論文 / 著書情報
Article / Book Information

題目(和文)	
Title(English)	Design and Development of Vibration Energy Harvesters using Tuned-Mass Systems for Bridge Structures
著者(和文)	竹谷晃一
Author(English)	Kouichi Takeya
出典(和文)	学位:博士(工学), 学位授与機関:東京工業大学, 報告番号:甲第10481号, 授与年月日:2017年3月26日, 学位の種別:課程博士, 審査員:佐々木 栄一,廣瀬 壮一,WIJEYEWICKREMA ANIL,北詰 昌樹,岩波 光保,小林 裕介
Citation(English)	Degree:Doctor (Engineering), Conferring organization: Tokyo Institute of Technology, Report number:甲第10481号, Conferred date:2017/3/26, Degree Type:Course doctor, Examiner:,,,,,
学位種別(和文)	博士論文
Type(English)	Doctoral Thesis

Doctoral Dissertation

Design and Development of Vibration Energy Harvesters using Tuned-Mass Systems for Bridge Structures

Tokyo Institute of Technology

Department of Civil Engineering

Supervised by Eiichi SASAKI

Kouichi TAKEYA

Contents

List of Figures

Chapter 1: Introduction

Chapter 2: Investigation on Characteristics of Electro-Mechanical Systems

Chapter 3: Proposal of Tuning Design Method

Chapter 4: Trial Application of TMG to an Actual Bridge

Chapter 5: Efficiency Enhancement of Power Generators for Energy Harvesting

Chapter 6: Proposal of Uses of the Developed Energy Harvesting System

List of Tables

Chapter 4: Trial Application of TMG to an Actual Bridge

Chapter 5: Efficiency Enhancement of Power Generators for Energy Harvesting

Chapter 6: Proposal of Uses of the Developed Energy Harvesting System

Acknowledgements

I wish to express my deepest gratitude to my supervisor, Associate Professor Eiichi Sasaki for his very kind supports, advices and encouragements. I am thankful for his aspiring guidance, invaluably constructive criticisms and friendly advices during the research work. A special gratitude I give to Professor Chitoshi Miki for his very kind supports, stimulating suggestions and encouragement.

I wish to express my gratitude to Associate Professor Yusuke Kobayashi, Dr. Atsushi Tanabe and Dr. Hisatada Suganuma for his accurate advice and kind encouragements. I am sincerely grateful to them for their truthful and constructive views on a number of issues related to this research. I would like also to thank sincerely Assistant Professor Hiroshi Tamura for his kind support, very friendly advices and encouragements.

Furthermore, I would like to mention about the support by NEXCO Co., LTD. My research works were financial supported by NEXCO Co., LTD. Furthermore, the member of NEXCO Co. gave me useful information and suggestions. Especially, I would like to thank Mr. Osafune, Mr. Kanno and Mr. Iwabuki. I would also like to mention about the support by E-stir Co. LTD., Scraft Co. LTD. and ITM Co. LTD. In order to develop electro-mechanical systems, I had technical help from them. Especially, I would like to thank Mr. Akazawa from E-stir Co., LTD., Mr. Hagiuda and Mr. Kato from Scraft Co. LTD. And Mr. Kataoka from ITM Co., LTD. I wish to express my gratitude to Mr. Kato, Mr. Hiyama, Mr. Hasegawa and Mr. Itami from Tokkyokiki Co., LTD. I would also like to thank to Mr. Nagoya and Mr. Arita from Subaru Co., LTD and President Sonobe from Sinwa-technos for their help of field experiments.

A special thanks goes to Ms. Ishihara and Ms. Hamada for her support in non-research field. They helped many office works. I would like to great thank PhD.

students Ms. Akutsu for her kind advice. She gave me useful view and remarks of my research works. It was good experience for me to help her research work. I learned many things from assisting her work and discussion with her. I wish to thank our laboratory members, Mr. Ando and Mr. Iizuka. It was good experience for me to help their research works. Mr. Itami friendly came to help my field experiment. PhD. student Mr. Natdanai gave me advices on my research works, and experiments. It was good experience for me to discuss on our research works with PhD. students Mr. Cao and Ms. Tuttipongsawat, Mr. Tominaga, Mr. Ota and Mr. Mishima.

I wish to special great thank Ms. Scorupski for her advice about my research work and English. She gave me useful view and remarks of my research works. Furthermore, I would like to thank our graduated laboratory members, Mr. Umekawa, Mr. Navicus, Mr. Ueda, Mr. Kanamori and Mr. Ebisawa for their kind help and friendship. Especially, I learned many things from assisting their research work and discussion with them.

Finally, I would like to thank to my parents Ms. Akiko and Mr. Shinichi Takeya and my grandfather Mr. Shoji Takeya for their long support and understanding.

Abstract

A method to harvest bridge vibration energy has been proposed in this paper using a tuned mass damper system, named hereafter Tuned Mass Generator (TMG). To harvest and make use of the unused reserve of bridge vibration energy the aforementioned damper system absorbs, a linear electromagnetic power generator has been applied. The benefits of using dual-mass systems over single-mass systems for power generation have been clarified according to the theory of vibrations. TMG parameters have been determined considering multi-physics parameters, and TMG has been tuned using a newly proposed parameter design method. Theoretical and numerical analysis results have found that for effective energy harvesting, it is essential that TMG has robustness against uncertainties in bridge vibrations and tuning errors, and TMG has demonstrated this feature when it was applied to an actual bridge. In addition, the design procedure of the TMG system, including the health monitoring system, has been proposed and the ability for continuous health monitoring has been demonstrated.

Keywords: *bridge vibration; energy harvesting; tuned mass damper; electromagnetic power generator, efficiency.*

Chapter 1

Introduction

Abstract

Vibration-based energy harvesting has been studied in various fields and one area of growing interest is the potential for this harvested vibration energy to supply electric power to wireless sensing devices, or other intelligent systems, for the health monitoring of bridges. An energy harvester, using a tuned dual-mass damper system and electromagnetic power generator, named hereafter Tuned Mass Generator (TMG), has subsequently been proposed.

1.1. Background

The importance of managing aging infrastructure has become of great concern in recent years, hence it is urgently required that effective maintenance management of infrastructures is established. One useful method is to monitor the dynamic behavior of structures, especially the vibrations of bridge structures **[1-6]**. However, due to the critical problem of continuous power supply required for monitoring, effective maintenance management has yet to be achieved. To supply electric power to monitoring sensing devices, vibration-based energy harvesting has become one area of growing interest and has been studied in various fields **[7-9]**. There is also the prospect for harvesting energy from large scale structures **[10-17]**.

To date, tuned mass damper or shock absorbing damper systems **[18-20]** have been studied to control bridge vibration which causes damage or noise. Considering these studies, tuned mass damper systems could, in particular, satisfactorily control bridge vibration when an ideal dynamic balance is achieved between its mass, springs and dampers **[21-27]**. If a power generator (or transducer) replaced the damper in a tuned mass damper system and could successfully absorb bridge vibration energy, it would have the capacity to harvest energy and control bridge vibration simultaneously. However, one problem of harvesting energy from bridge vibration is that the natural frequency of bridges is generally much lower than the mechanical vibrations which have so far been the main target of energy harvesting.

In recent years, harvesting energy from low frequency vibrations **[13]** or supplying harvested energy to monitoring systems has been studied using building model structures **[14]**, yet the amplitude of the target vibration in these cases is much higher than that of bridge vibration. In the case of bridge structures, the damping effect of electric power generators decrease in low frequency ranges, and as a result, the efficiency of energy harvesting or vibration control decreases. One solution to this problem could be to apply high performance power generators with large electric damping.

Many types of transduction mechanisms have already been developed to increase the efficiency of power generation, such as electromagnetic power generators using ferromagnetic devices **[7,12,28-31]**, piezoelectric power generators using piezoelectric

ceramics **[32-34]**, or even electrets **[35-39]**. Among these many new developments, electromagnetic power generators can, in particular, generate high electric power and produce large damping forces; it is thus considered that high performance electromagnetic power generators can produce enough electric damping for harvesting energy from even low frequency bridge vibrations **[40-43]**. However, the power generation level obtained from bridge vibrations has been around micro-watt to milli-watt and is not still satisfied to monitor dynamic behavior of bridge structures.

Another problem concerning harvesting energy from bridge vibration is that the natural frequency of bridges is uncertain due to many factors, including traffic conditions and temperature **[4,44-51]**. However, the performance of tuned mass damper systems is highly sensitive, and can drop with the slightest change in frequency when the forced excitation frequency is near the effective frequency. In other words, tuned mass damper systems have a narrow target frequency range, and have low robustness against changes in vibration frequency **[52]**.

One approach that has been proposed to reduce this sensitivity is to apply much higher damping than theoretically designed **[53]**. However, increasing the damping reduces the performance of tuned mass dampers, and vice versa, hence various parameter design methods have been proposed depending on the desired peak value of displacement for a given bridge **[54-56]**. There are parameter design methods that consider how the balance between robustness and the peak value of displacement can be adjusted through evaluation functions or band width parameters, and using multiple tuned mass dampers to improve this balance has also been investigated **[57-65]**. Still, further investigation is required to implement these various design parameters, due to the limitations of weight and accuracy when assembling these tuned mass dampers, including tuning errors, and these factors have been considered in this study. A further difficulty of the aforementioned parameter design methods is that they have been developed considering vibration control only; hence they cannot be applied directly to energy harvesting. In several studies, tuning methods for energy harvesting were proposed considering mechanical systems and electric circuits of energy harvesters **[66,67]**. Yet, these methods were found to be insufficient for efficient energy harvesting, since the performance of electromagnetic transducers should also be designed considering harvested energy from vibration of bridge structures.

1.2. Purpose and Objectives

To solve the aforementioned difficulties surrounding the energy harvesting from bridge structural vibrations, and achieve continuous health monitoring systems of bridges, the purpose of this study is to design and develop an efficient energy harvester to capture energy from vibrations of bridge structures. To achieve the purpose, an energy harvester using a tuned mass system and electromagnetic power generator (or transducer) is developed, named hereafter Tuned Mass Generator (TMG), which can then lead to continuous health monitoring systems of bridge structures. To be specific, efficiency enhancement of the TMG system is considered to achieve the energy harvesting from low frequency and uncertain bridge vibrations. To satisfy the aim of energy harvesting to obtain various required electricity for health monitoring such as dynamic behavior of bridge structures, efficient electromechanical structure design of TMG is required and maximum power generation should be higher than one watt, in brief, watt order. To achieve the aforementioned purpose, the following research objectives are considered.

I. Investigation of the structural characteristics of energy harvesters

II. Proposal of a parameter design method for effective energy harvesting

III. Evaluation of the applicability of TMG to an existing bridge

IV. Enhancement of a power generators efficiency

V. Development of a TMG system that includes a health monitoring system of bridge structures

1.3. Related Research

1.3.1. Health monitoring for Bridge Structures

Aging of infrastructure including bridges has rapidly progressed over the past decade **[68]**, and so the importance of infrastructure management has become of great

importance. Moreover, it is vital to recognize the condition of structures as soon as possible when abnormal events such as earthquakes occur. However, due to the decline in engineers and the limitation of available finance, sufficient inspection and maintenance methods have become difficult to carry out. To solve the aforementioned problems surrounding infrastructure, it is urgent to construct an effective maintenance management method to supplement the inspections that are being carried out by engineers.

One constructive maintenance management method is to monitor the dynamic behavior of structures, especially the vibrations of bridge structures, and so far various studies have been carried out **[1-3]**. Bridge structures are greatly affected by various dynamic traffic loads, such as heavy vehicles. Miki et al. **[4]** has established a monitoring system for the dynamic behavior of bridge structures such as by using accelerometers and displacement sensors. In addition, long-term operation of the monitoring system was carried out to inspect abnormalities in bridge structures and traffic conditions of large vehicles, and to detect damages quickly after disasters. Fukada et al. **[5]** carried out long-term monitoring of structural dynamic behaviors of a bridge to inspect the dynamic stress of the bridge girders and the total weight of trucks typically crossing a bridge.

As identified in these researches, the importance of health monitoring systems of bridge structures has been demonstrated, in particular, the long-term monitoring of dynamic structural behaviors. However, due to the critical problem of supplying continuous power to monitoring systems, the long-term health monitoring of bridge structures is currently limited. Nonetheless, vibration-based energy harvesting has the potential for using the harvested vibration energy to supply electric power for the health monitoring of bridges **[8]**.

1.3.2. Structural Design of Energy Harvester

Environmental vibration power generation is performed by converting mechanical energy from vibrations into electric energy using a power generator. The conversion efficiency highly depends on the power generation system and the vibration conditions. Among the various conversion systems, such as electromagnetic power generators using ferromagnetic devices **[7,12,29-31]**, piezoelectric power generators using

piezoelectric ceramics **[32-34]**, or even electrets **[35-38]**, piezoelectric and electromagnetic devices have an advantage of higher electrical power generation with simple implementation. Arroyo et al. investigated piezoelectric and electromagnetic vibration energy harvesters using normalized models **[69]**. Three parameters were considered in the normalized models, namely the coupling coefficient, loss coefficient and mechanical quality factor. Based on the findings in experiments and a theoretical study regarding piezoelectric and electromagnetic generators, it was determined that although electromagnetic generators demonstrate high resistive losses, this is compensated by high coupling coefficients. In addition, it was notably shown that the power density of an electromagnetic generator does not decrease in proportion to its volume as it is commonly observed. However, the power generation obtained is still low for efficient energy harvesting from vibrations of bridge structures.

Most researches on energy harvesting have been focused on vibration characterized by frequencies above 10Hz and below milli-watt power **[7-17]**. In contrast, the fundamental vibration frequency of large-scale structures, such as high-rise buildings or bridges, is typically around 1Hz. Since large-scale energy is expected in these vibrating structures **[70,71]**, power generators to harvest this vibration energy must be capable of extracting large power from low-frequency and low-velocity oscillations.

Cassidy et al. proposed an electromagnetic power generator for harvesting energy from large structures such as high-rise buildings or bridges **[72]**. To obtain large power generation, a ball screw coupled with a permanent-magnet synchronous machine was used in the proposed power generator (**Figure 1.1**). To evaluate this devices energy harvesting capability, impedance matching theory **[73-75]** was used, and the ability of harvesting energy was experimentally demonstrated. Although large power generation could be obtained, large power losses were also distinguished.

Other approaches to obtain large power generation density include using the Transverse Flux Linear Motor, namely TFLM (**Figure 1.2**) **[76]**, or using a magnet array **[77]**. TFLM is a type of linear motor with high power per volume since the magnetic circuit is separated from the electric circuit, and high thrust force density is obtained due to flux concentration **[78-84]**. To acquire higher power per volume, Hoang et al. considered several types of TFLM devices with various configurations of

the permanent magnet using the equivalent magnetic circuit network method **[76]**. However, disadvantages of TFLM such as mechanical loss including cogging and efficiency, and power factor, should also be considered.

Tang et al. proposed a new type of electromagnetic power generator with high power density by putting strong rare-earth magnet arrays in alternating directions and using high-magnetic-conductive casing (**figure 1.3**) **[77]**. However, through experiment it was shown that the maximum damping capacity obtained included large mechanical loss.

To obtain large power generation density, kinematic devices, such as a crank, cam or ball screw, are generally required in electromagnetic power generators. However, the mechanical transmission loss in these kinematic devices cause a reduction in efficiency of electric power generation and the power generator also becomes larger in size. In addition, although the power density increases, the more permanent magnets that are used, the lower the efficiency and the higher the cost.

Akazawa et al. **[40-43]** proposed a new type of free-piston linear electromagnetic power generator to attain high efficiency and a compact design. Linear systems have advantages such as low mechanical loss. In particular, the free-piston linear electric power generator has advantages not only for low mechanical loss but also high efficiency power generation. In addition, the volume of strong rare-earth magnets in the power generators can be reduced using the free-piston linear power generator system. Although the proposed device was originally designed for stirring engine systems, this technology could improve the efficiency of harvesting energy from structural vibrations due to its compact design and ability to obtain high power efficiency.

1.3.3. Tuned Mass Systems for Bridge Vibrations

Among tuned mass systems, tuned mass dampers could, in particular, satisfactorily control vibrations when an ideal dynamic balance is achieved between its mass, springs and dampers **[21-23,27]**. If a power generator replaced the damper in a tuned mass damper system and could successfully absorb bridge vibration energy, it would have the capacity to harvest energy and control bridge vibration simultaneously. Zhu et al. **[85]** proposed an application of electromagnetic power generators, namely EM

dampers, for both vibration damping and energy harvesting in buildings. Theoretical and experimental studies of linear EM dampers was presented. Based on the results, EM dampers replaced traditional viscous fluid dampers for vibration mitigation of lightly damped and flexible structures, such as high-rise buildings. Zuo et al. **[66,67]** modeled two energy harvesters with tuned mass damper systems, single-mass and dual-mass systems, and concluded that dual-mass systems provide greater power generation with an increase in electrical damping if the energy harvester is under forced excitation, or base displacement excitation is applied. However, in the case of energy harvesting from vibrations of bridge structures, the forced excitation is from traffic vibrations and not a forced excitation directly applied to the energy harvester. In addition, since vibration characteristics of bridge structures depend on vibration amplitude, it is considered that the vibration characteristics, in small vibration amplitudes such as a micro-tremor and in large vibration amplitudes such as traffic of large vehicles or earthquakes, significantly differ **[48,49]**. Consequently, it is difficult to achieve effective vibration control on real bridges in addition to harvesting energy. For the above reasons, an effective model and practical design method for bridge vibration energy harvesting has yet to be established.

1.3.4. Monitoring System of Bridge Structures using Energy Harvesting

A prototype monitoring system using a piezoelectric device and an electric circuit was developed and examined at an existing bridge by Yoshida et al. **[8,9]**. The aim was to obtain electricity from train-induced vibrations of the actual bridge. Not only were advantageous shapes and materials of piezoelectric power generators examined, electric circuits, for effectively harvesting energy from train load induced vibrations of bridge structures was also examined. The generated electric power when trains pass through the bridge was demonstrated. In addition, based on the experimental results, a prototype monitoring system was proposed. The prototype system demonstrated measured and transmitted data five times with the power generated from bridge vibrations induced by a train composed of ten cars, and the train received this transmitted data wirelessly. Yoshida's study demonstrated that it is possible to harvest electricity from railway bridge vibrations and transmit small monitoring data wirelessly.

Although vibration-based energy harvesting for supplying electric power to structural health monitoring systems is of growing interest, generated voltage signals have yet to be practically used. Yamaguchi et al. **[11]** developed a new passive type vibration velocity sensor by using the power generation characteristics of vibrated electret. Based on the findings in a numerical simulation, a vibration velocity sensor using an electret electrode structure was proposed. As a basic experimental result, a relationship between generated voltage per unit velocity and frequency was obtained as transfer functions for converting voltage signals to velocities. Finally, experiments of voltage signal responses from vibration of an existing bridge were carried out to examine the applicability of the proposed sensors. Yamaguchi's study demonstrated a new use of energy harvesting from vibrations of bridge structures.

1.4. Outline of this Dissertation

The research objectives are discussed in the five main chapters respectively as outlined below (**Figure 1.4**).

Chapter 1. Introduction

Background, related research, purpose and objectives were discussed.

Chapter 2. Investigation on Characteristics of Electro-Mechanical Systems

In order to develop an advantageous design of energy harvesters for vibrations of bridge structures, electro-mechanical characteristics of a Tuned Mass Generator (TMG) were investigated. Advantages of dual-mass systems over single-mass systems were evaluated for power generation from vibrations of bridge structures.

Chapter 3. Proposal of Tuning Design Method

The tuning design method of TMG for efficient energy harvesting of vibrations from bridge structures has been proposed. Based on parametric studies, the effect of parameters on robustness regarding frequency change and tuning errors was determined.

Chapter 4. Trial Applications of TMG to an Actual Bridge

TMG was designed and developed for application on an actual bridge. The characteristics of power generation from bridge vibrations were investigated and discussed.

Chapter 5. Efficiency Enhancement of Power Generators for Energy Harvesting

In order to improve the applicability of TMG, electromechanical structure of a power generator for efficient energy harvesting was considered and developed.

Chapter 6. Proposal of Uses of the Developed Energy Harvesting System

Based on the findings in the previous chapters, a practical use of TMG for monitoring systems of bridge structures has been proposed and its capability is experimentally verified.

Chapter 7. Conclusion and Recommendations

The results of each chapter are summarized in this chapter. Based on the findings obtained in this study, recommendations for an efficient energy harvesting system and practical use of the developed TMG are proposed.

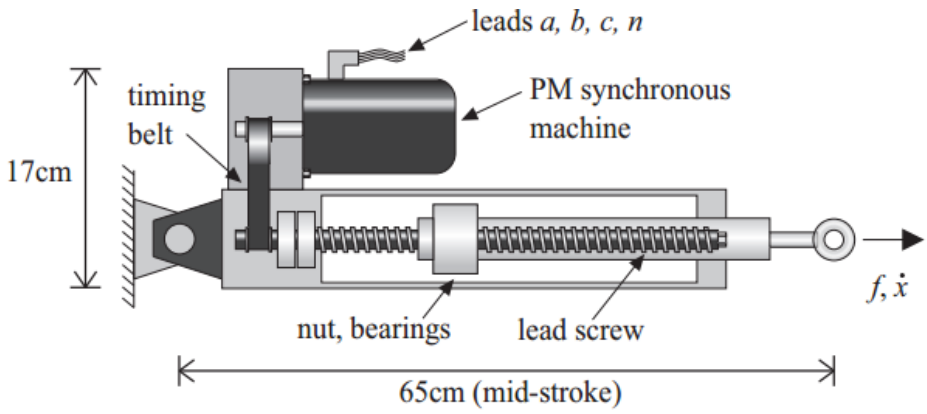

Figure 1.1 Configuration for a power generator consisted of a ball screw

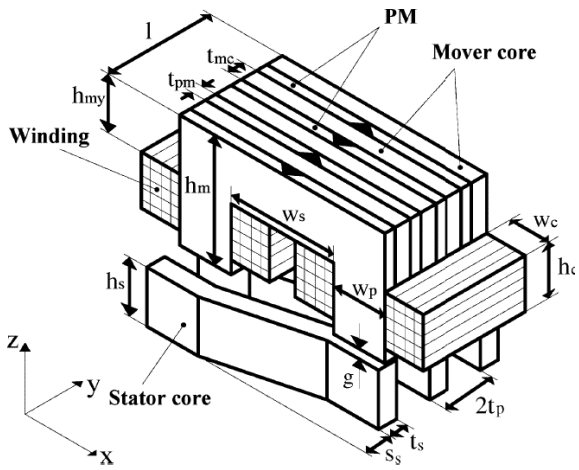

Figure 1.2 Configuration for a transverse flux linear motor (TFLM) with full permanent magnet

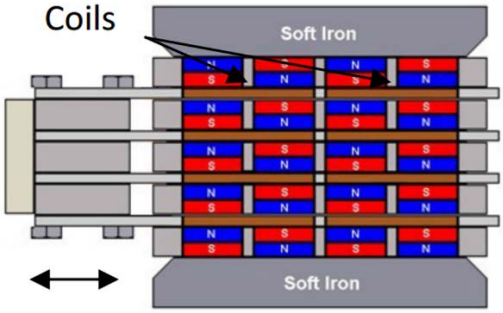

Figure 1.3 Configuration for an electromagnetic power generator using a coil and magnet array

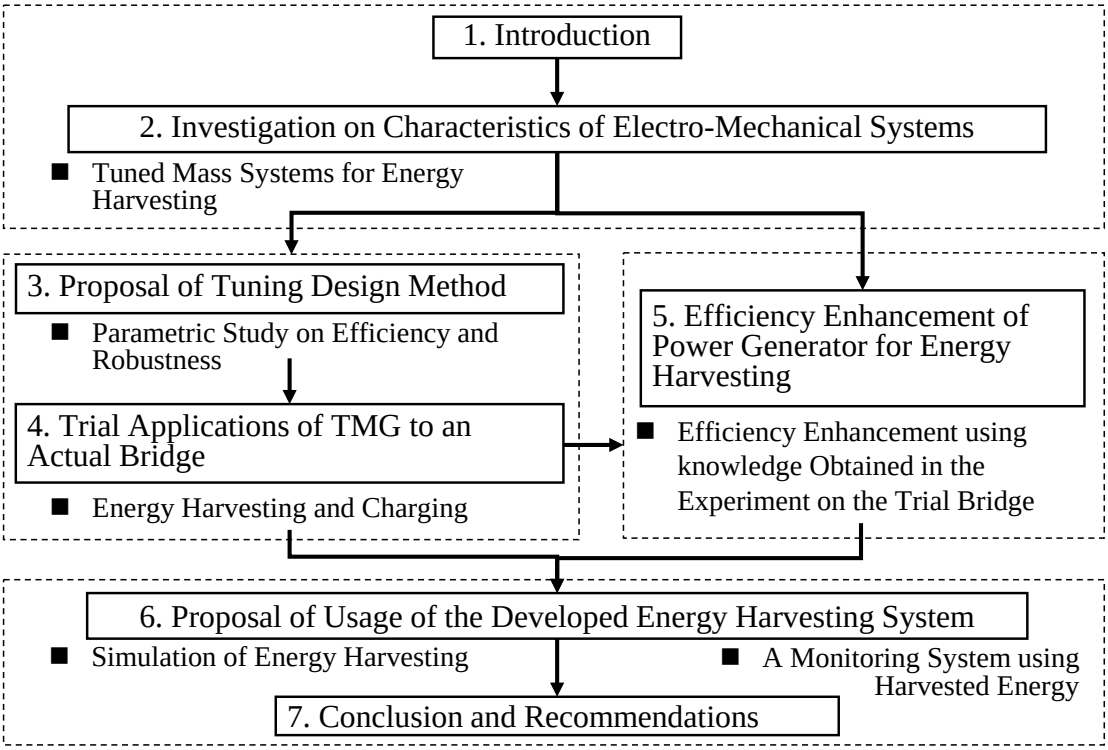

Figure 1.4 Flow of this dissertation

Chapter 2

Investigation on Characteristics of Electro-Mechanical Systems

Abstract

In this chapter, advantages of dual-mass systems over single-mass systems for power generation from vibrations of bridge structures have been theoretically investigated. Results from the theoretical study show that for effectively using harvested energy for charging, it is essential to consider the robustness against changes in the electric damping, and dual-mass systems were found to successfully demonstrate this ability. Moreover, it was found that dual-mass systems have advantages over single-mass systems for robustness against tuning errors and changes in natural frequencies of bridges.

2.1. Overview

To date, tuned mass damper systems have been found to satisfactorily control bridge vibration when an ideal dynamic balance is achieved between its mass, springs and dampers. If the damper in a tuned mass damper system was replaced with an electromagnetic power generator and could successfully absorb bridge vibration energy, it would have the capacity to harvest energy. However, one problem of harvesting energy from bridge vibration is that the natural frequency of bridges is generally much lower than the mechanical vibrations which have so far been the main target of energy harvesting. Another factor to be considered is that large-scale energy is expected in vibrating bridge structures **[72,73]**, and so energy harvesters should be capable of extracting large power from low-frequency and low-velocity oscillations.

Zuo et al. **[66,67]** modeled two energy harvesters with tuned mass systems, namely a single-mass and a dual-mass system, and concluded that dual-mass systems provide greater power generation with an increase of electric damping if the energy harvester is under forced excitation, or base displacement excitation is applied. However, in the case of harvesting energy from bridge vibrations, the forced excitation is from traffic vibrations and is thus not a forced excitation that is directly applied to the energy harvester. It is therefore still controversial as to whether a single-mass system or a dual-mass system is more efficient for harvesting energy from bridge vibrations. Due to the above reasons, an effective structural system to harvest energy from vibrations of bridge structures has yet to be established.

In this chapter, characteristics of electro-mechanical systems of an energy harvester for vibration of bridge structures has been investigated when using both single-mass and dual-mass systems. It was concluded that an energy harvester using a tuned dual-mass system was more advantageous and this system along with an electromagnetic power generator, named hereafter Tuned Mass Generator (TMG), has subsequently been proposed. In addition, the characteristics of TMG have been theoretically explained to investigate how TMG can achieve greater power generation from vibrations of bridge structures.

2.2. Theoretical Explanation of Single-Mass and Dual-Mass Systems

2.2.1. Single-Mass Vibration Energy Harvesters

Figure 2.1 shows a single-mass vibration energy harvester, where mass m_1 is connected to the bridge mass M with spring k_1 and an electromagnetic power generator is installed. $F(t)$ is the excitation force, $F_e(t)$ is the damping force by the electromagnetic power generator. Bridge mass M is connected to the base with an equivalent spring K and a damping coefficient C_M. $x(t)$ and $X(t)$ express the displacement of the mass m_1 and the bridge mass M. As shown in **Figure 2.2**, an equivalent circuit is introduced to represent the linear generator and is formularized as

$$L\frac{dI(t)}{dt} + rI(t) + RI(t) = E(t) \tag{2.1}$$

where L is the inductance [H], r is the internal resistance [Ω], R is the resistance of the circuit [Ω], I is the current [A] and E is the electromotive force [V]. Based on Faraday's law, the electromotive force $E(t)$ has been defined as

$$E(t) = k_{emf}\frac{dx(t)}{dt} \tag{2.2}$$

in which k_{emf} is an electromotive force coefficient [Vs/m], and $dx(t)/dt$ is the velocity of the moving part of the electromagnetic power generator. The damping force by electromagnetic power generator $F_e(t)$ is formularized as

$$F_e(t) = k_{emf} I(t) \tag{2.3}$$

Harvested electric power and electrical loss from electromagnetic power generators is expressed as

$$W(t) = RI^2(t), \quad W_{loss}(t) = rI^2(t) \tag{2.4}$$

The total electric power generation [VA or Nm/s] from combining the above, and considering the electromagnetic power generator to include equivalent damping is

$$W_{total}(t) = (c_{eh} + c_{el})x_1^2(t) \tag{2.5}$$

where $\dot{x}$ is the velocity, and c_{eh} and c_{el} are damping coefficients due to harvested electric power and electrical loss respectively. These equivalent electrical damping coefficients can be defined as

$$c_{eh} = \frac{k_{emf}^2}{r}\frac{R_r}{(1+R_r)^2}, \quad c_{el} = \frac{k_{emf}^2}{r}\frac{1}{(1+R_r)^2} \tag{2.6}$$

where $R_r = R/r$ is the resistance ratio. **Equation (2.6)** demonstrates that the equivalent electrical damping coefficients increase when the resistance ratio R_r decreases. The ratio of harvested electric power to total electric power generation, which the electromagnetic power generator absorbs, is hereafter called converting ratio and is formularized as

$$h = \frac{c_{eh}}{c_{eh} + c_{el}} \tag{2.7}$$

Next, the power factor of the electric circuit is introduced as follows

$$P_f = \frac{1+R_r}{\sqrt{L_r^2 + (1+R_r)^2}} \tag{2.8}$$

where $L_r = \omega L/r$ is the impedance ratio. Thus, the resistance ratio R_r and L_r can be expressed, using the converting ratio h and power factor P_f, as

$$R_r = \frac{h}{1-h}, \quad L_r = \frac{\sqrt{P_f^{-2} - 1}}{1-h} \tag{2.9}$$

When subjected to forced excitation $F(t) = F_0 sin(\omega t)$ as shown in **Figure 2.1**, the governing equation for the vibration energy harvester is expressed as

$$\begin{aligned} &m_1\ddot{x}_1(t) + k_1(x_1(t) - X(t)) = -F_e(t) \\ &M\ddot{X}(t) - k_1(x_1(t) - X(t)) + KX(t) + C_M\dot{X}(t) = F_e(t) + F(t) \end{aligned} \tag{2.10}$$

The following non-dimensional quantities are introduced.

$$\zeta_M = \frac{C_M}{2\sqrt{M \cdot K}}, \quad \zeta_{e1} = \frac{c_e}{2\sqrt{m_1 \cdot k_1}}, \quad \mu_1 = \frac{m_1}{M}, \quad \gamma_1 = \frac{\sqrt{K/M}}{\sqrt{k_1/m_1}}, \quad \lambda = \frac{\omega}{\sqrt{K/M}}$$

where ζ_M is the damping ratio of the bridge, ζ_{e1} is the equivalent damping ratio due to the electric load, μ_1 is the mass ratio, γ_1 is the frequency ratio, and λ is the normalized excitation frequency. The equivalent damping coefficient due to the electric load c_e is formularized as follows

$$c_e = \frac{k_{emf}^2}{r} \frac{1+R_r}{L_r^2 + (1+R_r)^2} \tag{2.11}$$

Dimensionless displacement $\overline{X}$ is defined as the ratio of displacement to static displacement X_0 as follows

$$\overline{X}(t) = \frac{X(t)}{X_0} = \frac{X(t)}{F_0 / K} \tag{2.12}$$

The following dimensionless harvesting power can also be introduced as

$$\overline{W}(t) = \frac{RI^2(t)}{F_0^2 \sqrt{M \cdot K}} \tag{2.13}$$

When the excitation force $F(t)$ in **equation (2.10)** is harmonic, the corresponding transfer function of the current GI_1 and the displacement GX_1 can be formularized by using the Laplace transform as follows

$$GI_1(s) = -\frac{M \cdot k_{emf} \cdot \mu_1 \cdot s^3}{k_{emf}^2 \cdot s\{d_2(s) + d_3(s)\} + d_1(s) \cdot d_2(s) \cdot d_3(s) - d_4(s)} \tag{2.14}$$

$$GX_1(s) = \frac{k_{emf}^2 \cdot s + d_1(s) \cdot d_2(s)}{k_{emf}^2 \cdot s\{d_2(s) + d_3(s)\} + d_1(s) \cdot d_2(s) \cdot d_3(s) - d_4(s)} \tag{2.15}$$

Where

$$d_1(s) = r\left(s \cdot \sqrt{M/K} \cdot L_r / \lambda + R_r + 1\right)$$
$$d_2(s) = M \cdot \mu_1 \cdot s^2 + K \cdot \mu_1 / \gamma_1^2$$
$$d_3(s) = K + C_M \cdot s + M \cdot s^2 + K \cdot \mu_1 / \gamma_1^2$$
$$d_4(s) = d_1(s) \cdot K^2 \cdot \mu_1^2 / \gamma_1^4 + 2 \cdot s \cdot K \cdot k_{emf}^2 \cdot \mu_1 / \gamma_1^2$$

In order to consider the characteristics of single-mass vibration energy harvesters for energy harvesting and vibration control, steady-state harvesting power and vibration amplitude responses with various electric damping ratios ζ_e are obtained as shown in **Figure 2.3** and **Figure 2.4**. If the bridge damping ratio ζ_M is 0.02, and the mass ratio μ_1 is 0.0011 (1.1 ‰), the value of mass ratio is equal to the total mass ratio of dual-mass systems mentioned in the next chapter. If the bridge damping is low or the mass ratio μ_1 is high, the efficiency of energy harvesting and vibration control increases. The dashed line in **Figure 2.3** shows the electric damping ratio, where the maximum harvesting power response is indicated by the red point. The dashed line in **Figure 2.4** shows the electric damping ratio where the minimum value of local maximum vibration amplitude response is indicated by the blue point. These two electric damping ratios

are not equal, as the appropriate design of parameters is for energy harvesting or vibration control. **Figure 2.5** and **Figure 2.6** show the response of harvesting power and vibration amplitude, respectively. The responses are sensitive to the tuning of electric damping ratio ζ_e hence the efficiency of energy harvesting drops with the slightest change in ζ_e.

2.2.2. Dual-Mass Vibration Energy Harvesters

Figure 2.7 indicates a dual-mass vibration energy harvester, where two masses m_1 and m_2 are connected in series with springs k_1 and k_2. An electromagnetic power generator is installed between the two masses. $F(t)$ is the excitation force, $F_e(t)$ is the damping force by the electromagnetic power generator. Bridge mass M is connected to the base with an equivalent spring K and a damping coefficient C_M. $x_1(t)$, $x_2(t)$ and $X(t)$ express the displacement of the mass m_1, mass m_2 and the bridge mass M. When subjected to forced excitation, the governing equations for the vibration energy harvester can be expressed as

$$\begin{aligned} &-m_2\ddot{x}_2(t)+k_2(x_2(t)-x_1(t))=-F_e(t) \\ &m_1\ddot{x}_1(t)+k_1(x_1(t)-X(t))+k_2(x_2(t)-x_1(t))=+F_e(t) \\ &M\ddot{X}(t)-k_1(x_1(t)-X(t))+KX(t)+C_M\dot{X}(t)=F(t) \end{aligned} \tag{2.16}$$

In addition, the following non-dimensional quantities are defined as follows

$$\mu_2=\frac{m_2}{m_1}, \qquad \gamma_2=\frac{\sqrt{k_2/m_2}}{\sqrt{k_1/m_1}}, \qquad \zeta_{e2}=\frac{c_e}{2\sqrt{m_2\cdot k_2}}$$

where μ_2 is the mass ratio, γ_2 is the frequency ratio, and ζ_{e2} is the electric damping ratio of the dual-mass system. When the forced excitation $F(t)$ in **equation (2.16)** is harmonic, the corresponding transfer function of the current GI_2 and the displacement GX_2 can be formulated by using the Laplace transform as follows

$$GI_2(s)=\frac{-s^3K\cdot M\cdot k_{emf}\cdot\mu_1^2\cdot\mu_2/\gamma_1^2}{d_3(s)\cdot d_6(s)-K^2\cdot\mu_1^2/\gamma_1^4\cdot d_1(s)\cdot d_2(s)+k_{emf}^2\cdot s-d_3(s)\cdot d_4(s)} \tag{2.17}$$

$$GX_2(s)=\frac{d_6(s)-d_4(s)}{d_3(s)\cdot d_6(s)-K^2\cdot\mu_1^2/\gamma_1^4\cdot d_1(s)\cdot d_2(s)+k_{emf}^2\cdot s-d_3(s)\cdot d_4(s)} \tag{2.18}$$

Where

$$d_1(s) = r \cdot \left(s \cdot \sqrt{M/K} \cdot L_r / \lambda + R_r + 1 \right)$$
$$d_2(s) = M \cdot \mu_1 \cdot \mu_2 \cdot s^2 + K \cdot \mu_1 \cdot \mu_2 \cdot \gamma_2^2 / \gamma_1^2$$
$$d_3(s) = K + C_M \cdot s + M \cdot s^2 + K \cdot \mu_1 / \gamma_1^2$$
$$d_4(s) = d_1(s) \cdot K^2 \cdot \mu_1^2 \cdot \mu_2^2 \cdot \gamma_2^4 / \gamma_1^4 + 2 \cdot s \cdot K \cdot k_{emf}^2 \cdot \mu_1 \cdot \mu_2^2 \cdot \gamma_2^2 / \gamma_1^2$$
$$d_5(s) = M \cdot \mu_1 \cdot s^2 + K \cdot \left(\mu_1 / \gamma_1^2 + \mu_1 \cdot \mu_2 \cdot \gamma_2^2 / \gamma_1^2 \right)$$
$$d_6(s) = k_{emf}^2 \cdot s \cdot \left(d_2(s) + d_5(s) \right) + d_1(s) \cdot d_2(s) \cdot d_5(s)$$

To consider the characteristics of dual-mass vibration energy harvesters for energy harvesting and vibration control, steady-state harvesting power and vibration amplitude responses with various electric damping ratios ζ_{e2} have been demonstrated as shown in **Figure 2.8** and **Figure 2.9**. If bridge damping ratio ζ_M is 0.02, and mass ratio μ_1 and μ_2 are set to be 0.001 and 0.1, the total mass ratio of dual-mass systems is equal to the mass ratio of single-mass systems 0.0011 (1.1 ‰). If bridge damping is low or the mass ratio μ_1 is high, the efficiency of energy harvesting and vibration control increases. The dashed line in **Figure 2.8** indicates the electric damping ratio, where the maximum harvesting power response is indicated by the red point. The dashed line in **Figure 2.9** shows the electric damping ratio, where the minimum value of local maximum vibration amplitude response is indicated by the blue point. These two electric damping ratios are not equal; in other words, the appropriate design of parameters for energy harvesting or vibration control is similar to single-mass systems. **Figure 2.10** and **Figure 2.11** show the response of harvesting power and vibration amplitude, respectively. The responses are less sensitive against the tuning of electric damping ratio ζ_{e2} compared to single-mass systems namely the efficiency of energy harvesting does not drop with a slight change in electric damping ratio.

2.3. Comparison between Single-Mass and Dual-Mass Systems

To consider the unstable bridge vibration, the electric power response spectrums of dual-mass systems and single-mass systems are shown in **Figure 2.12** and **Figure 2.13**. The displacement response spectrums are shown in **Figure 2.14** and **Figure 2.15**. The response spectrums in 2% and 4% reduce of γ_1 are shown in these figures. As shown in **Figure 2.12** and **Figure 2.13**, the peak value of electric power response

reduces when γ_1 reduces. To adapt this phenomena, the tuning of the mass or springs can be considered. However, it is difficult to tune these parameters on the field. The tunable parameter of single mass systems is only the electric damping ratio of the electromagnetic power generator ζ_e. Meanwhile, only the peak value can be changed by tuning electric damping ratio ζ_e, the frequency cannot be tuned. Therefore, this method is not effective to adapt TMG to the unstable bridge vibration. On the other hand, the parameters of second mass in dual-mass systems, such as mass ratio μ_2 and frequency ratio γ_2 are available to tune on the field. The frequency which gives the peak value can be shifted by tuning the mass ratio μ_2 and the peak value can be tuned by the frequency ratio γ_2 or electric damping ratio ζ_e. **Figure 2.16** and **Figure 2.17** show the tuned frequency response spectrum of the power generation and the displacement by changing the combination of γ_2 and μ_2. Generally, it is hard to tune parameters exactly same as the designed values. Therefore, the robustness against tuning errors is important. As a consequent, the dual-mass systems have an advantage over single-mass systems for the applicability of tuning parameters.

From the results obtained in this chapter, a vibration energy harvester using a dual-mass system, named Tuned Mass Generator (TMG) has been deemed most appropriate for this study.

2.4. Summary

Based on the aforementioned researches and issues encountered in this chapter, an energy harvester, using a tuned dual-mass system and electromagnetic power generator (or transducer), named hereafter Tuned Mass Generator (TMG), has subsequently been proposed. In addition, the characteristics of TMG have been theoretically explained for energy harvesting to achieve greater power generation from bridge vibrations. The findings from this chapter are summarized below.

(a) The electromagnetic power generator is represented by an equivalent electric circuit for modeling TMG. The corresponding transfer function of the power generation and the displacement can be formulated by using Laplace transform.

(b) In dual-mass systems, the efficiency of energy harvesting does not drop with a

slight change in electric damping ratio as in the case of single-mass systems. Consequently, dual-mass systems have an advantage over single-mass systems for effectively using harvested energy for charging.

(c) The appropriate design of parameters for energy harvesting or vibration control is different for single-mass and dual-mass systems. The balance between the two designs can be controlled by changing the electric damping ratios of the electromagnetic power generator.

(d) Robustness of TMG against tuning errors is important. Accordingly, dual-mass systems have an advantage over single-mass systems for the applicability of tuning parameters.

Dual-mass systems have several advantages over single-mass systems for power generation, such as efficiency of harvesting energy in charging and robustness of tuning. Based on this finding, a bridge vibration energy harvester using a dual-mass system, named Tuned Mass Generator (TMG), has been proposed and will be further enhanced to enable TMG to harvest energy.

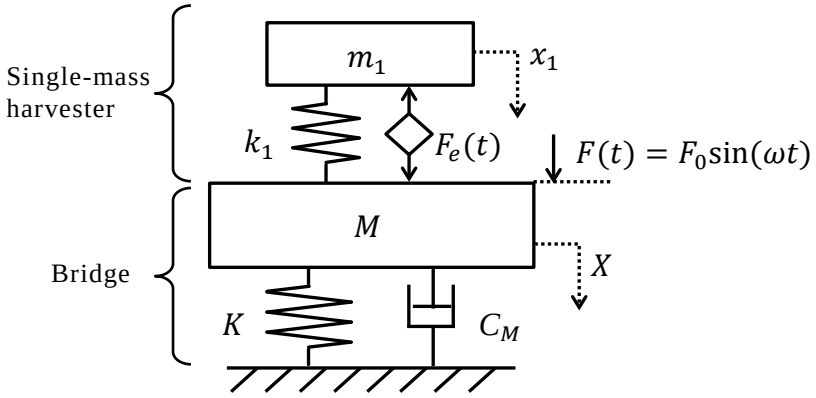

Figure 2.1 Analysis model of single mass systems

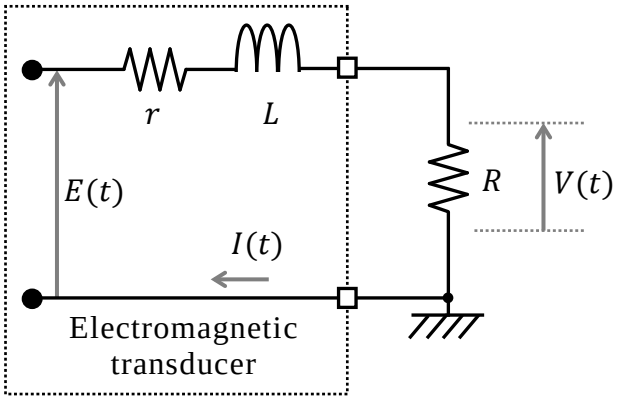

Figure 2.2 Electric circuit

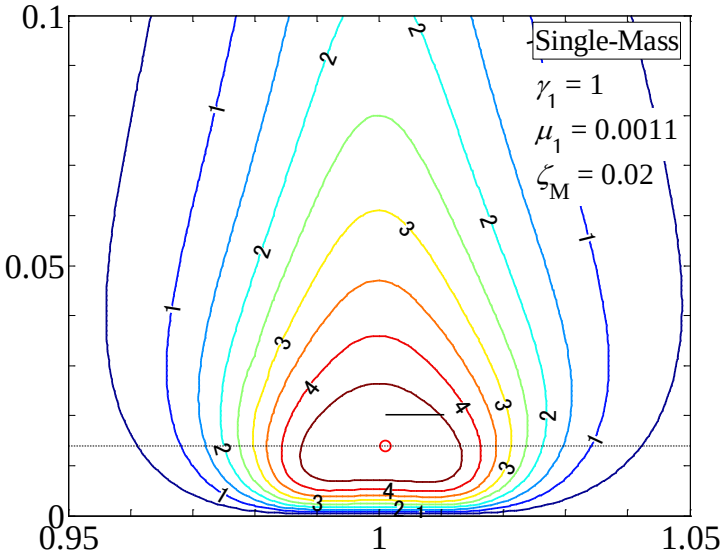

Figure 2.3 Harvesting power $\overline{W_{max}}$ response of single mass systems with various electric damping ratios ($0 \leq \zeta_e \leq 5$)

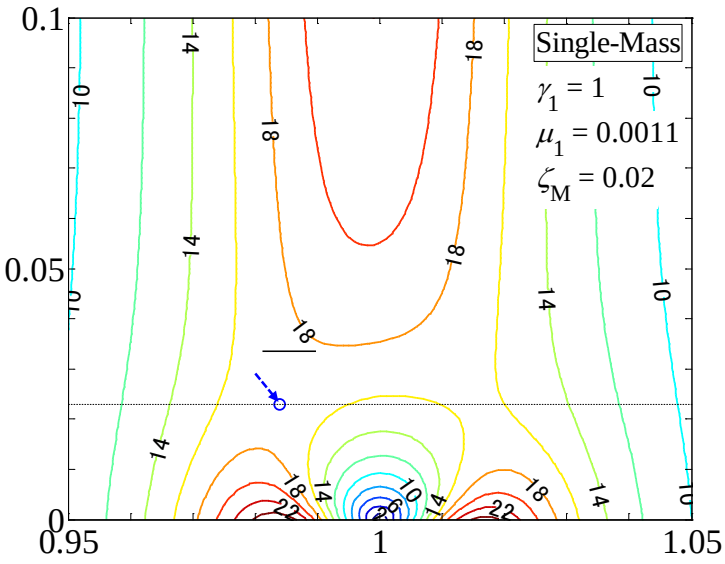

Figure 2.4 Bridge vibration displacement $\overline{X_{max}}$ response of single mass systems with various electric damping ratios ($0 \leq \zeta_e \leq 5$)

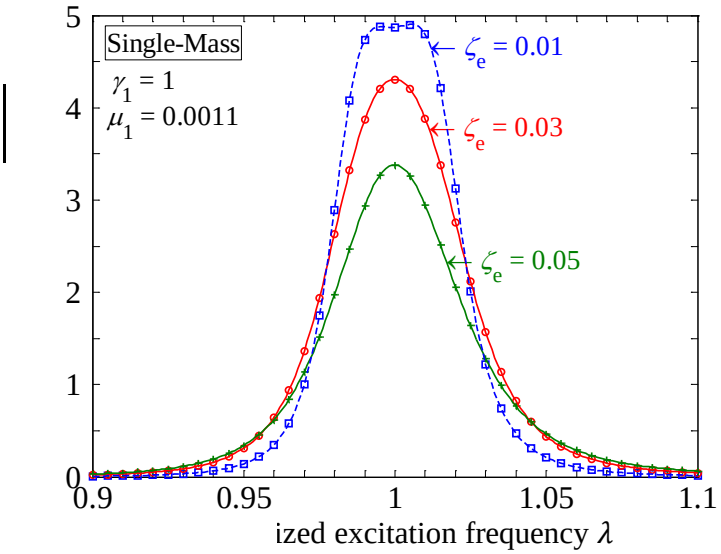

Figure 2.5 Harvesting power $\overline{W_{max}}$ response of single mass systems with different electric damping ratios (ζ_e = 0.01, 0.03, 0.05)

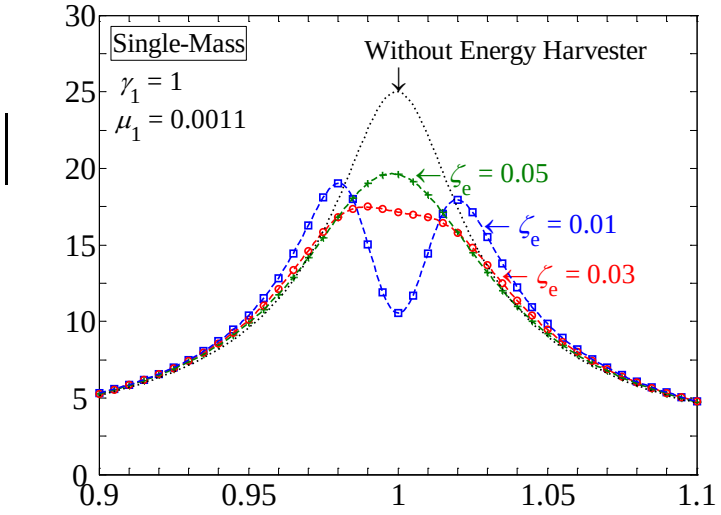

Figure 2.6 Bridge vibration displacement $\overline{X_{max}}$ response of single mass systems with different electric damping ratios (ζ_e = 0.01, 0.03, 0.05)

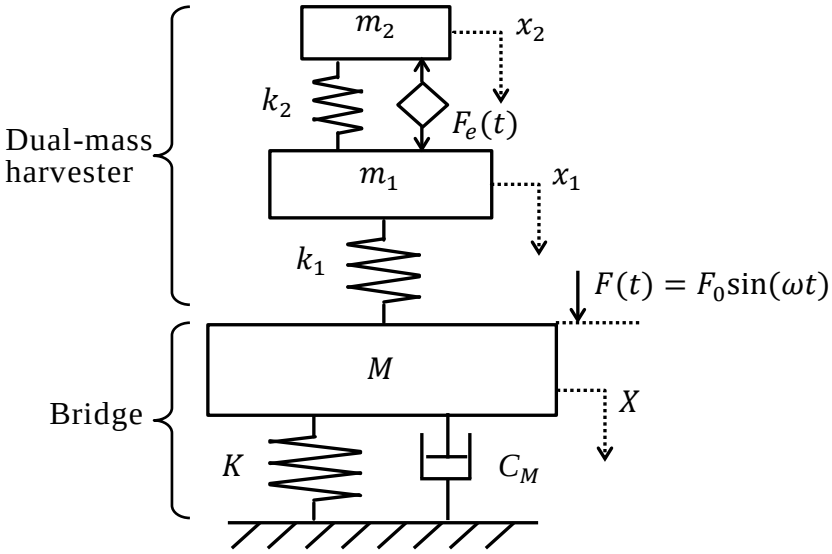

Figure 2.7 Analysis model of dual-mass systems

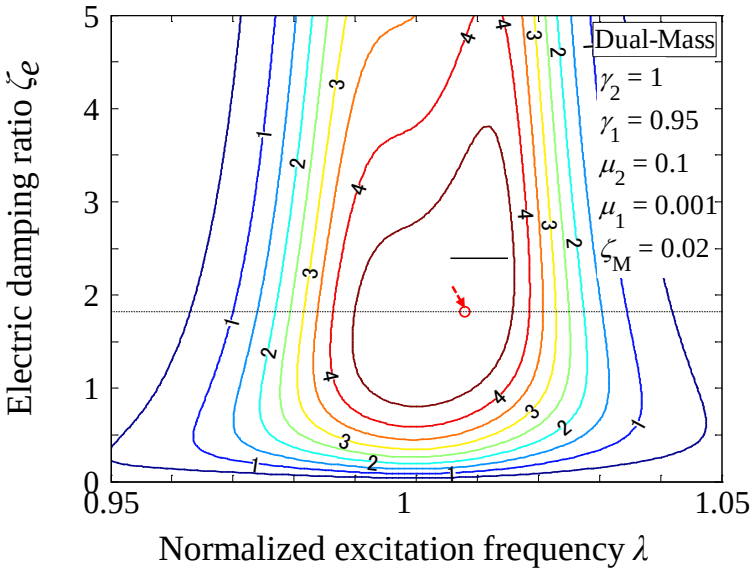

Figure 2.8 Harvesting power $\overline{W_{max}}$ responses of dual-mass systems with various electric damping ratios ($0 \leq \zeta_e \leq 5$)

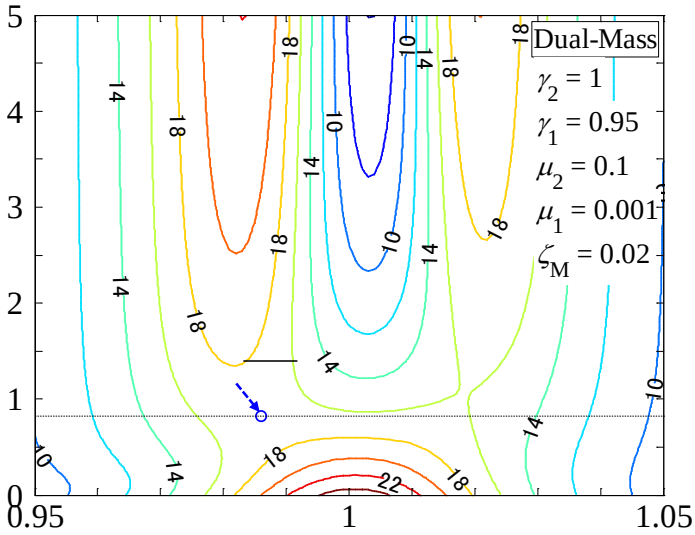

Figure 2.9 Bridge vibration amplitude $\overline{X_{max}}$ responses of dual-mass systems with various electric damping ratios ($0 \leq \zeta_e \leq 5$)

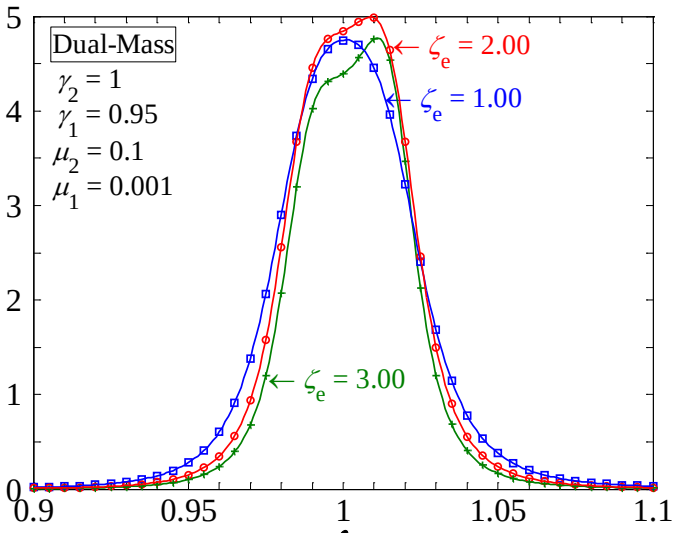

Figure 2.10 Harvesting power $\overline{W_{max}}$ responses of dual-mass systems with different electric damping ratios (ζ_e = 0.01, 0.03, 0.05)

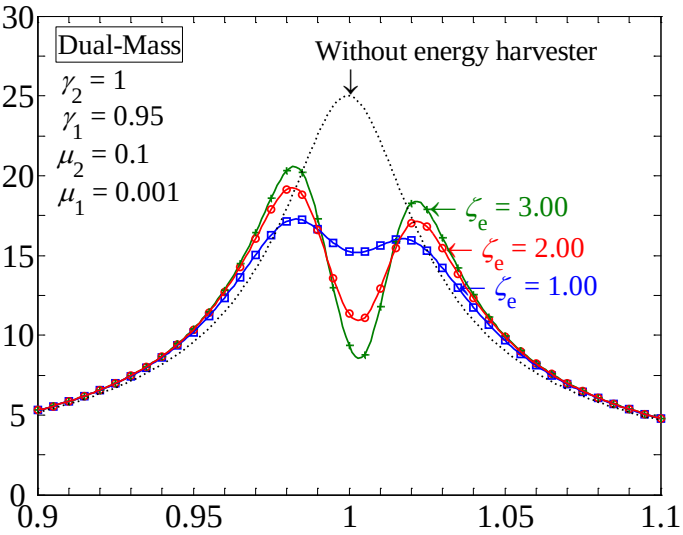

Figure 2.11 Bridge vibration amplitude $\overline{X_{max}}$ responses of dual-mass systems with different electric damping ratios (ζ_e = 0.01, 0.03, 0.05)

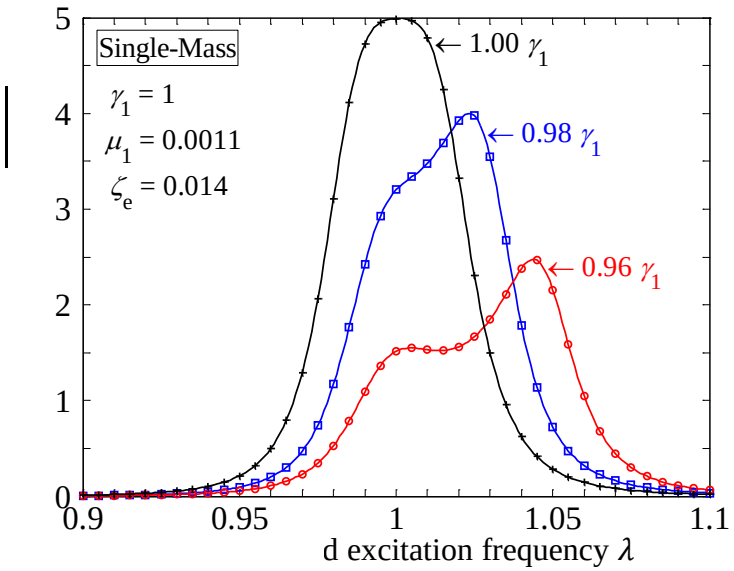

Figure 2.12 Harvesting power $\overline{W_{max}}$ responses of single-mass systems with different frequency ratio

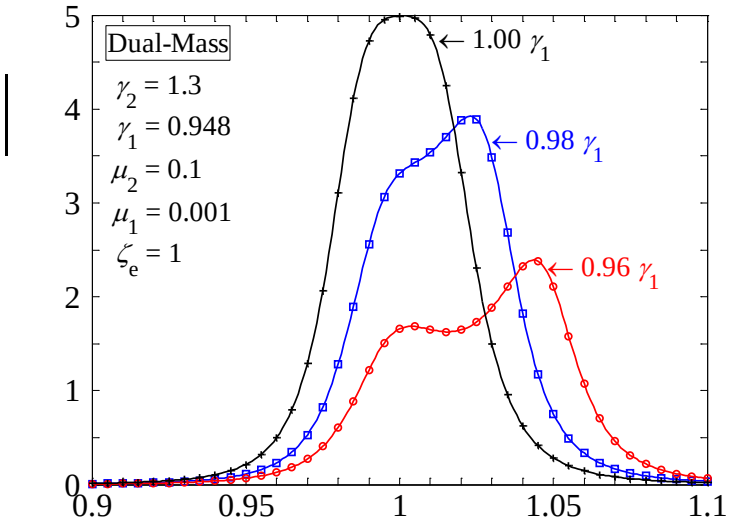

Figure 2.13 Harvesting power $\overline{W_{max}}$ responses of dual-mass systems with different frequency ratio

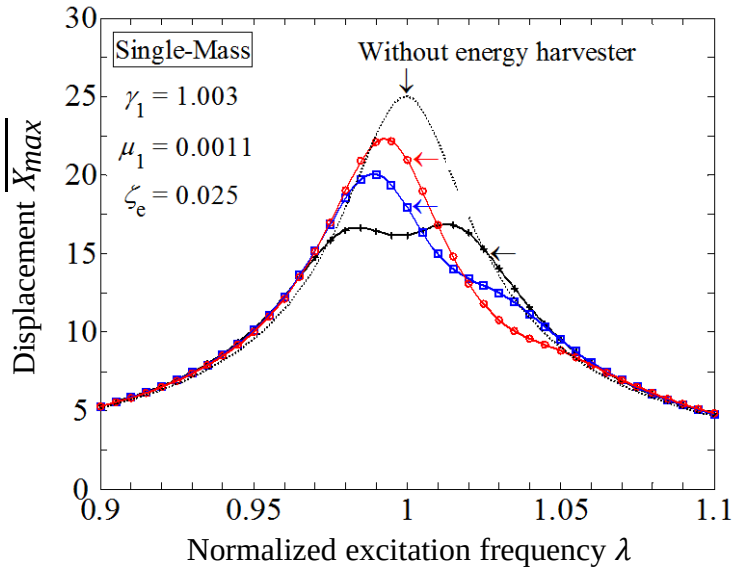

Figure 2.14 Vibration amplitude $\overline{X_{max}}$ responses of single-mass systems with different frequency ratio

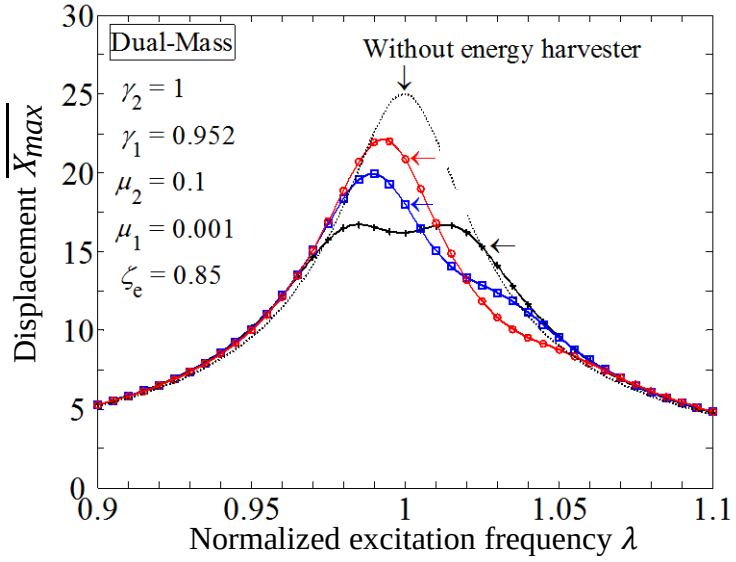

Figure 2.15 Vibration amplitude $\overline{X_{max}}$ responses of dual-mass systems with different frequency ratio

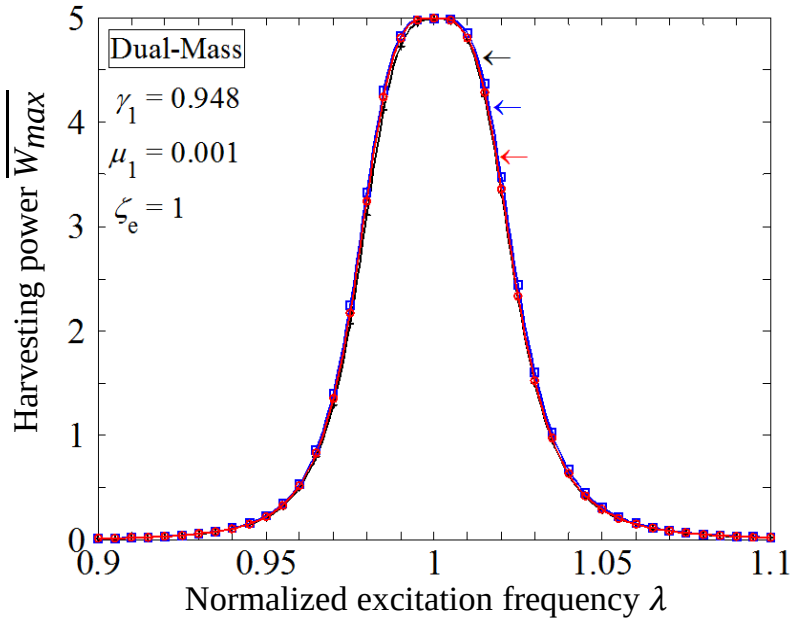

Figure 2.16 Tuning of harvesting power responses of dual-mass systems with second mass ratio and frequency ratio

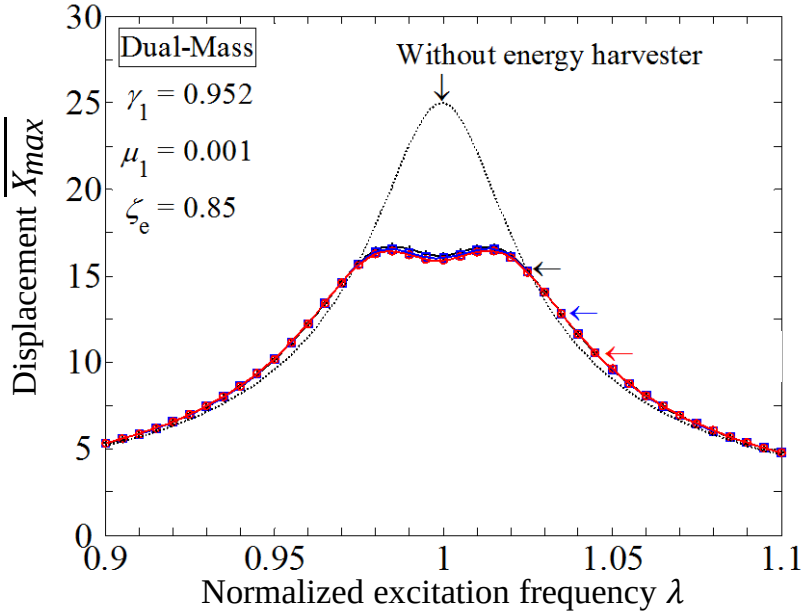

Figure 2.17 Vibration amplitude $\overline{X_{max}}$ responses of dual-mass systems with second mass ratio and frequency ratio

Chapter 3

Proposal of Tuning Design Method

Abstract

In the previous chapter, advantages of dual-mass systems over single-mass systems for power generation from vibrations of bridge structures were explained. Based on the results, a bridge vibration based energy harvester using a tuned dual-mass system and electromagnetic power generator, named Tuned Mass Generator (TMG), has been proposed. In addition, characteristics required to design TMG have been formulated using an equivalent electric circuit of an electromagnetic power generator. In this chapter, a multi-physics parameter design method has been developed to tune TMG. Results from parametric studies show that for effective energy harvesting, first, it is essential to determine the relationship between the required characteristics for the electromagnetic power generator, and second, that TMG requires a robust parameter design for uncertain bridge vibrations, accuracy of assembling TMG and tuning errors.

3.1. Overview

In the previous chapter, characteristics of energy harvesters using tuned mass systems have been formulated using an equivalent electric circuit of a linear electromagnetic power generator. In addition, advantages of dual-mass systems over single-mass systems for power generation from vibrations of bridge structures were investigated. Based on the findings, a bridge vibration energy harvester using dual-mass systems and an electromagnetic power generator, named Tuned Mass Generator (TMG), has been proposed. However, an appropriate tuning design is necessary to enable the most effective performance of TMG for power generation from the vibrations of bridge structures.

In this chapter, effects of parameters on energy harvesting were investigated for efficient energy harvesting from bridge structural vibrations. In addition, a multi-physics parameter design method has been developed to tune TMG.

3.2. Effects of Parameters on Energy Harvesting in Dual-Mass Systems

In order to evaluate the effect of parameters on the efficiency of energy harvesting, first, the energy flow of the bridge-TMG vibration system was considered. **Figure 3.1(a)** and **Figure 3.1(b)** show the energy flow in a bridge-TMG model for every vibration cycle. A part of the bridge vibration energy flows into the main mass of TMG (A) in mechanical form, although the damping from bridge structures (O) dissipates the main part of bridge vibration energy. In the mechanical domain, the vibration energy of the main mass flows into the second mass (E), where some of the energy continues to cycle as the vibration of the main mass (M), while some mechanically dissipates (C). The electromagnetic power generator converts some of the mechanical energy into electrical energy (D and F). In the electrical domain, some electrical energy is harvested (J), while the remaining electrical energy is converted into thermal energy from the internal resistance of the electromagnetic power generator (H), or continues to cycle as reactive energy (I).

The sole target of this study is energy harvesting. In order to maximize the efficiency of energy harvesting, there are three possible options. First, increase the energy flow into TMG (A), second, increase the transducing energy from the mechanical domain to the electrical domain (D and F), and thirdly, increase the power factor or converting ratio of electrical energy to energy harvesting (H, I and J). The energy flow into TMG increases with an increase in the mass ratio μ_1. When using the same mass ratio, an appropriate frequency ratio exists to maximize the energy flow. In order to increase the transducing energy from the mechanical domain to the electrical domain, an appropriate electrical damping for the electromagnetic power generator should be designed.

The electric circuit and characteristics of the electromagnetic power generator design the converting ratio of electrical energy. For the aforementioned reasons, frequency ratios and electrical damping ratio are considered as the key parameters that need tuning, whereas the mass ratio μ_1 is fixed as 0.001 (1 ‰). The mass ratio was designed by considering watt-order power generation from bridge structural vibrations. The damping ratio of a bridge ζ_M is fixed as a generally used value of 0.02. The power factor and converting ratio predominantly depend on the specifications of the electromagnetic power generator; if the power factor and converting ratio take a maximum value, all electrical energy is harvested. The power factor can become the maximum using the power factor correction (PFC) circuit. The PFC circuit uses a phase advanced capacitor and its capacitance C^* is designed as follows

$$C^* = \frac{1}{\omega^2 L} \tag{3.1}$$

where ω is the angular frequency [rad] and L is the inductance of the coil in the electromagnetic power generator [H]. As previously shown in **equation (3.1)**, the converting ratio cannot become 1 except for in extreme cases where the internal resistance $r = 0$ or resistance $R = \infty$. Considering general cases, the power factor and converting ratio are fixed as 1 and 0.8, respectively.

To analyze the influence of parameters on the efficiency of energy harvesting, parametric study was conducted. First, a frequency response of power ratio based on the response function in **equation 2.13** and **equation 2.17** in **Chapter 2** was calculated where parameters were designed as follows: $\mu_2 = 0.1$, $\gamma_1 = 0.948$, $\gamma_2 = 1.4$,

$\zeta_e = 1$. These parameters were designed using the parameter design method as mentioned next. Next, parameters were varied from this combination of parameters. The normalized cross-correlation coefficient of harvesting power response with a lag of zero was introduced as follows

$$\hat{R}_{xy}(0) = \frac{\sum_{\lambda_l}^{\lambda_h} \{\overline{W}(\lambda) \cdot \overline{W}_0(\lambda)\}}{\sum_{\lambda_l}^{\lambda_h} \{\overline{W}_0(\lambda)\}^2} \tag{3.2}$$

where normalized excitation frequencies λ_l, λ_h are in the range of $-\infty < \lambda_l \leq \lambda \leq \lambda_h < +\infty$, $\overline{W}$ is the harvesting power response in dimensionless form, and $\overline{W_0}$ is the harvesting power response with $\mu_2 = 0.1$, $\gamma_1 = 0.948$, $\gamma_2 = 1.4$, $\zeta_e = 1.0$, named A1. The closer the normalized harvesting power response $\overline{W}$ gets to $\overline{W_0}$, the closer the normalized cross-coefficient of harvesting power response with a lag of zero gets to the value of 1.

Figure 3.2 shows the normalized cross-correlation coefficient of harvesting power response with a lag of zero, for various electric damping ratios ζ_e and frequency ratios γ_2. The normalized cross-correlation coefficient with a lag of zero has one maximum value at A1. In **Figure 3.2**, B1 shows the value with $\gamma_2 = 1.4$ and $\zeta_e = 0.5$, C1 shows the value with $\gamma_2 = 0.95$ and $\zeta_e = 1.0$, and D1 shows the value with $\gamma_2 = 0.95$ and $\zeta_e = 1.6$. Other parameters, $\mu_2 = 0.1$ and $\gamma_1 = 0.948$, are fixed. **Figure 3.3** shows the frequency responses of power ratio of the four cases, A1, B1, C1 and D1. As shown in **Figure 3.2**, the normalized cross-correlation coefficient with a lag of zero is obtained almost the same as the maximum value when the combination of parameters corresponds to the dashed line (D1 is an example case), whereas the harvesting power value decreases when the combination of parameters moves away from the dashed line (such as B1 and C1). Consequently, the appropriate combination of parameters ζ_e and γ_2 gives almost the same harvesting power response as the maximum response, although only one combination of parameters exists to maximize the efficiency of energy harvesting. Fundamentally, it is practically impossible to tune parameters to be identical to the designed values, yet this characteristic can be used to minimize the tuning error through an appropriate combination of parameters.

Figure 3.4 shows the normalized cross-correlation coefficient with a lag of zero for various combinations of mass ratio μ_2 and frequency ratio γ_1 parameters. A2 is the case when the harvesting power response in dimensionless form with $\mu_2 = 0.10$,

γ_1 = 0.948, γ_2 = 1.3, ζ_e = 1.0. The normalized cross-correlation coefficient with a lag of zero has one maximum value at A2. B2 shows the value with μ_2 = 0.12 and γ_1 = 0.948, C2 shows the value with μ_2 = 0.10 and γ_1 = 0.938, and D2 shows the value with μ_2 = 0.12 and γ_1 = 0.938. Other parameters, γ_2 = 1.3 and ζ_e = 1.0, are fixed. **Figure 3.5** shows the frequency responses of power ratio of the four cases, A2, B2, C2 and D2. As shown in **Figure 3.4**, the normalized cross-correlation coefficient at a lag of zero takes almost the same maximum value when the combination of parameters corresponds to the dashed line, whereas the harvesting power value decreases when the combination of parameters moves away from the dashed line. Therefore, if the appropriate combination of parameters μ_2 and γ_1 are used a harvesting power response almost the same as the maximum response can be obtained. However only one combination of parameters can maximize the efficiency of energy harvesting. Precise tuning of μ_2 is comparatively less difficult than tuning of γ_1 since there is a limitation in the variety of springs or the size of the main mass m_1. From these parametric studies, the parameters γ_1, γ_2 and ζ_e were determined as the parameters to be designed, while μ_2 is fixed as 0.1.

3.3. Multi-Physics Parameter Design Method for Power Generation

Since the natural frequency of bridges is uncertain due to many factors, including traffic conditions and temperature **[4,44-51]**, the purpose of multi-physics parameter design is to maximize power generation and ensure robustness against changes in vibration frequency. **Figure 2.7** showed the analysis model. All input and output parameters have been transformed into dimensionless form, and thus any reference to parameters or outputs henceforth are dimensionless. Harvesting power response in steady-state vibration is obtained by changing the frequency ratios γ_1, γ_2 and the equivalent electrical damping ratio ζ_e. In this study, it has been proposed that to ensure robustness against changes in vibration frequency, the amplitude of harvesting power response $\overline{W}$ in **equation (2.13)** must satisfy the minimum amplitude of harvesting

power $\overline{W_c}$ in the range between the normalized excitation frequencies λ_l and λ_h, using the constraint function. Similarly, the harvesting power response must maximize electric power generation when λ = 1, using the objective function. The constraint function and objective function are defined as follows

$$Q_1 = \min\left(\overline{W}(\gamma_1, \gamma_1, \zeta_e, \lambda)\Big|_{\lambda=\lambda_l,\lambda_h}\right) \tag{3.3}$$

$$G_1 = \overline{W}(\gamma_1, \gamma_1, \zeta_e, \lambda)\Big|_{\lambda=1} \tag{3.4}$$

The balance between robustness and peak power generation can be adjusted through the constraint function Q_1. **Figure 3.6** shows some harvesting power responses using the constraint function **equation (3.3)** and objective function **equation (3.4)**, with different parameters. Normalized excitation frequencies λ_l, λ_h and minimum power generation $\overline{W_c}$ can be modified depending on the purpose of energy harvesting. **Figure 3.7** shows the sequence of the proposed design method. For various combinations of the aforementioned parameters, γ_1, γ_2 and ζ_e, the harvesting power spectrum is calculated by reiterating the sequence of the presented analysis procedure. This sequence of iterations is continued until the maximum objective function G_1 is obtained. The parameters are designed to maximize the objective function G_1 by using a Sequential Quadratic Programming (SQP) method. SQP method can be considered as a generalized version of Newton's method, and it is one of the most effective methods for nonlinear constrained optimization problems. However, various local maximum power generation were found for various combination of parameters by only applying the SQP method. In this study, not only by using SQP method, but also by using the proposed objective function G_1 by considering the upper and lower limits of electric damping, a local maximum value equal to a global maximum value can be found. The distribution of G_1 using variations of the three tuning parameters γ_1, γ_2 and ζ_e is shown in **Figure 3.8(a)** to demonstrate the local maximum value. **Figure 3.8(b)** shows the upper view of the three-dimensional **Figure 3.8(a)**. As shown in **Figure 3.8(b)**, the local maximum values of G_1 have a wide distribution range when the electric damping ratio ζ_e is modified. However, when the electric damping ratio is low, the density of G_1 which satisfies the constraint function Q_1 is also low. In other words, if the electric damping ζ_e is low, the efficiency of energy harvesting is highly sensitive to tuning

errors, and can drop with the slightest change of tuning parameters (**Figure 3.8(b)**). It is therefore essential to consider robustness not only against changes in vibration frequency, but also against tuning errors, hence, the electric damping ratio should be high. Nonetheless, the converting ratio decreases if the electrical damping ratio increases when a fixed value of electromotive force coefficient k_{emf} is used. Thus, robustness against tuning errors (or changes of tuning parameters) and efficiency of energy harvesting have a trade-off relationship. Upper and lower limits of electric damping and converting ratio can be used to design the balance of this trade-off relationship.

3.4. Multi-Physics Parameter Design Method for Energy Storage

The purpose of multi-physics parameter design regarding energy storage is to maximize energy storage and ensure robustness against changes in vibration frequency. **Figure 3.9** shows the electric circuit for storing energy into a battery (capacitor). Equations for this electric circuit are derived as follows.

$$\begin{cases} E'(t) = rI(t) + L\dfrac{dI(t)}{dt} & \left[\begin{matrix} E'(t) > 0 \\ E(t) \geq 0 \end{matrix}\right] \\ -E'(t) = rI(t) + L\dfrac{dI(t)}{dt} & \left[\begin{matrix} E'(t) > 0 \\ E(t) < 0 \end{matrix}\right] \\ E'(t) = 0 & \left[\begin{matrix} else \end{matrix}\right] \end{cases} \tag{3.5}$$

Where

$$E'(t) = |E(t)| - V_b(t) - V_d$$

$$V_b(t) = \frac{1}{C}\int_0^t |I(t)|dt + V_b(0)$$

Where $E(t)$ is the electromotive force, $E'(t)$ is induced voltage to the battery, $V_b(t)$ is the battery voltage, V_d is the voltage dropped by diodes in a rectifier circuit, $I(t)$ is the current, r is the internal resistance of a coil of the power generator, L is the self-inductance of the coil and C is the capacitance of the battery. If the capacitance C is enough large, a change in battery (capacitor) voltage is negligible; the battery voltage

can be treated as a fixed value. The electric circuit experiences energy loss caused by the internal resistance *r*, and the diode's voltage drop V_d. The reactive energy generated from coils of the electromagnetic power generator does not charge any energy to the battery; it keeps cycling the energy in the electric circuit. The critical vibration frequency of bridges usually has low natural frequency, hence, the diode's voltage drop V_d can be simplified as a fixed value in low-frequency circuits. The dimensionless parameters are defined as follows.

$$B_r = \frac{V_b \cdot k_{emf}}{F_0 \cdot r}, \qquad D_r = \frac{V_d \cdot k_{emf}}{F_0 \cdot r}, \qquad \zeta_e = \frac{k_{emf}^2}{2r\sqrt{k_2 \cdot m_2}}$$

Where B_r is the battery voltage ratio, and D_r is the diode's voltage drop ratio. The following non-dimensional quantities were also introduced.

$$\overline{W_2} = \frac{V_b \cdot A}{F_0^2 \sqrt{K \cdot M}} \tag{3.6}$$

$$\overline{W_{rms}} = \frac{V_b}{F_0^2 \sqrt{K \cdot M}} \frac{\omega}{2\pi} \int_0^{2\pi} A(t)dt \tag{3.7}$$

where $\overline{W_2}$ is the harvesting power response when battery circuits are used, $\overline{W_{rms}}$ is the route mean square value of harvesting power response, and the current to the capacitor is corrected to $A(t) = |I(t)|$ by the rectifier. All input and output parameters have once again been made into dimensionless form, and thus any reference to parameters or outputs henceforth are dimensionless. In the case of energy storage, the route mean square value of harvesting power is more important than amplitude, unlike power generation. The route mean square value of harvesting power response in steady-state vibration is obtained by changing the frequency ratios γ_1, γ_2, and the battery voltage ratio B_r. In this study, it has been shown that to ensure robustness against changes in vibration frequency, the root mean square value of harvesting power response in steady-state vibration $\overline{W_{rms}}$ must satisfy the minimum power $\overline{W_c}$ in the range between the normalized excitation frequencies, λ_l and λ_h, using the constraint function. Concurrently, the spectrum for power generation must maximize electric power generation when $\lambda = 1$, using the objective function. The constraint function and objective function for energy storage are defined as

$$Q_2 = \min\left(\overline{W_{rms}}(\gamma_1, \gamma_1, B_r, \lambda)\Big|_{\lambda=\lambda_l,\lambda_h}\right) \tag{3.8}$$

$$G_2 = \overline{W}_{rms}(\gamma_1, \gamma_1, B_r, \lambda)\big|_{\lambda=1} \tag{3.9}$$

The balance between robustness and route mean square values of harvesting power can be adjusted through the constraint function Q_2. Normalized excitation frequencies λ_l, λ_h and minimum power $\overline{W_c}$ can be modified depending on the purpose of energy harvesting. **Figure 3.10** shows the sequence of the proposed design method. For various combinations of the aforementioned parameters, γ_1, γ_2 and B_r, the harvesting power response is calculated by reiterating the presented sequence of analysis. This sequence of iterations is continued until the maximum objective function G_2 is obtained using the SQP method. In general, by this method a local maximum value of G_2, equal to a global maximum, could be found. Therefore, as shown in **Figure 3.11(a)**, varying the three design parameters γ_1, γ_2 and B_r, influences the distribution of G_2. **Figure 3.11(b)** shows the side view of the three-dimensional **Figure 3.11(a)**. These figure enables a better comprehension of the local maximum. As shown in **Figure 3.11(b)** the local maximum values of G_2 have a distribution range between the frequency ratios γ_1 and γ_2. However, if the battery voltage ratio B_r is high, the density of G_2 which satisfies the constraint function Q_2 is low. In other words, the efficiency of energy harvesting is highly sensitive to tuning errors. Conversely, as shown in **Figure 3.11(a)**, if the battery voltage ratio is low, the robustness against tuning errors of γ_1 or γ_2 increases, while the harvesting power response becomes highly sensitive to changes in B_r. Fundamentally, the battery voltage ratio B_r is variable as it depends on the amplitude of forced excitation F_0. It is vital to consider robustness against not only changes in vibration frequency, but also against tuning errors, and against changes in B_r. Therefore, robustness against tuning errors of γ_1 or γ_2 and changes in B_r are a trade-off relationship. Upper and lower limits of the battery voltage ratio can be designed to balance this trade-off relationship.

3.5. Summary

Effects of parameters on energy harvesting have been investigated for efficient energy harvesting from bridge structural vibrations. To achieve the efficient energy

harvesting, three important factors were revealed. First, increase the energy flow into TMG, second, increase the transducing energy from the mechanical domain to the electrical domain, and thirdly, increase the power factor or converting ratio of electrical energy to energy harvesting. In addition, a multi-physics parameter design method has been developed to tune TMG. Results from parametric studies have shown that for effective energy harvesting, first, it is essential to determine the relationship between the required characteristics for the electromagnetic power generator, and second, that TMG requires a robust parameter design for random bridge vibrations, accuracy of assembling TMG and tuning errors.

It should be noted that there is also the potential for the proposed TMG to be further developed so that nonlinear characteristics of the energy harvester during charging can be controlled under variable bridge vibrations due to heavy traffic.

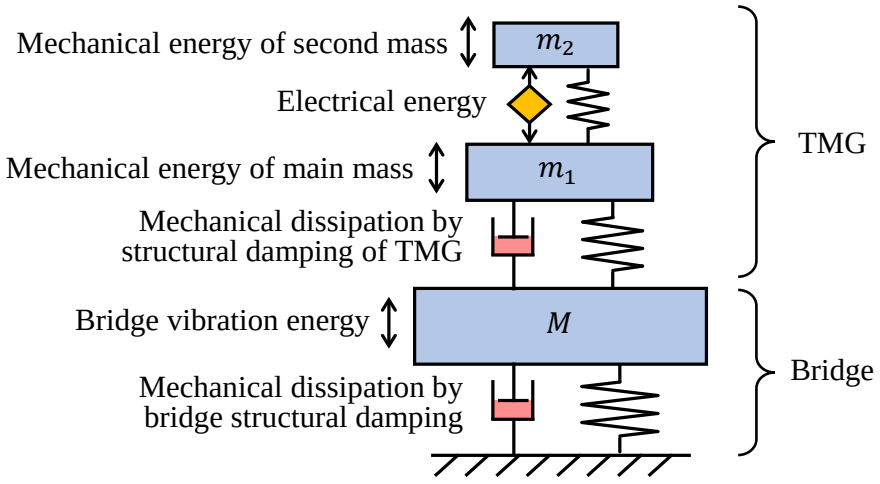

Figure 3.1(a) Energy flow model of bridge-TMG system

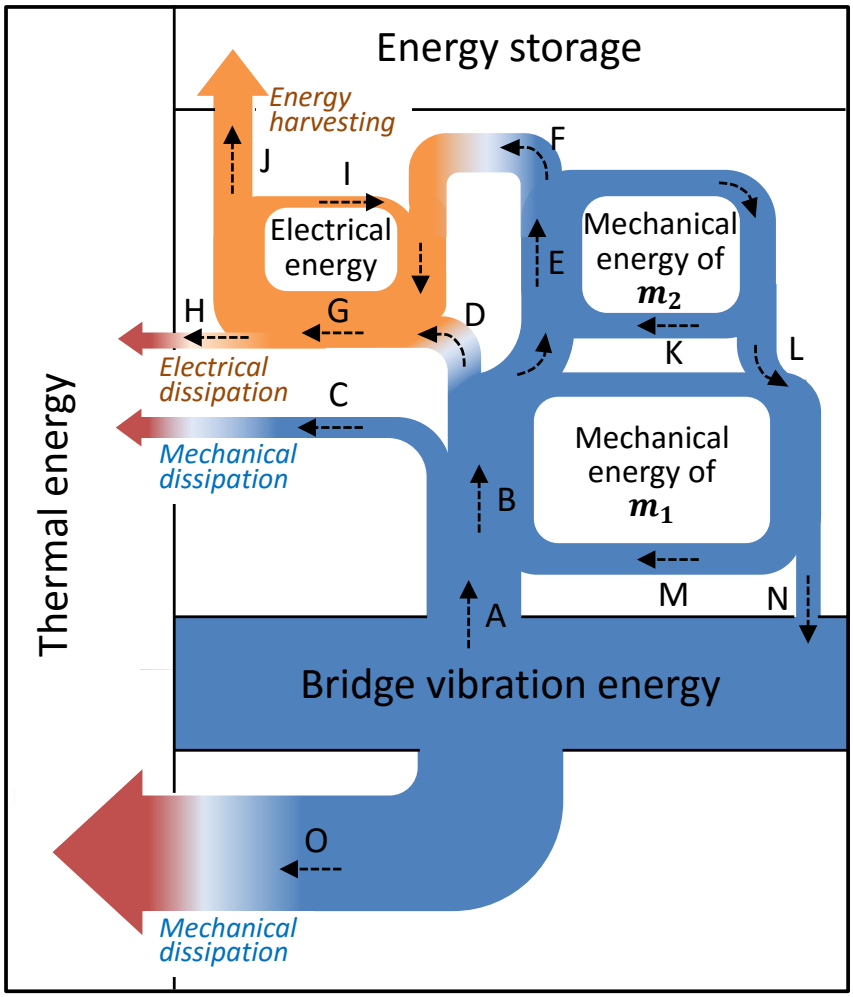

Figure 3.1(b) Energy flow of TMG with a dual-mass system on the bridge

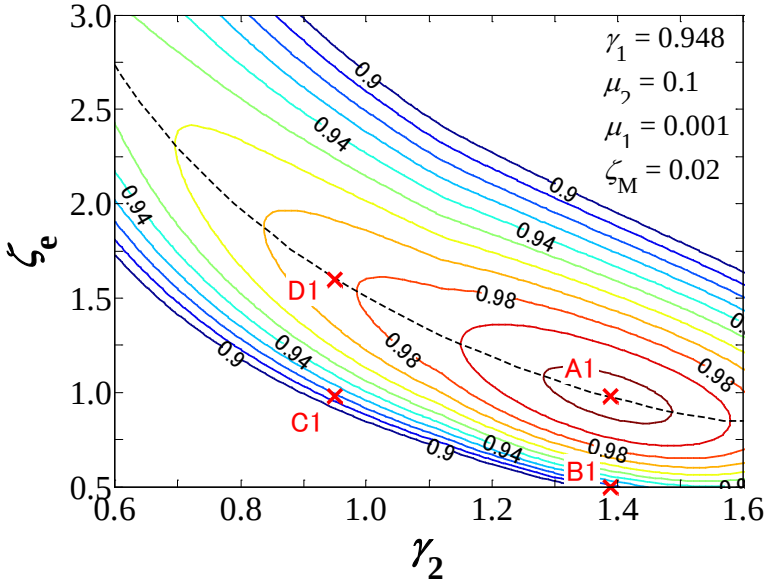

Figure 3.2 Distribution of harvesting power responses of the dual-mass system for various combinations of γ_2 and ζ_e

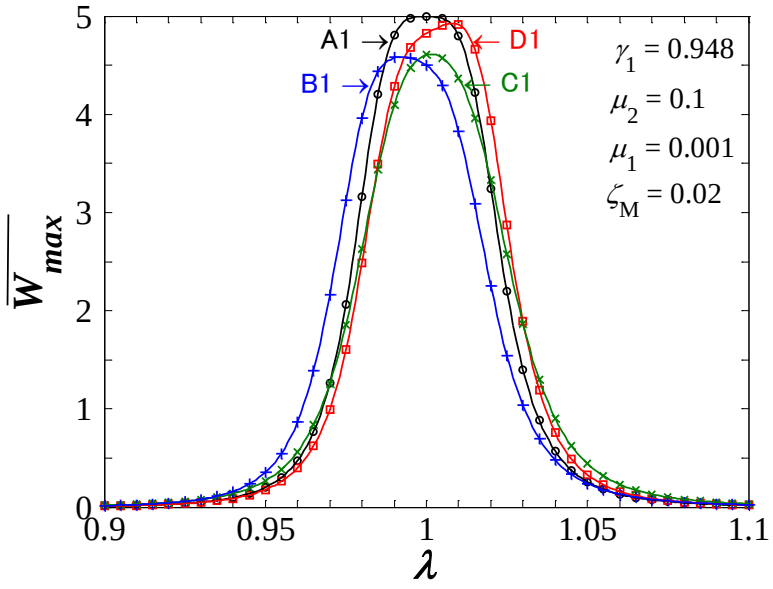

Figure 3.3 Harvesting power responses of the dual-mass system for different combinations of γ_2 and ζ_e

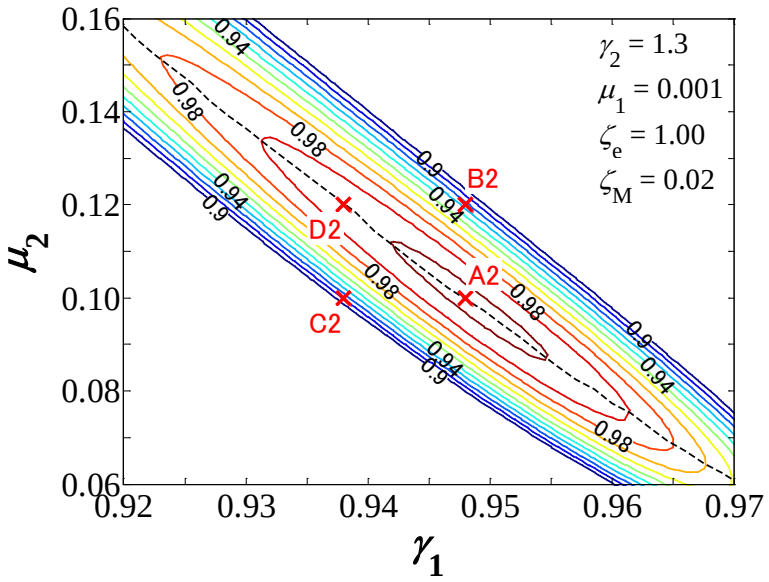

Figure 3.4 Distribution of harvesting power responses of the dual-mass system for various combinations of γ_1 and μ_2

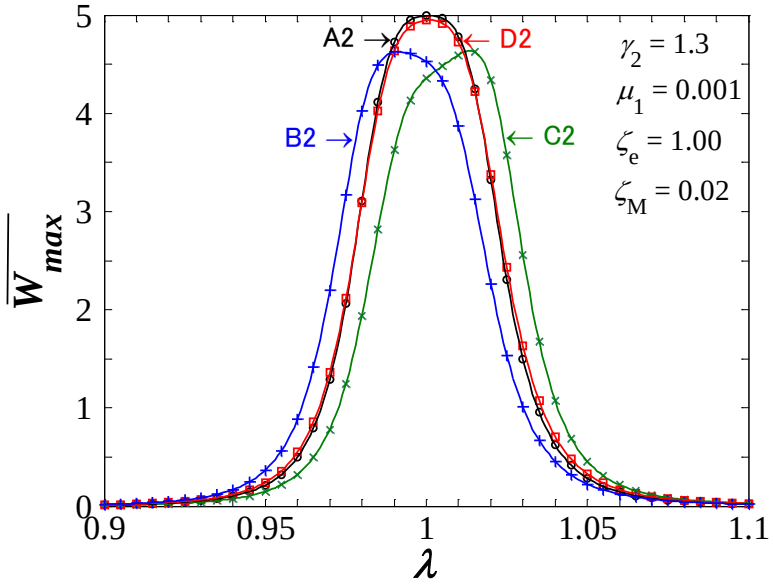

Figure 3.5 Harvesting power responses of the dual-mass system for different combinations of γ_1 and μ_2

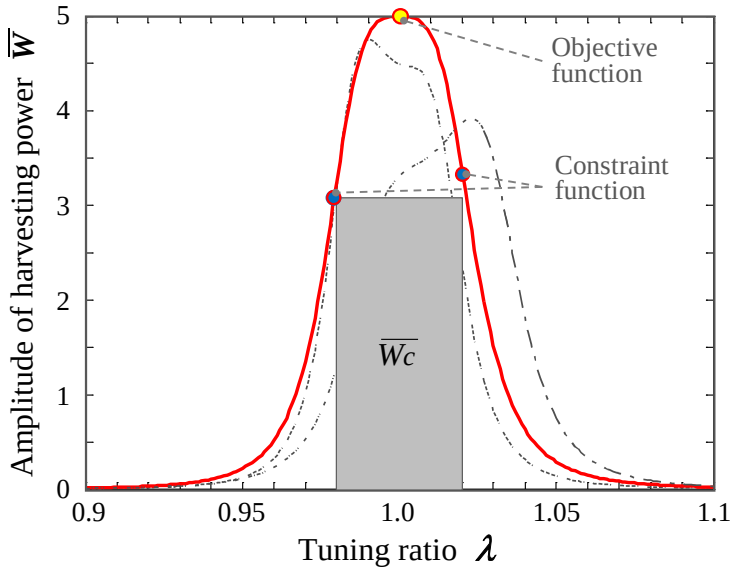

Figure 3.6 Objective and constraint functions of the proposed parameter design method and frequency responses of power generation in dimensionless form

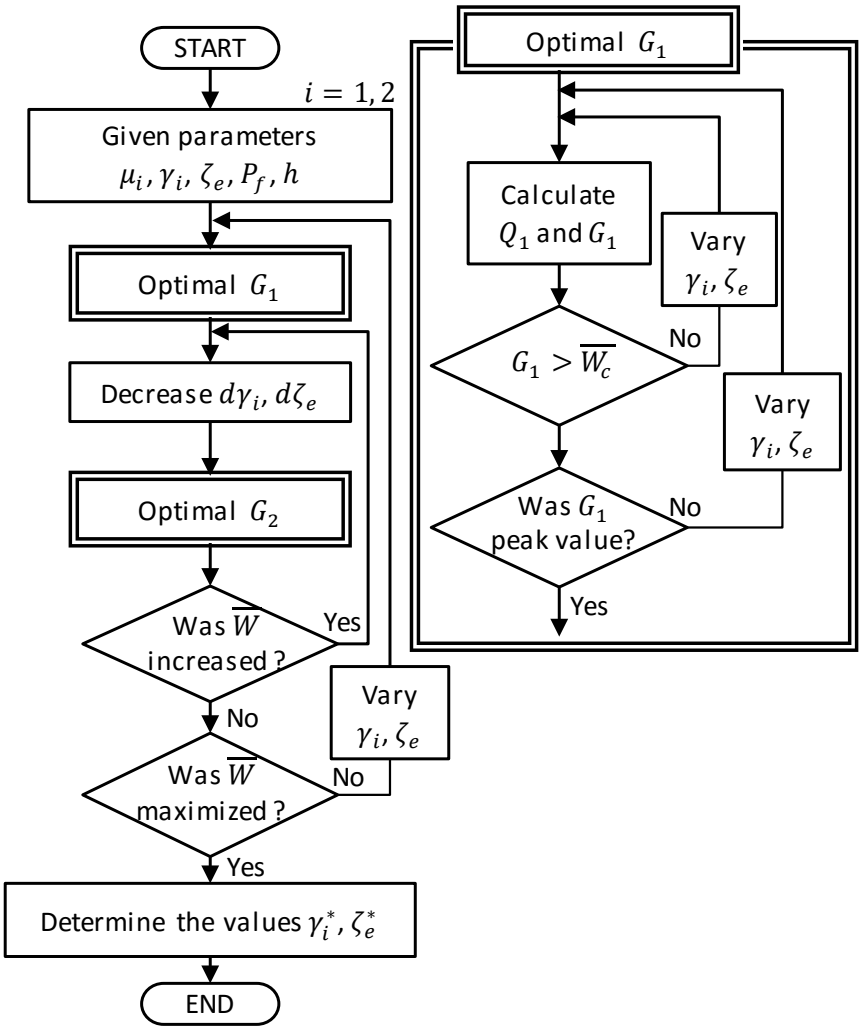

Figure 3.7 Flow of the multi-physics parameters design method

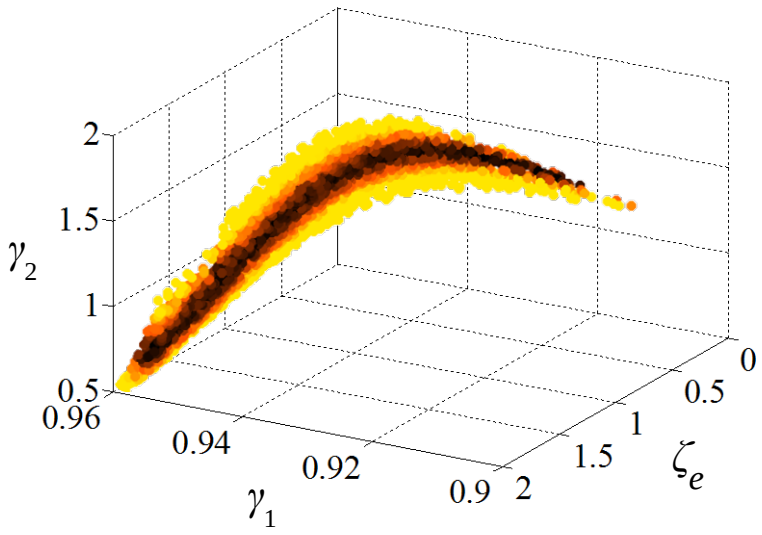

Figure 3.8(a) 3D view of distribution of amplitude of $\overline{W}$ with variations of three design parameters γ_1, γ_2 and ζ_e

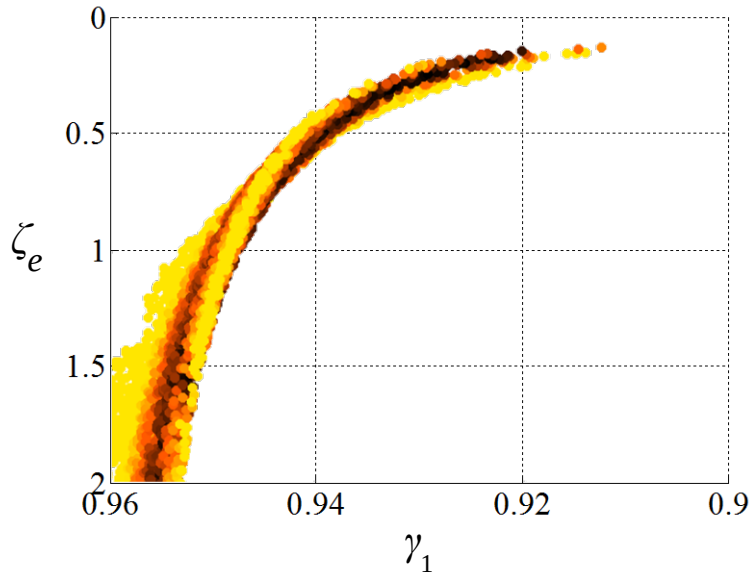

Figure 3.8(b) 2D view of distribution of amplitude of $\overline{W}$ with variations of three design parameters γ_1, γ_2 and ζ_e

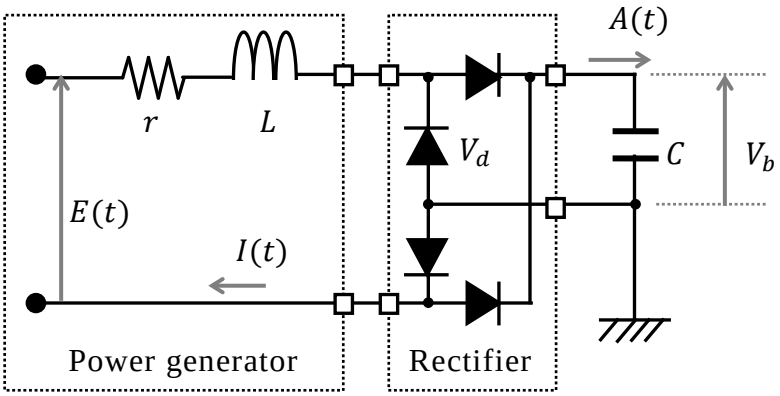

Figure 3.9 Electric circuit for charging

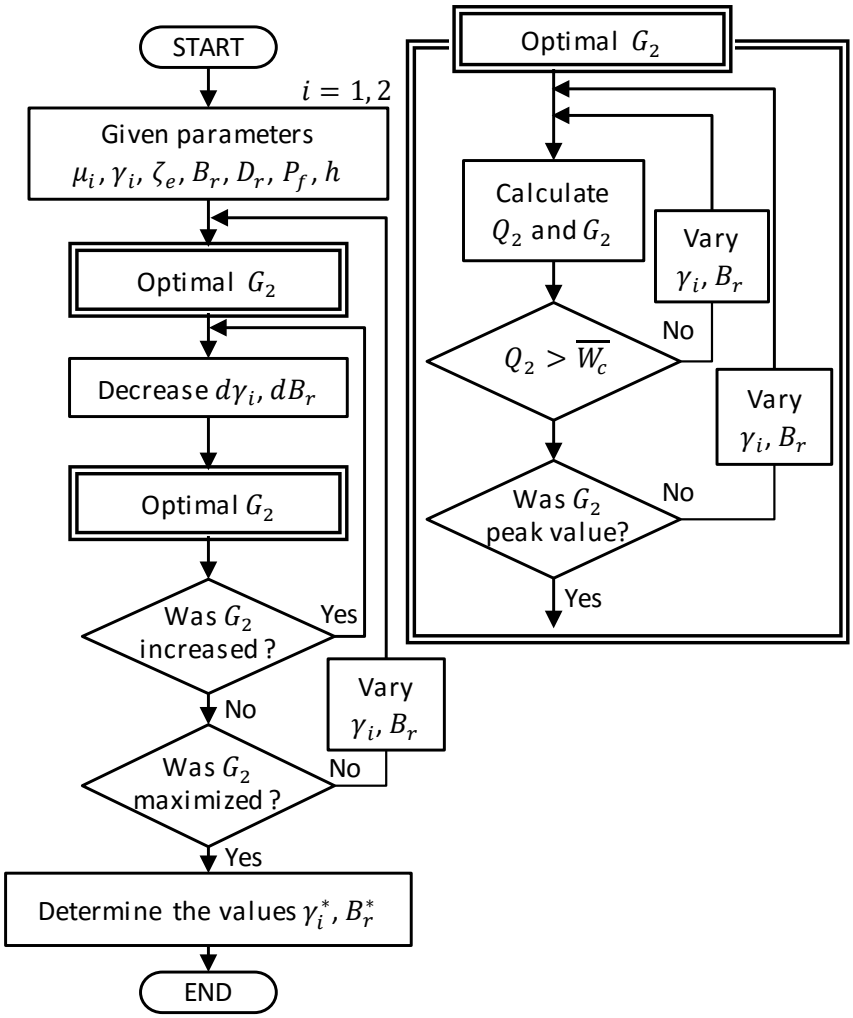

Figure 3.10 Flow of the multi-physics parameters tuning method for energy storage

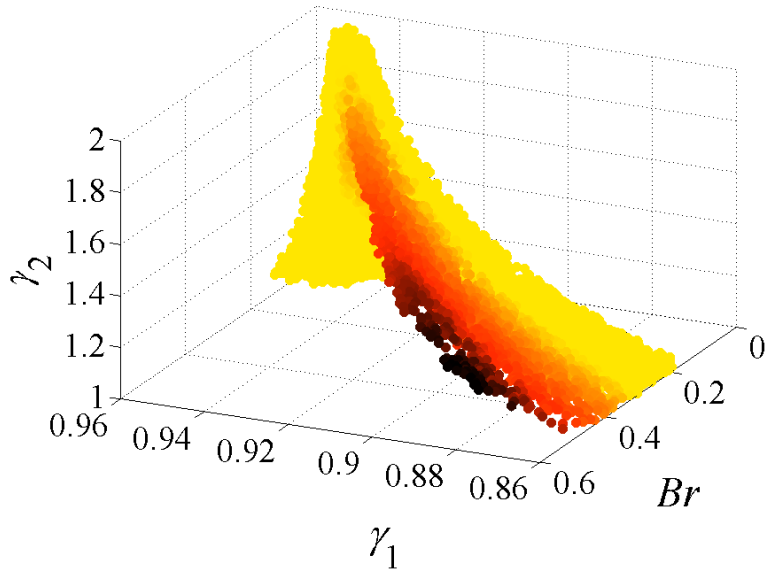

Figure 3.11(a) 3D view of distribution of amplitude of $\overline{W_{rms}}$ under variations of three design parameters γ_1, γ_2 and B_r

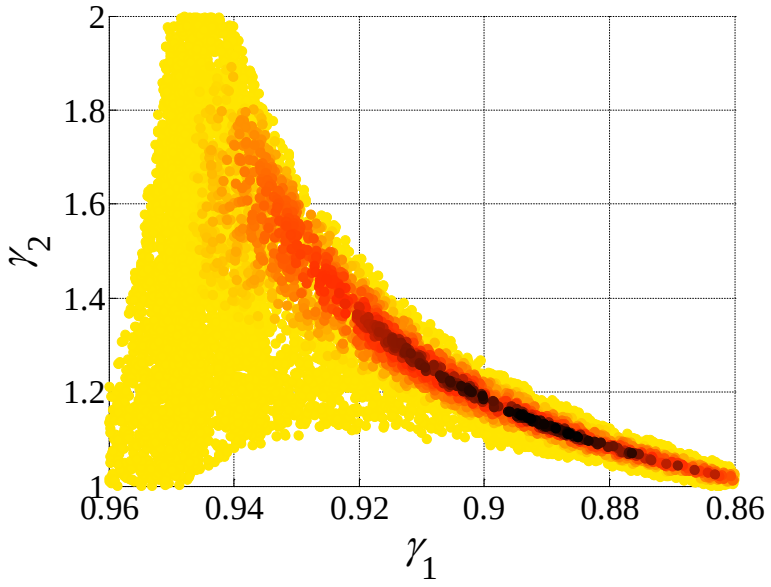

Figure 3.11(b) 2D view of distribution of amplitude of $\overline{W_{rms}}$ under variations of three design parameters γ_1, γ_2 and B_r

Chapter 4

Trial Applications of TMG to an Actual Bridge

Abstract

In this chapter, a prototype TMG was developed. To investigate the configuration of TMG considering the performance of energy harvesting, first, an application procedure and installation location of TMG were considered, and next, a tuned mass generator was applied to an actual expressway bridge. According to the experiments on the existing bridge, it has been demonstrated that TMG can generate electric power on a watt scale, which is required for the structural health monitoring of bridges. This indicates that TMG can compensate for the energy consumed by monitoring systems or other low-power devices. In addition, the relationship between electric power generation and the traffic of large vehicles has been investigated.

4.1. Overview

In the previous chapters, parametric studies demonstrated that for effective energy harvesting, TMG requires a robust parameter design for uncertain bridge vibrations, accuracy when assembling the TMG, and tuning errors. To enable the most effective performance of TMG, a multi-physics parameter design method has been developed. Consequently, a prototype TMG using a dual-mass system and electromagnetic power generator has been developed.

In this chapter, to investigate the configuration of TMG considering the performance of energy harvesting, first, an application procedure and installation location of TMG were considered, and next, a prototype TMG was applied to an actual expressway bridge. In addition, it was tested to see whether batteries could be charged to make use of the energy harvested from the unused reserve of bridge vibrations. If batteries could be successfully charged, TMG could be used for monitoring systems of bridge structures. It would therefore be possible to establish sustainable health monitoring systems which do not require physical access for periodic battery replacement or power supply construction.

4.2. Target Power Generation and Application Procedure

For health monitoring, bridge structural vibrations are generally measured to detect conditions of bridge structures. To date, energy harvesting devices from vibration energy have been developed **[9, 13, 14, 28, 39]**, however, the power generation level obtained from bridge vibrations has generally been around micro-watt to milli-watt and is not still satisfied. In this study, to achieve a required power generation for the monitoring system of bridge structures with the smallest mass ratio, the aim has been to obtain watt order power generation to supply energy to monitoring devices. Therefore, TMG was developed as a prototype energy harvester using bridge vibrations, and the mass ratio of TMG over bridge mass was set as 0.05 %, which is one order smaller than mass ratios of conventional tuned mass dampers used for

vibration control of bridge structures. To achieve the target power generation, it is essential to bring out the ability of TMG by considering an application method of TMG and vibration characteristics of bridge structures. To evaluate the ability of power generation from actual bridge vibrations, the efficiency of converting absorbed energy by TMG to power generation has been investigated.

The proposed application procedure of TMG is shown in **Figure 4.1**. First, a target vibration mode of bridge structures and installation locations of TMG were considered. Characteristics of bridge structures, such as modal masses and modal damping ratios were then investigated. Next, parameters of TMG were determined through an experimental evaluation procedure. The parameters of TMG were then tuned using the proposed parameter design method. Finally, TMG was designed and developed. This TMG was then applied on an existing bridge to investigate the characteristics of power generation from vibrations of bridge structures.

4.3. Target Vibration Frequency and Installation location

First, target vibration modes and installation locations of the TMG were examined to obtain the best performance of the developed TMG. TMG was designed to obtain electricity for health monitoring systems from vibrations of bridge structures due to traffic loads of large vehicles. Higher the traffic volume, higher the induced energy. To discuss the generality of TMG, the traffic volume should therefore be considered. Dominant vibration frequencies of typical bridges are generally within 1 to 15 Hz on vertical stringers or main girders. As an example of application to actual bridges, a trial bridge, which is a 216 meters three span continuous steel truss bridge located on an expressway in Gifu prefecture, was selected as shown in **Figure 4.2**. The target bridge was selected by considering the traffic volume and dominant natural vibration frequencies of the bridge. The traffic volume of large vehicles is around five to eight thousands per day, and dominant natural vibration frequencies on the vertical girder of the bridge occur within 1 to 15 Hz.

4.3.1. Detection of Natural Vibration Frequency of the Trial Bridge

To detect the natural vibration frequencies of the trial bridge, acceleration measurements were conducted. A strain gauge based accelerometer (sensitivity: 1 $\mu\varepsilon.s^2/m$) was installed one quarter of the way along the first span of the target bridge (18 m from the start of the bridge) and a 500 Hz logging sampling rate was selected. The frequency power spectrum density of the bridge vibration acceleration was obtained as shown in **Figure 4.3**.

4.3.2. Decision of the TMG Installation Location

To determine an effective TMG installation location for energy harvesting from vibrations of the bridge, acceleration measurements on the trial bridge were conducted using two piezoelectric-based accelerometers (sensitivity: 6.42 $pC.s^2/m$). One accelerometer (named hereafter accelerometer A) was installed 18 m from the bridge start as a fixed measuring point, and another accelerometer (named hereafter accelerometer B) was installed onto various measuring locations as shown by the red points in **Figure 4.2**, for taking multiple measurements. Accelerometer A is expressed by the blue point. Target vibrations of TMG are the vertical vibrations of bridge structures, therefore, acceleration measurements were taken from the central vertical girders of the bridge. Since vibrations on the first span of the bridge are highest, a greater number of measuring points were located on the first span compared to other spans. Acceleration measurements were then taken during two minutes in each measurement step, with a sampling rate of 256 Hz.

To determine bridge vibration mode shapes, a modal analysis method of structures vibrating under variable external loadings proposed by Kaito et al. **[86]** was applied. First, the first five vertical vibration modes were focused on as they normally have large vibration energy. The detected five vertical vibration modes are shown in **Figure 4.4(a)** to **Figure 4.4(e)**. Oscillation amplitudes of the detected vibration mode shapes were then normalized. From the modal analysis, the vibration mode at 14.2 Hz had the largest vibration acceleration among the natural frequencies of the target bridge, and so has been considered as the local structural vibration. To investigate the applicability of TMG, two vibration frequencies of the bridge were focused on; (a) large vibration accelerations, (b) a low bridge vibration mode. By considering the tunable range of TMG (higher than 5 Hz or more), the target vibration frequencies were determined as

(a) 14.2 Hz and (b) 6.1 Hz. TMG can therefore generate maximum power where the mode has the highest amplitude. From these results, the TMG installation location has been decided to be one quarter of the way along the first span of the bridge (18 m from the bridge start).

In this research, to accurately identify the vertical vibration modes due to traffic loads, acceleration measurements were taken at multiple locations. However, it should be noted that for practical use, the number of vibration measurement locations can be further reduced.

4.4. Modal Mass and Damping

Characteristics of the bridge such as modal equivalent masses and modal damping ratios were determined to design TMG.

4.4.1. Modal Equivalent Masses

The modal mass of the bridge was calculated using an eigenvector method **[87]** which is generally used for modal analysis. Normalized eigenvectors of vibration modes and a mass matrix are used to calculate the modal mass at a particular location. In the case of a N degree-of-freedom system as shown in **Figure 4.5**, the modal mass of the *i*-order mode at *j* point-mass is formulated as follows.

$$M_{ij} = \{X_{ij}\}^T [M] \{X_{ij}\} \tag{4.1}$$

Where, $[M]$ is mass matrix, $\{X_{ij}\}$ is the eigenvector of the *i*-order mode which is normalized by the *j* point-mass as follows

$$\{X_{ij}\}^T = x_{ij}^{-1} \{x_{i1}, x_{i2}, ..., x_{ij}, ...x_{iN}\} \tag{4.2}$$

In this study, a 21 degree-of-freedom point-mass model was considered. The mass matrix $[M]$ of the analysis model was created by assuming a uniform distribution of the total mass of the bridge. The determined vertical vibration modes were used for eigenvector $\{X_{ij}\}$. Using **equation (4.1)** and **equation (4.2)**, the modal masses at 18m from the start of the bridge were determined as shown in **Table 4.1**.

4.4.2. Modal Damping Ratio

The modal damping ratio was determined using the free vibration in each vibration mode, using band-pass filters. The modal damping influences the efficiency of energy harvesting since the bridge damping consumes vibration energy. To evaluate the harvested energy of TMG, the normal distribution of damping ratios was considered and the modal damping ratio ζ_i (90 %) was determined as the upper limit value. This ratio was selected for practical analysis of harvesting energy, since the variation below the average modal damping ratio is advantageous for power generation and is not a problem. The proportion above the upper limit value is therefore set to be 10 % of the total. The determined modal damping ratios of the bridge are shown in **Table 4.1**.

4.5. Determination of Characteristics of TMG

Figure 4.6 shows images of the developed prototype TMG and the power generator. **Figure 4.7** shows the analysis model which consists of a bridge and TMG. The bridge is expressed by a modal mass M, modal stiffness K and modal damping coefficient C_M. The TMG model consists of two masses, m_1 and m_2, and the two masses and the bridge are connected in series with springs k_1 and k_2. When the external excitation force $F(t)$ is induced to the bridge mass M, displacement of the bridge mass M is expressed by $X(t)$. $x_1(t)$ and $x_2(t)$ indicate the displacement of each mass of TMG. A power generator is introduced between the two masses m_1 and m_2, and the electric damping force of the power generator is expressed by $F_e(t)$. For effective design of TMG using the proposed tuning design method in **Chapter 3**, characteristics of TMG should be evaluated first. Mechanical and electric experiments for evaluating TMG characteristics have thus been conducted by using an excitation vibration machine and an electric circuit.

4.5.1. Mechanical Damping Characteristics of TMG

To evaluate the mechanical damping effect of TMG, the half power method **[88]** has been applied. The half power method is a classical method using the experimental

responses under random excitation forces. The applicable range of the damping ratio is 10 % or less. The evaluation formula of the damping ratio ζ is shown as follows.

$$\zeta = \frac{1}{2}\frac{f_b - f_a}{f_p} \tag{4.3}$$

Where f_a and f_b are the frequencies at -3dB from the peak value of frequency response spectrum ($f_a < f_b$) [Hz], and f_p is the resonant frequency [Hz].

A sweep excitation force from 1 Hz to 20 Hz was induced to TMG using the excitation machine shown in **Figure 4.8**. The accelerations of the two masses and the actuator of the excitation machine were then measured. The frequency acceleration response spectrums were obtained and the mechanical damping were experimentally evaluated as follows.

$$c_1 = 82.5 \text{ Ns/m}, \quad c_2 = 118.0 \text{ Ns/m}$$

Where, the frequency spectrums used are expressed as follows.

$$H_1(j\omega) = \frac{\ddot{x}_1(j\omega)}{\ddot{X}(j\omega)}, \quad H_2(j\omega) = \frac{\ddot{x}_2(j\omega)}{\ddot{x}_1(j\omega)} \tag{4.4}$$

4.5.2. Mechanical Coil Spring Characteristics of TMG

Regarding the long-term serviceability of TMG systems, it is essential that the coil spring is used within the allowable deflection range. Therefore, stoppers above and below each mass were designed to prevent the allowable deflection from being exceeded. Also, the fatigue life of the coil springs was evaluated using a fatigue strength diagram for helical compression springs according to JIS B 2704-1 (2009) **[89]**. If springs are operated at 80 % of the full stroke, the fatigue life is in the order of 10^6 to 10^7. In actual bridge vibrations, this level of vibration amplitude occurs several times per hour. Therefore, if vibration of this level occurs 100 times per hour, the fatigue life is in the order of ten years or more.

4.5.3. Electric Characteristics of Power Generator

In **Chapter 2**, the characteristics of power generators were theoretically explained using an equivalent circuit of a power generator. The equivalent circuit of the power generator and an external electric load *R* is shown in **Figure 4.9**. The power

generator is expressed by the DC resistance r and the self-inductance L in the equivalent circuit. The DC resistance r is related to the conversion efficiency when electric power is generated from voltage induction. The smaller the DC resistance, the higher the conversion efficiency. AC impedance $\sqrt{(2\pi \cdot f \cdot L)^2 + r^2}$ is related to the power ratio, where f is frequency [Hz]. The smaller the AC impedance, the higher the power ratio. Hence evaluation of the electric characteristics of the power generator is highly important to achieve the best performance of the power generator.

4.5.4. Electromotive Force Coefficient: k_{emf}

To evaluate the electromotive force coefficient k_{emf}, experiments using an excitation machine were conducted. The sine wave vibration was induced to the moving part of the power generator from the actuator of the excitation machine. The induced voltage at the coil of the power generator were measured, and the electromotive force coefficient was determined using the formula shown as follows.

$$k_{emf} = \frac{V_{rms}}{v_{rms}} \tag{4.7}$$

Where, V_{rms} is the root mean square value of induced voltage at the coil [V], and v_{rms} is the root mean square value of velocity of the moving part [m/s]. The velocity of the moving part was obtained from the displacement signal of the actuator. The electromotive force coefficient k_{emf} has been experimentally obtained as follows.

$$k_{emf} = 250\,\text{V.s/m}$$

4.5.5. DC Resistance of the Internal Coil: r

To evaluate the DC resistance of the internal coil of the power generator, a classical method named I-V method was applied. I-V method evaluates the impedance of the electric circuit by measuring the current and the voltage. The electric circuit used in the experiment is shown in **Figure 4.10**. A voltage source and a shunt resistance (r_s = 40 mΩ) were connected in series, where the voltage differential at the internal coil V_1 [V] and the induced voltage at the shunt resistance V_2 [V] were measured. The DC resistance of the internal coil was obtained using the formula below.

$$r = \frac{V_1}{V_2} R \tag{4.8}$$

From the experimental evaluation, the DC resistance of the internal coil has been obtained as follows.

$$r = 5.7\,\Omega$$

4.5.6. Inductance of the Internal Coil: *L*

The self-inductance of the internal coil was experimentally determined by using the I-V method. The electric circuit used in the experiment is shown in **Figure 4.11**. The AC voltage source and shunt resistance (r_s = 40 mΩ) were connected in series to the power generator. The root mean square value of the induced voltage at the power generator V_{1rms} [V] and the detected voltage at the shunt resistance V_{2rms} [V] were measured. The self-inductance of the internal coil L is obtained using the formula below

$$L = \frac{1}{\omega}\sqrt{\frac{V_{1rms}^2}{V_{2rms}^2}R^2 - r^2} \tag{4.9}$$

Where, ω is the radial frequency of the AC voltage source [rad/s]. The determined self-inductance of the internal coil L [H] is a function of radial frequency and can be approximately expressed by the following equation.

$$L = -0.099\log(\omega) + 0.742 \text{ H} \tag{4.10}$$

4.6. Parameter Design

To determine the effective parameters of TMG to maximize the power generation from vibrations of bridge structures, a numerical analysis of power generation was conducted using the equivalent forced excitations estimated from the acceleration measurements of the target bridge. The analysis model is shown in **Figure 4.7**. The equivalent force was calculated using the proposed method by Taguchi et al. **[90]**.

In this study, the mass ratio of the first mass of TMG to the bridge mode mass is around 0.05 % with the aim to obtain watt order power generation from bridge vibration. The weight of the first mass of TMG was therefore determined as 104 kg.

The damping ratio of the bridge vibration mode was obtained using the measured free vibration acceleration data of the bridge using a band-pass filter. The mechanical damping coefficients of TMG were obtained using the half power method. The target tuning parameters were the frequencies of two masses f_1, f_2 and the electric damping coefficient of the power generator c_e. The parameters aiming to maximize the energy harvested were determined using the proposed analysis iteration flow shown in **Figure 3.7** in **Chapter 3**. A target frequency range of harvesting energy was 5.7 Hz to 6.1 Hz, considering the frequency response of the target bridge, and the determined parameters f_1^*, f_2^*, c_e^* for two target vibration modes are shown in **Table 4.2** and **Table 4.3** respectively. According to researches on the bridge vibration monitoring **[4,50,51]**, seasonal changes of natural frequency of bridges are less than 0.1 % (or less than 0.2 Hz). The target frequency range of harvesting energy includes therefore general seasonal changes of natural frequency of bridges. According to another research on the bridge vibration monitoring **[46]**, it is considered that the damages on local bridge structural members, such as fatigue clacks and corrosion, has little influence on vibration characteristics of whole bridges. Therefore, when TMG is designed to correspond to a whole vibration mode of bridge structures, the long-term influence by damages of bridge structures on the harvesting energy can be comparatively smaller than the influence by seasonal changes of natural frequency of bridges.

4.7. Application of TMG to the Trial Bridge

4.7.1. Experiment for Power Generation

The designed TMG for the two different vibration modes, namely 6.1 Hz and 14.2 Hz, was installed onto the selected location of 18 m from the start of the bridge as shown in **Figure 4.12**. To evaluate the characteristics of power generation on the actual bridge, a one-day experiment was conducted. Regarding the long-term serviceability of the TMG system, the TMG was covered with an aluminum case to protect it from weather influences, and the electric circuit was covered with a waterproof and dustproof housing. The electric circuit for the power generation shown in **Figure 4.12**

was used in this experiment. To improve the efficiency of electric circuit, a power factor correlation capacitor *C* was introduced in this electric circuit. As shown in **Figure 4.13** and **Figure 4.14**, the hourly harvested energy was obtained from the measured voltage generation of TMG. The hourly traffic of large vehicles was also measured and plotted. The blue line shows the hourly harvested energy, and the bar chart shows the hourly traffic of large vehicles measured by a traffic counter device located 1.2 km away from the trial bridge. The results of each target frequency are explained below.

4.7.1.1. Target Frequency of 14.2 Hz

As shown in **Figure 4.13**, the average hourly energy harvested in the one-day measuring period was 2.9 mWh. The maximum power generation was around 0.5 to 2 W when large vehicles passed. This power obtained is several orders higher than previous vibration energy harvesting in low frequency vibrations **[8,9,12-14]**. Power generation is analyzed in further detail in **section 4.8.3**. The hourly energy harvested is strongly related to the traffic of large vehicles. As can be seen the peak value of the energy harvested and traffic of large vehicles occurred at midnight, and the hourly energy harvested changed with traffic.

4.7.1.2. Target Frequency of 6.1 Hz

As shown in **Figure 4.14**, The average hourly energy harvested in the one-day measuring period was 2.9 mWh. The maximum power generation was around 0.5 to 3 W when large vehicles passed. **Table 4.4** shows the basic power consumption of sensing devices and data loggers. The power supply ratio expresses the average power generation of TMG to the power consumption of sensing devices. TMG can compensate all electric energy when the power supply ratio is over 100 %. On the other hand, TMG can only compensate a part of electric energy and extend the service life of sensing devices when the power supply ratio is less than 100 %. The energy harvested is planned to mainly charge batteries, and be periodically used to monitor the bridge's structural condition. Therefore, the experimentally harvested energy of TMG from vibrations of bridge structures can satisfy the general use of monitoring systems.

4.7.2. Experiment for Charging Batteries using Harvested Energy

For effective charging of batteries using harvested energy, it is important to reduce the two negative effects as follows; (i) charging power loss and (ii) natural discharge of batteries. (i) Charging power loss is mainly caused by a voltage drop in the rectifier circuit and internal resistance of batteries. The natural discharge of batteries can be reduced if the battery voltage is small. Therefore, to increase the charging efficiency of batteries using the energy harvested, Schottky Barrier Diodes (SBD) were applied to reduce the voltage drop in the rectifier circuit. In addition, electric double-layer capacitors (named hereafter super capacitors) were selected as the batteries for this study since their internal resistance is generally smaller than other batteries. Moreover, the super capacitors have the advantage of long-term reliability, longer life from charge and discharge, and larger temperature ranges over a normal capacitor. SBD also have an advantage in efficiency of rectification over a general-purpose rectification diode as the voltage drop is lower. The charged energy to the super capacitors was obtained as follows.

$$J(t) = \frac{1}{2} C_b \left(V^2(t) - V^2(0) \right) \tag{4.11}$$

Where, C_b is the capacitance [F], $J(t)$ is the charged energy [J], $V(t)$ is the capacitor voltage [V] and $V(0)$ is the initial capacitor voltage. The charging electric circuit used in the experiment is shown in **Figure 4.15**. A super capacitor array, witch the capacitance C_b = 80 F, 7.5 V withstand voltage and 38 mΩ of DC resistance, was used. To consider the effect of the natural discharge of the super capacitor array, a natural discharging experiment was conducted in laboratory. **Figure 4.16(a)** shows the charging circuit used in the experiment, and **Figure 4.16(b)** shows the experimental results. The voltage drop V_d was larger when the capacitor voltage was higher. On the other hand, the voltage drop rate was constant when the capacitor voltage was less than around 3 V. The current supplied to the charging electric circuit was in the order of around 1 to 10 mA, and the voltage drop of the rectifier circuit using SBD was around 0.4 to 0.6 V. The charging experiments to the supper capacitor array were conducted for each target bridge vibration mode.

4.7.2.1. Target Frequency of 14.2Hz

Figure 4.17 shows the charged electric energy to the super capacitor array with a blue line. The initial voltage was around 1 V because charging energy loss is higher

when the capacitor voltage $V(t)$ is near 0 V. As shown in **Figure 4.17**, the increase in rate of charged energy was smaller on November 9th, 15th, 16th and 22th, 2014, because the traffic of large vehicles was lower. Furthermore, the increase in rate of the charged energy was higher when the capacitor voltage was lower. On the other hand, the increase in rate of the charged energy was lower when the capacitor voltage was higher. One reason is that harvested electric energy is dependent on the capacitor voltage, hence the efficiency of charging electric energy changes. Moreover, the natural electrical discharge of the capacitor increases when the capacitor voltage is high. Based on the natural electrical discharge characteristics of the super capacitor array (**Figure 4.16(b)**), the natural discharged energy in a charging experiment can be obtained. The energy harvested by TMG can be expressed as the summation of the charged energy and the natural discharged energy, as shown by the red dashed line in **Figure 4.17**. The increase in rate of energy harvested by TMG was higher when the capacitor voltage was higher. However, the natural electrical discharged energy increased with an increase in the capacitor voltage. Therefore, the increase in the charged energy ratio reduced with an increase in the capacitor voltage. Based on these results obtained in the charging experiment, the natural electrical discharge effect should be considered to improve the charging efficiency.

4.7.2.2. Target Frequency of 6.1 Hz

Figure 4.18 shows that the charged energy in the super capacitor array is shown with a blue line. The initial voltage $V(0)$ was 1.7 V. The total charged energy in the experiment lasting two weeks was 280 J. The increase in rate of charged energy was smaller on November 30th, December 1st, 6th and 7th, 2014, because the traffic of large vehicles was low. The discharged energy from the super capacitor array was obtained, and the energy harvested by TMG was expressed as the summation of the measured charged energy and discharged energy, as shown by the red line in **Figure 4.18**. According to these results from the charging experiment, the increase in rate of harvested energy of TMG was higher when the capacitor voltage was around 2 V. The natural discharged energy increased with an increase in the capacitor voltage. Therefore, the increase of charged energy ratio reduced with an increase in the capacitor voltage. Based on the charging experiment results, the capacitor voltage

could be determined as the parameter to improve energy harvesting and energy charging.

4.7.3. Efficiency of Power Generation

Figure 4.19 to **Figure 4.21** indicate an example of traffic-induced bridge acceleration, generated voltage and power generation data in time domain, during 30 seconds of the one-day measuring period. The accelerations of the two masses of TMG were also measured. From these measured data, the energy flow of the bridge-TMG system was obtained and is shown in **Figure 4.22**. The maximum generated power was 3.2 W. This power is several orders higher than previous vibration energy harvesting methods, namely micro-watt to milli-watt orders in low frequency vibrations **[10-17]**. It is therefore a significant result. The equivalent masses depend on bridge vibration modes, therefore, band-pass filters were used to separate the first to fifth vibration modes. The vibration energy in each bridge vibration mode were separately obtained and summated. As shown in **Figure 4.22**, the total induced energy from the external traffic load was 143 J. Most of the energy was dissipated by the bridge's structural damping as shown in **Table 4.1**. 3.3 J or 2.3 % of the total energy was harvested and converted to electric energy using TMG. This efficiency is two orders higher than the mass ratio of around 0.05 %, which is another significant result. The energy flow of each vibration mode are shown in **Figure 4.23(a)** to **Figure 4.23(e)**, respectively. **Figure 4.24** shows the combined band-pass filters used to separate the vibration modes. As shown in **Figure 4.23**, over 99 % of the total electric energy was generated in the 6.1 Hz bridge vibration mode. The absorbed energy using TMG is expressed as the summation of the consumed energy in mechanical damping (3.0 J) and energy harvested (3.3 J). The converting efficiency of TMG is around 52 %, which is obtained by dividing the energy harvested by the total absorbed energy. Hence, TMG could generate electric energy from more than half of the absorbed energy.

4.7.4. Vibration Energy

To consider the vibration energy of bridge structures, the modal vibration energy distributions were examined. First, the vibration modes of the bridge were identified, and second, the vibration energy of each vibration mode was obtained. To identify the

modal vibration energy distributions, a method using vibration measurements of bridges was considered. The modal vibration energy distribution has been obtained using the excitation force due to traffic loads. This method was proposed by Taguchi et al. **[90]** and to evaluate the modal vibration energy from traffic loads, bridge characteristics such as modal mass and damping were used (**Table 4.1**).

The modal vibration energy distribution was evaluated from acceleration measurements of the target bridge. **Figure 4.25(a)** shows the hourly traffic of large vehicles, **Figure 4.25(b)** shows the hourly modal vibration energy distribution, and **Figure 4.25(c)** shows the total modal vibration energy distribution between the 8th and 9th November 2014. **Figure 4.26** show the results between the 25thand 26th November 2014, and **Figure 4.27** show the results between 17th and 18th November 2015. As shown in these figures, the second vertical vibration mode at 3.1 Hz had the highest energy, around half of the total bridge vibration energy, and the third vertical vibration mode at 6.1 Hz had the second highest energy. The efficiency of energy harvesting by TMG could be further improved if TMG could be tuned for the lower vibration frequency. Although the total vibration energy depended highly on the traffic of large vehicles and had peaks at midnight, the modal vibration at 6.1 Hz was induced not only at midnight, but also during daytime. Since the total traffic including normal vehicles is large during daytime, it is considered that the third vertical mode at 6.1 Hz is induced by not only the traffic of large vehicles, but also small vibrations. This finding can be advantageous for harvesting energy from bridge vibration. Namely, harvesting energy from the third vertical mode at 6.1 Hz of this bridge is effective if electric energy can be harvested from not only large vibrations by traffic of large vehicles, but also small vibrations. The characteristics of power generators can be further designed to improve the efficiency of power generation.

4.8. Summary

To harvest and make use of the unused reserve of vibration energy from bridge structures, a prototype of TMG was developed. To investigate the configuration of

TMG considering the performance of energy harvesting, TMG has been applied to an actual expressway bridge. The findings are summarized below.

A) Installation and tuning procedures of TMG were proposed and demonstrated from acceleration measurements on the trial bridge. The target vibration modes and installation locations of TMG were provisionally determined by using the proposed method of vibration modal analysis.

B) By using the proposed tuning design method, TMG was tuned to adapt to two different bridge vibration modes. The ability of the two tuning designs were demonstrated through an experiment on the trial bridge.

C) TMG was found to achieve watt order power generation, which was the aim of the tuning design. The energy harvested by TMG from experiment was found to satisfy the energy required for the general use of monitoring systems.

D) TMG could generate electric energy greater than 2 % of the traffic-induced vibration energy of the bridge. This efficiency is two orders higher than the mass ratio of the bridge and TMG, which is around 0.05 %, and so is satisfactory. It was also demonstrated that TMG could generate electric energy from more than half of the unused reserve of energy which conventional tuned mass dampers absorb.

In addition, the applicability of TMG could be further improved if TMG could be applied to lower bridge vibration modes (less than 5 Hz) since large energy is expected in low bridge vibration modes. The tunable range of TMG was mechanically limited by the nominal stroke of coil springs. Moreover, the characteristics of the power generator could be designed to improve the efficiency of power generation or to reduce the magnetic force.

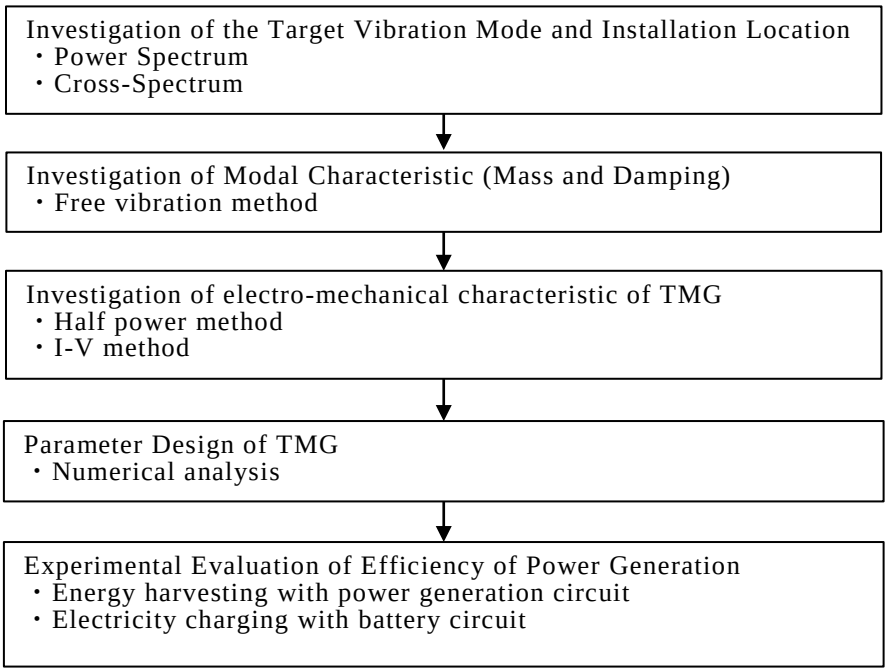

Figure 4.1 Flow of the proposed application method of TMG

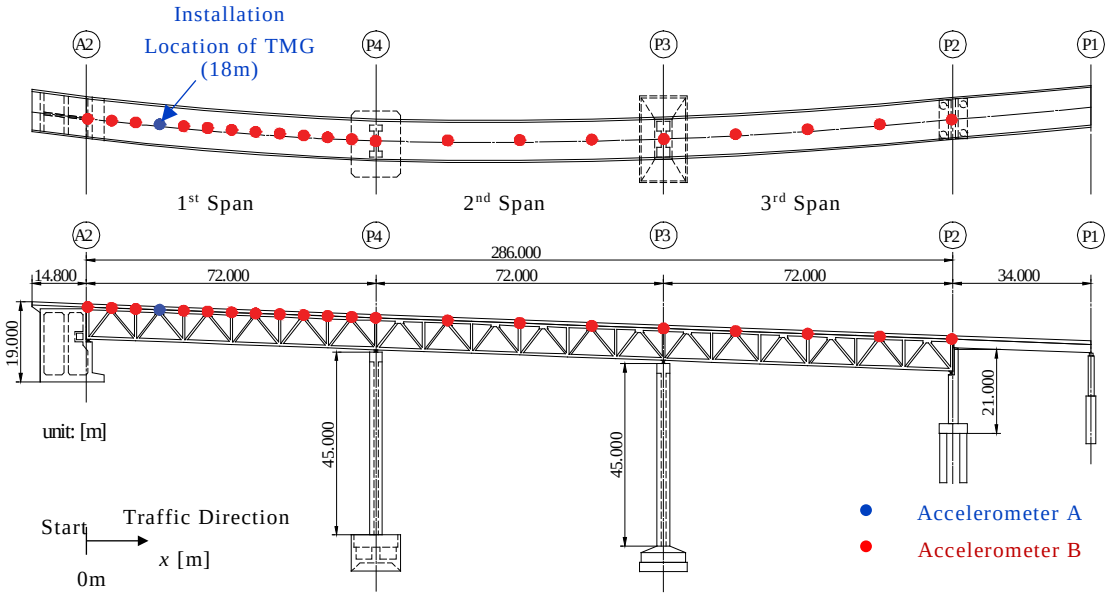

Figure 4.2 Trial bridge and installation location of TMG and accelerometers

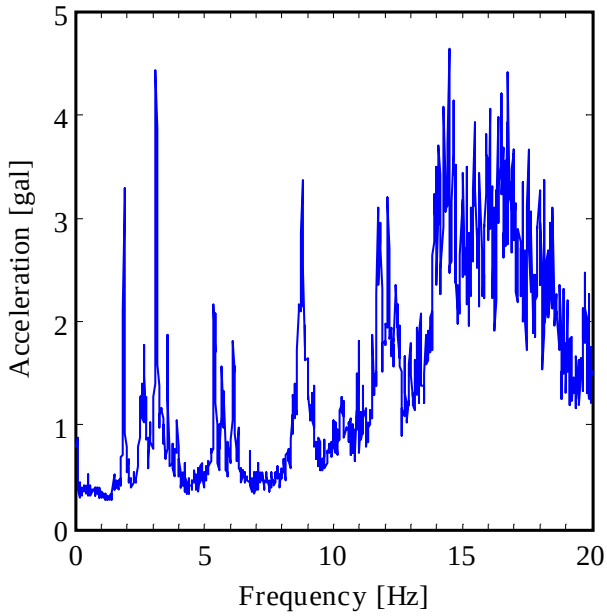

Figure 4.3 Frequency spectrum of acceleration of bridge

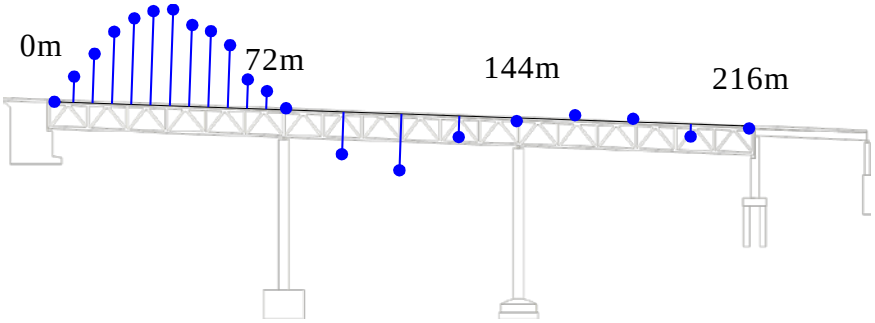

Figure 4.4(a) Bridge vibration mode at 1.5Hz

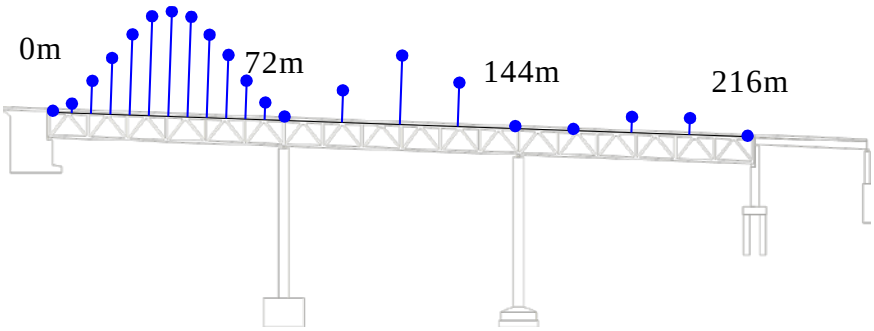

Figure 4.4(b) Bridge vibration mode at 3Hz

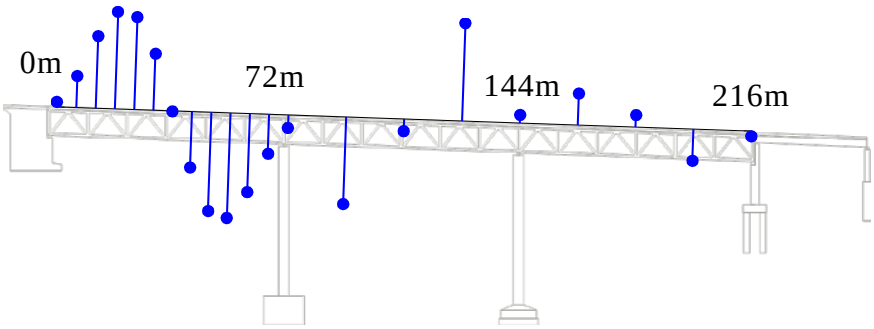

Figure 4.4(c) Bridge vibration mode at 6Hz

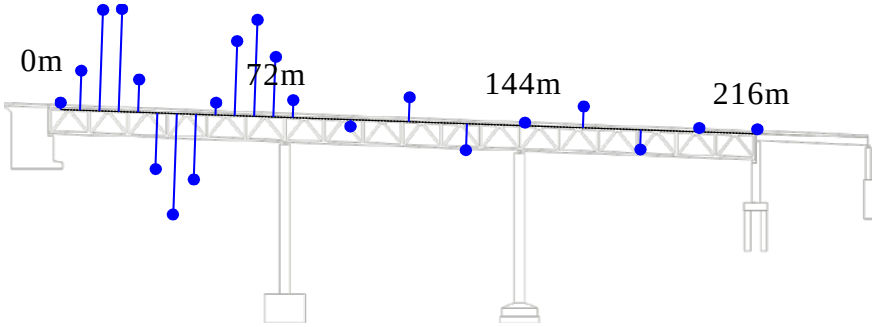

Figure 4.4(d) Bridge vibration mode at 9Hz

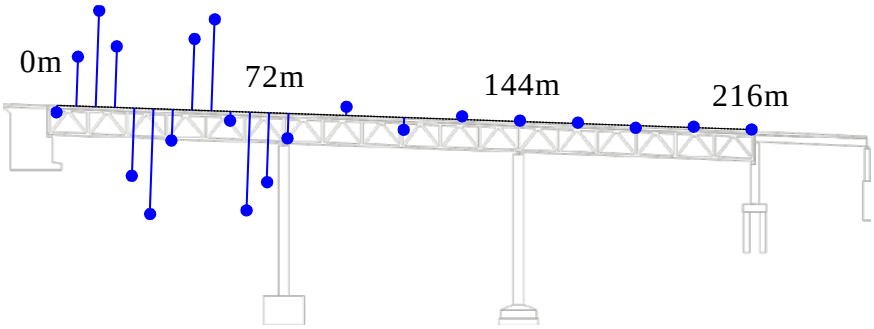

Figure 4.4(e) Bridge vibration mode at 12Hz

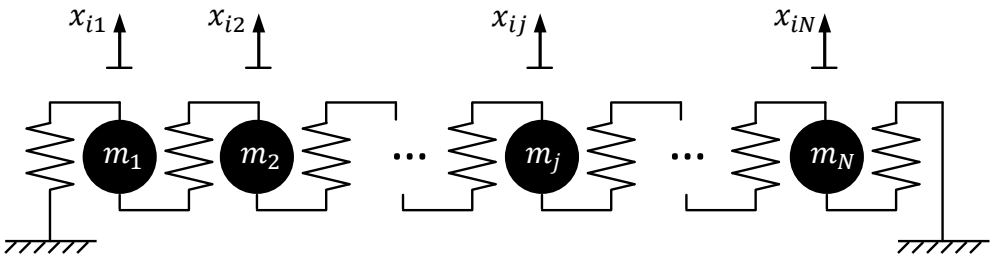

Figure 4.5 *N*-degree of freedom model in *i*-order modal vibration

Table 4.1 Natural frequency in each vibration mode of bridge and equivalent mass at installation location of TMG

	1st mode	2nd mode	3rd mode	4th mode	5th mode
Vibration Frequency	1.6Hz	3.1Hz	6.1Hz	9.1Hz	12.5Hz
Equivalent Mass *M* (Mass Ratio over Total Bridge Mass)	245ton (34.8%)	470ton (66.8%)	233ton (33.2%)	129ton (18.4%)	361ton (51.4%)
Damping Ratio of Bridge	0.035	0.019	0.017	0.031	0.012

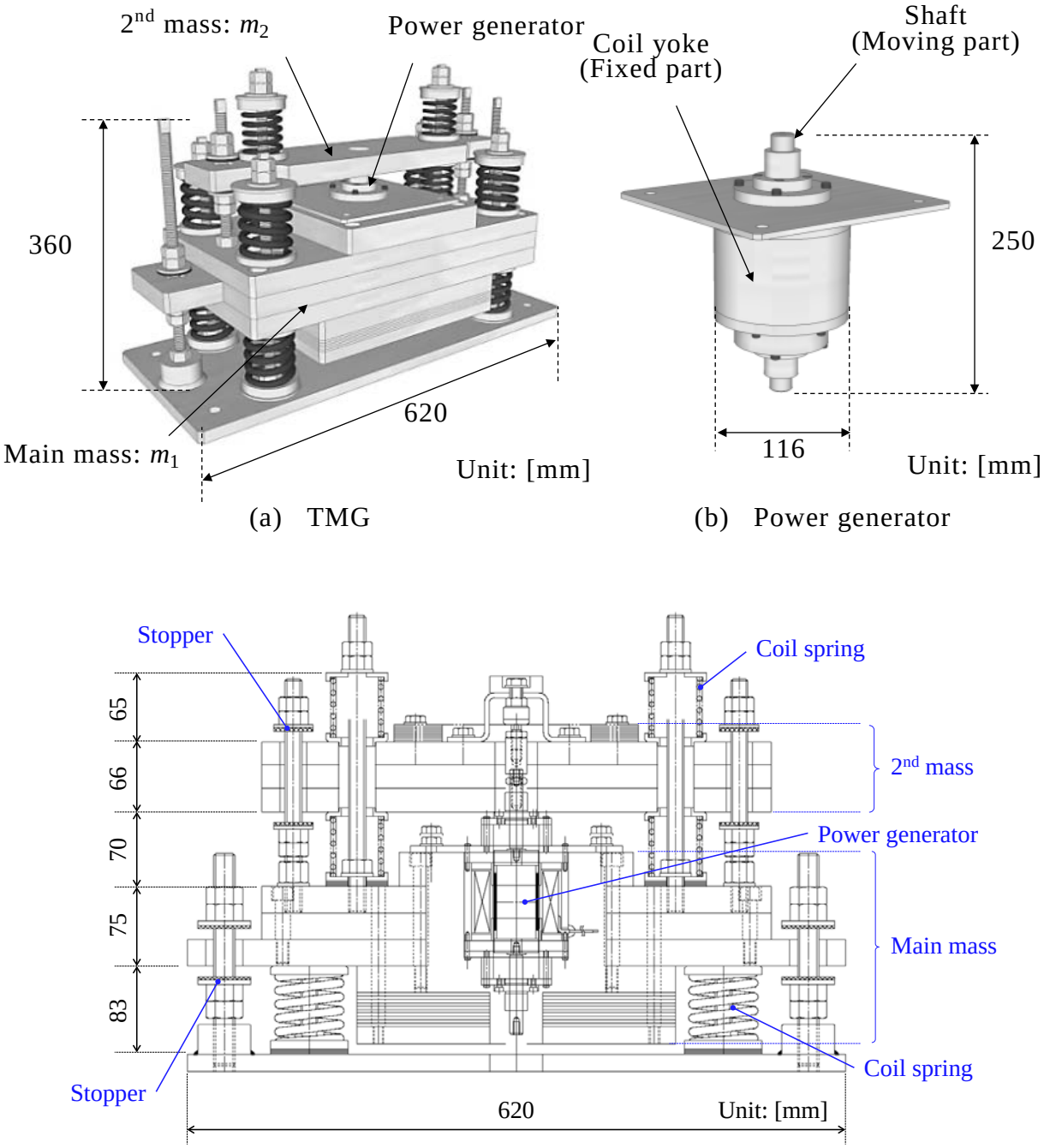

Figure 4.6 Image of TMG and the electromagnetic power generator

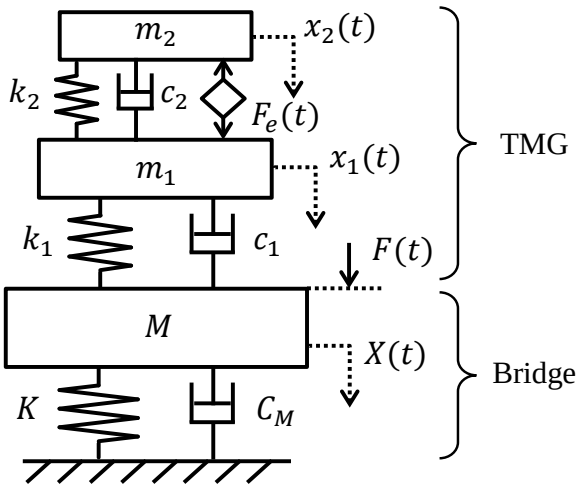

Figure 4.7 Analysis model of TMG and bridge system

Figure 4.8 Setup of TMG on an excitation machine

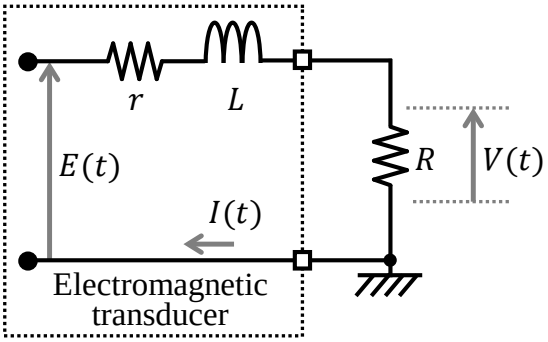

Figure 4.9 Electric circuit for power generation

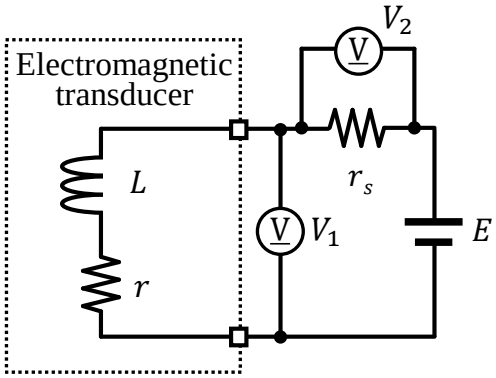

Figure 4.10 Electric circuit for evaluation of DC resistance of the internal coil of the power generator

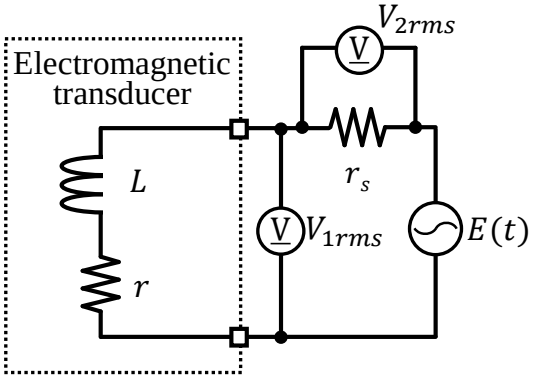

Figure 4.11 Electric circuit for evaluation of self-inductance of the internal coil of the power generator

Table 4.2 Tuning parameters for 14.2Hz vibration mode

Second mass	m_2 = 12 kg
Main mass	m_1 = 104 kg
Natural frequency of second mass	f_2^* = 18.50 Hz
Natural frequency of main mass	f_1^* = 16.98 Hz
Damping of second mass	c_2 = 118.0 Ns/m
Damping of main mass	c_1 = 82.5 Ns/m
Electric damping	c_e^* = 1615 Ns/m
Capacitance for power factor correlation	C = 220 μF

Table 4.3 Tuning parameters for 6.1Hz vibration mode

Second mass	m_2 = 31 kg
Main mass	m_1 = 104 kg
Natural frequency of second mass	f_2^* = 10.2 Hz
Natural frequency of main mass	f_1^* = 6.92 Hz
Damping of second mass	c_2 = 118.0 Ns/m
Damping of main mass	c_1 = 82.5 Ns/m
Electric damping	c_e^* = 1972 Ns/m
Capacitance for power factor correlation	C = 1200 μF

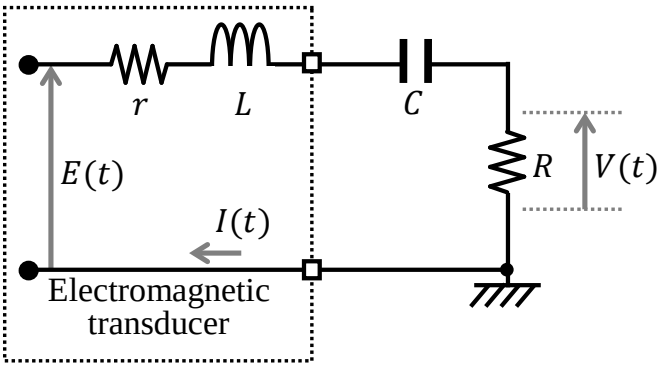

Figure 4.12 Electric circuit model used in the experiment

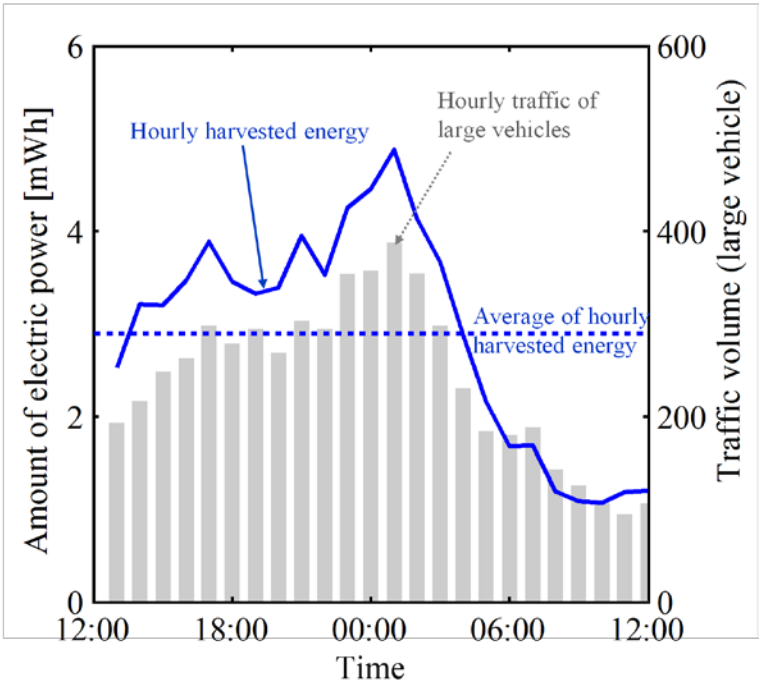

Figure 4.13 Generated electric energy and traffic per hour (target frequency: 14.2 Hz)

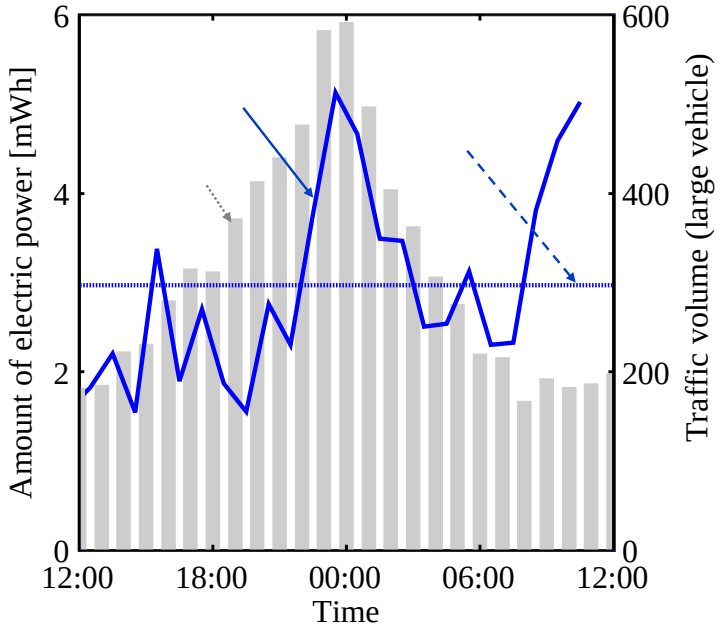

Figure 4.14 Generated electric energy and traffic per hour (target frequency: 6.1 Hz)

Table 4.4 Power consumption of general monitoring devices of bridge structures and power supply ratio by TMG

Monitoring Device	Power Consumption	Power Supply Ratio by TMG
MEMS accelerometers	0.1~1mW	300% or more
MEMS Temperature sensors	0.01~0.3mW	1000% or more
Low-power consumption data logger	1mW~	300% or less

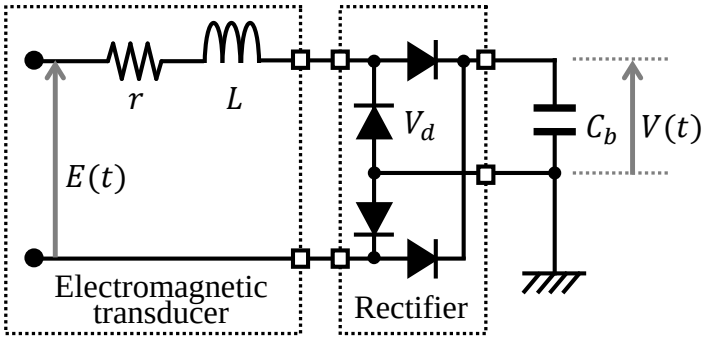

Figure 4.15 Charging circuit

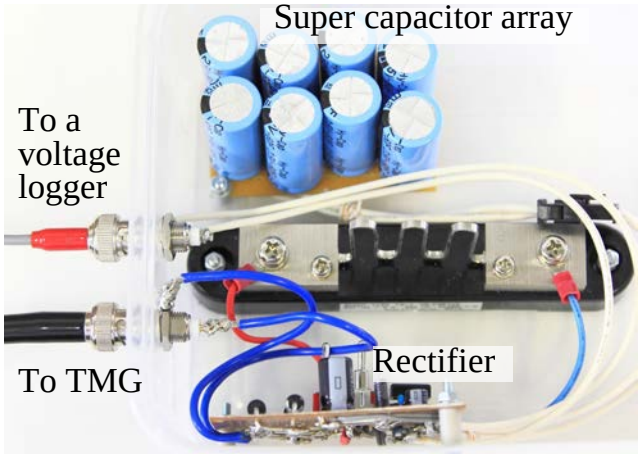

Figure 4.16(a) Setup of the charging circuit with a super capacitor array used in the experiment

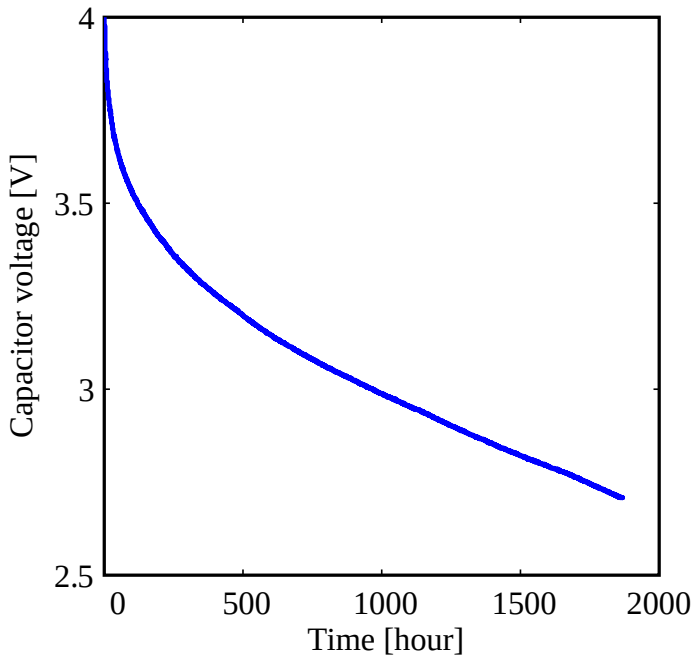

Figure 4.16(b) Discharge characteristic curve of the super capacitor array

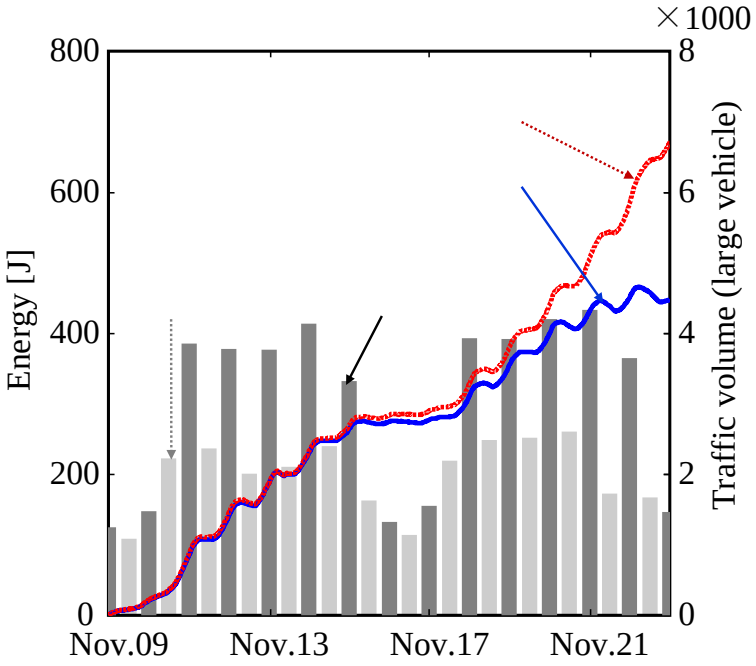

Figure 4.17 Storage electric energy and hourly traffic (target frequency: 14 Hz)

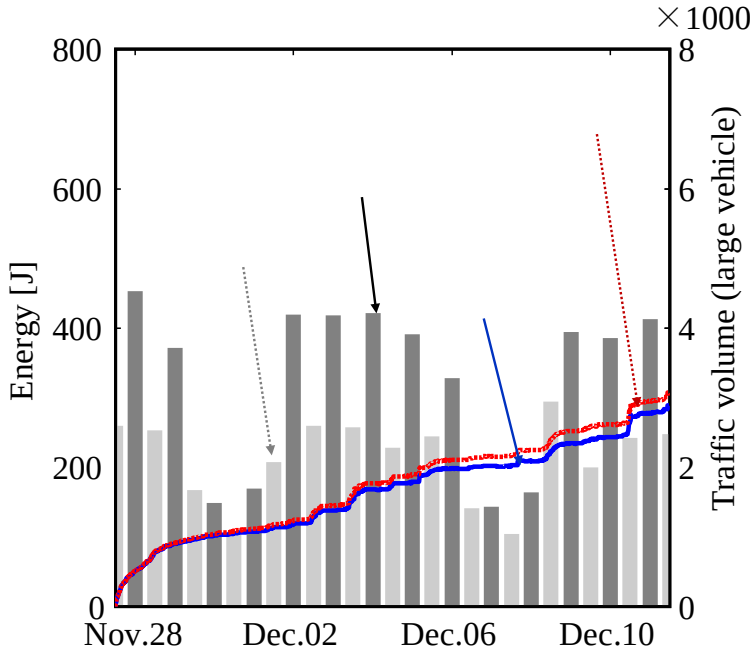

Figure 4.18 Storage electric energy and hourly traffic (target frequency: 6.1 Hz)

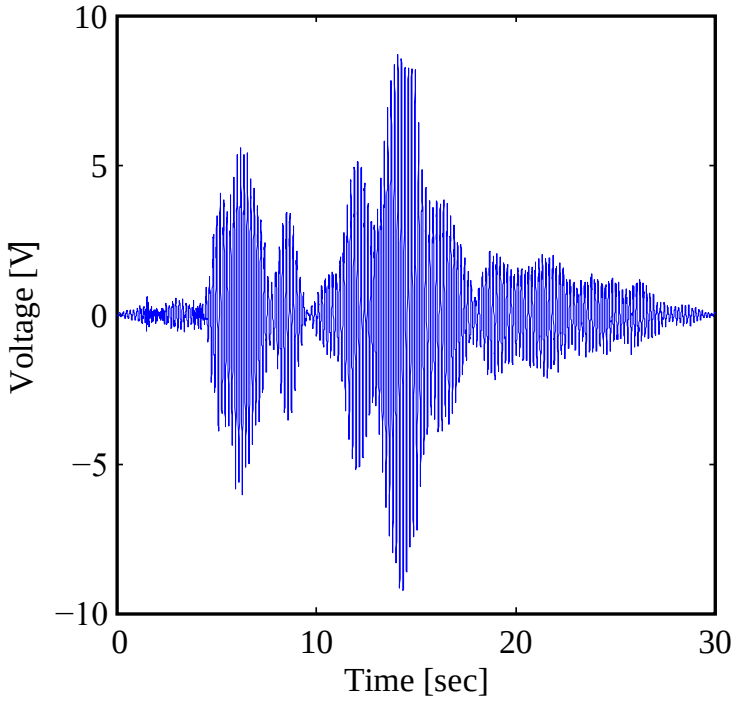

Figure 4.19 Generated voltage by TMG

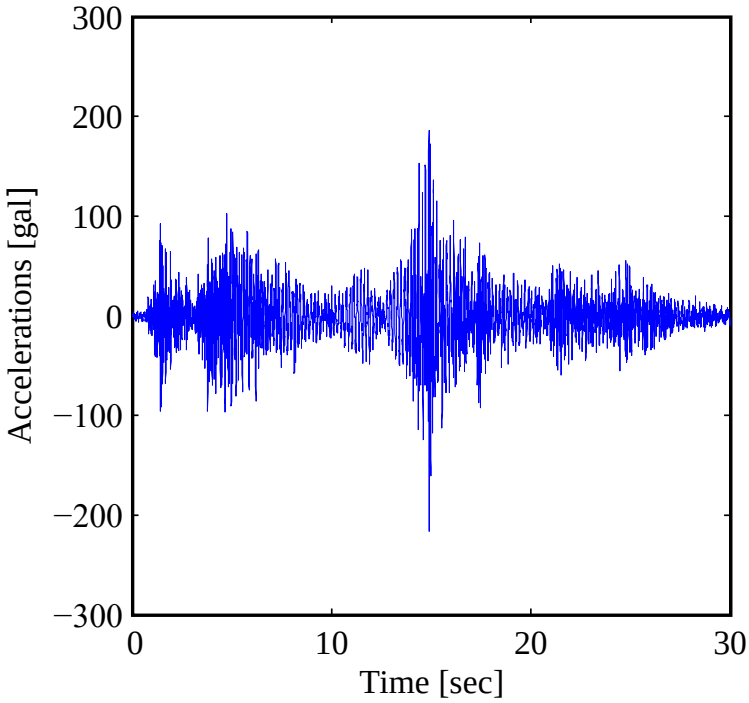

Figure 4.20 Bridge acceleration measured at 18m from the bridge start at the installation location of TMG

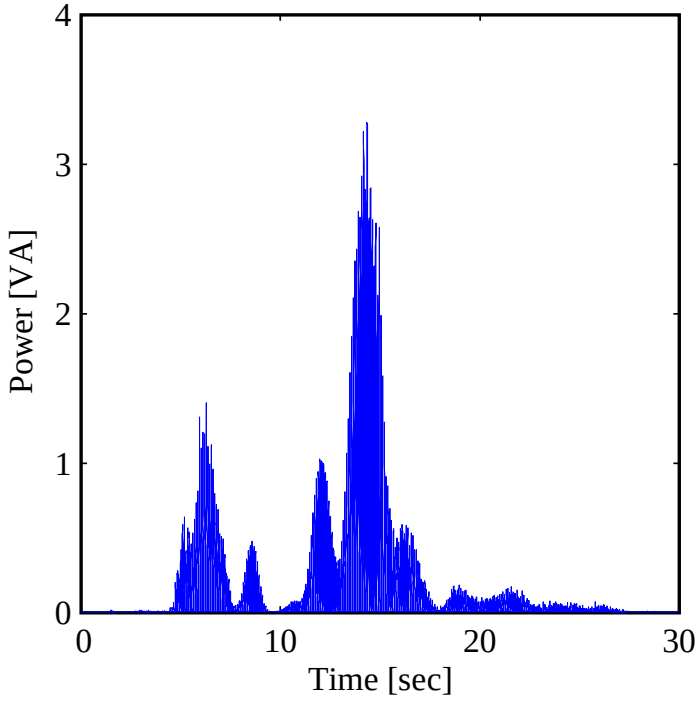

Figure 4.21 Generated power by TMG

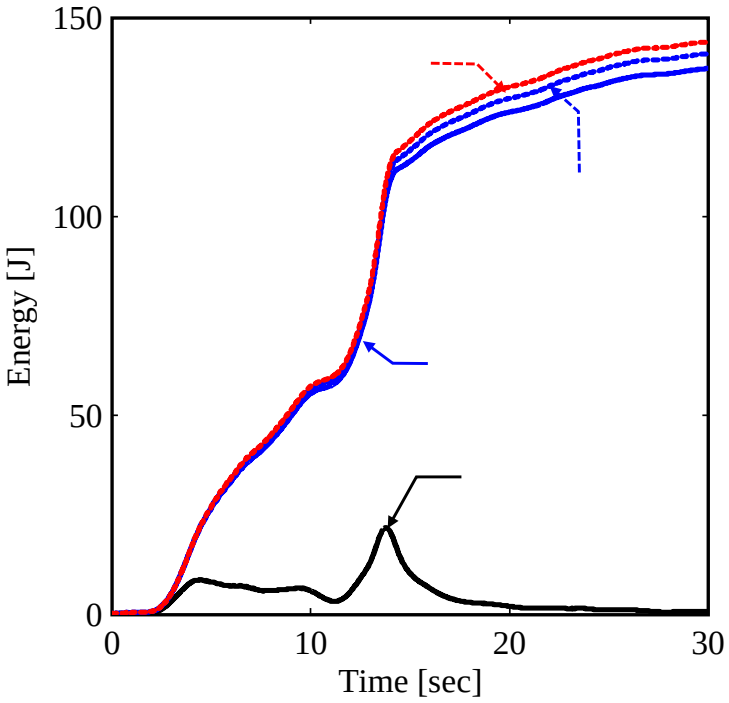

Figure 4.22 Energy flow in the bridge-TMG vibration system

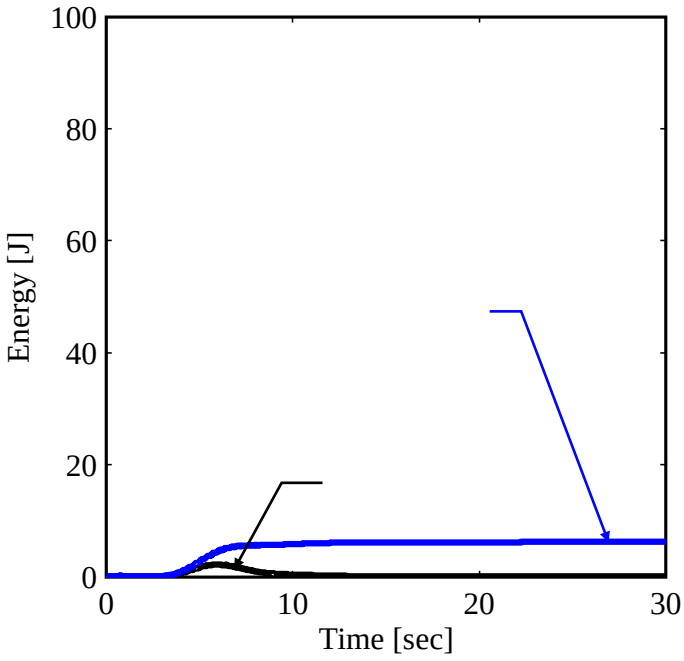

Figure 4.23(a) Energy flow of 1.5Hz vibration mode in the bridge-TMG vibration system

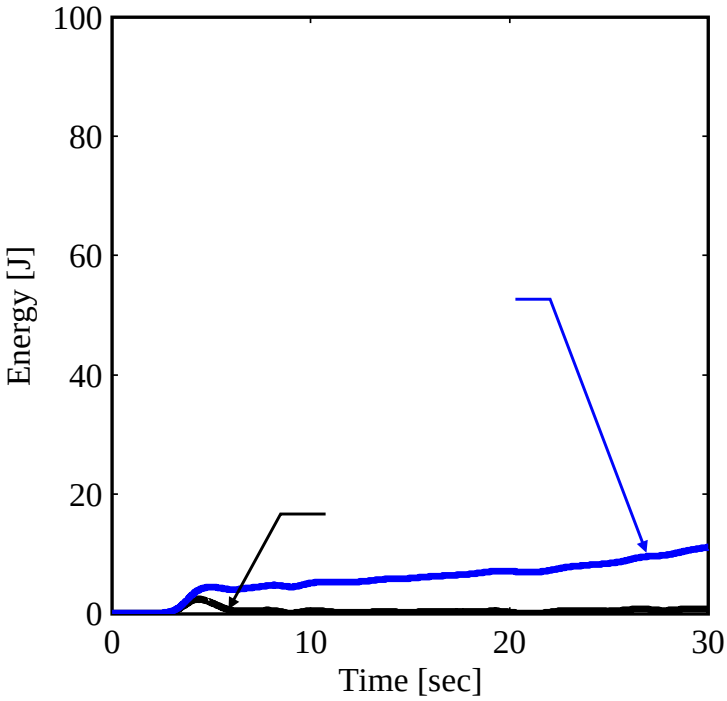

Figure 4.23(b) Energy flow of 3Hz vibration mode in the bridge-TMG vibration system

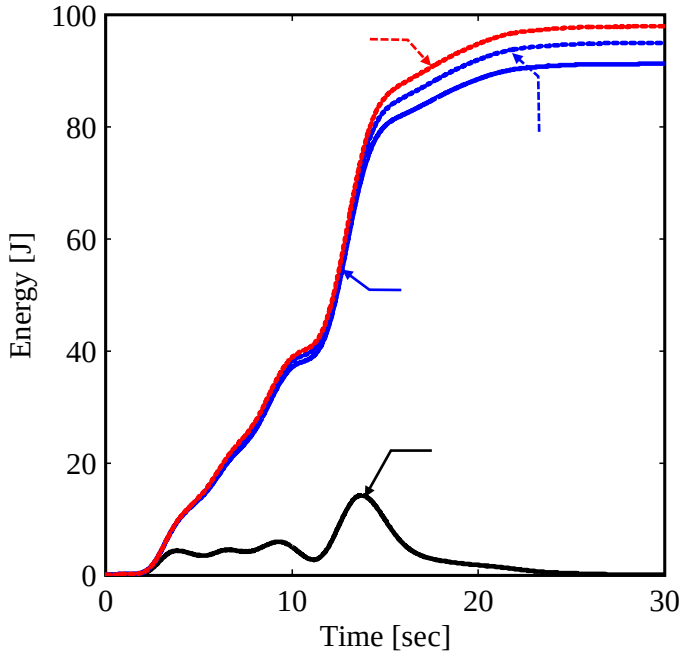

Figure 4.23(c) Energy flow of 6Hz vibration mode in the bridge-TMG vibration system

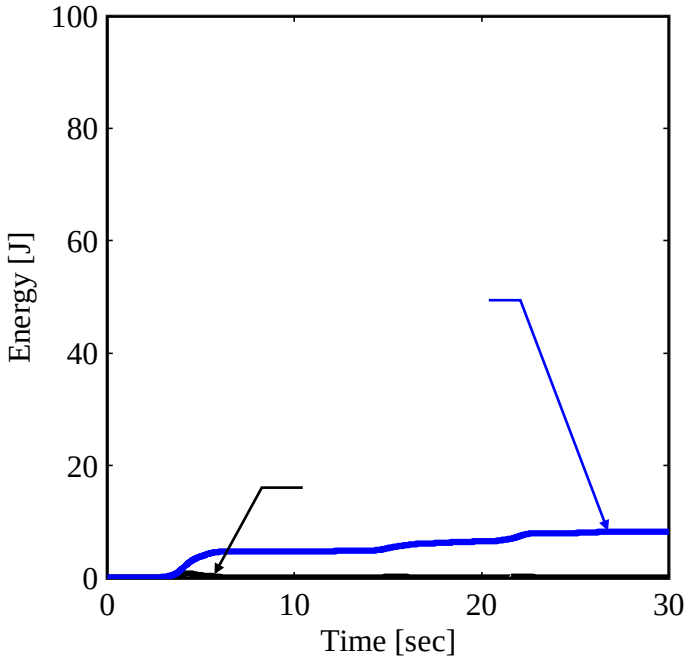

Figure 4.23(d) Energy flow of 9Hz vibration mode in the bridge-TMG vibration system

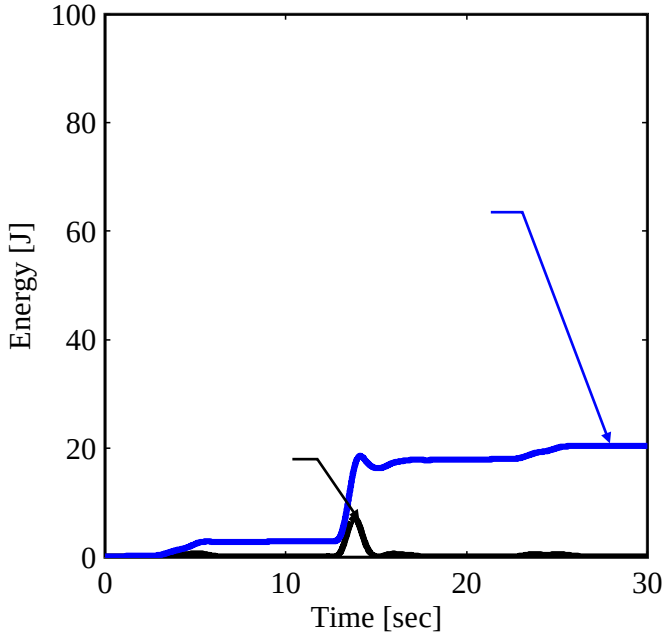

Figure 4.23(e) Energy flow of 12Hz vibration mode in the bridge-TMG vibration system

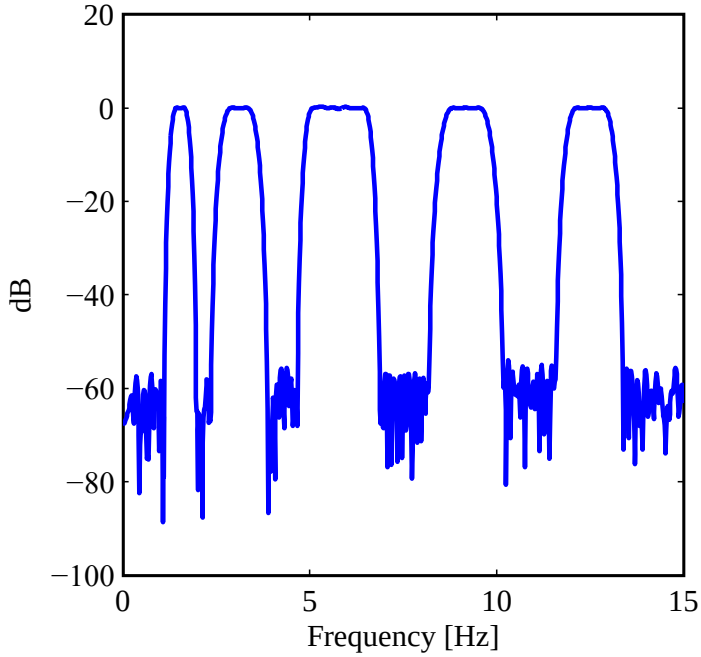

Figure 4.24 Summation of band-pass filters that was used in the modal analysis of energy flows

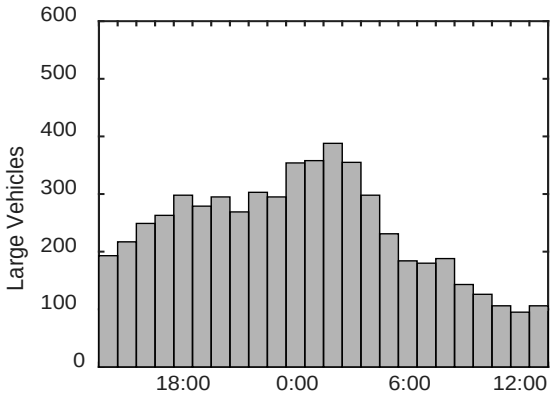

Figure 4.25(a) Hourly traffic of large vehicles between 8th and 9th November 2014

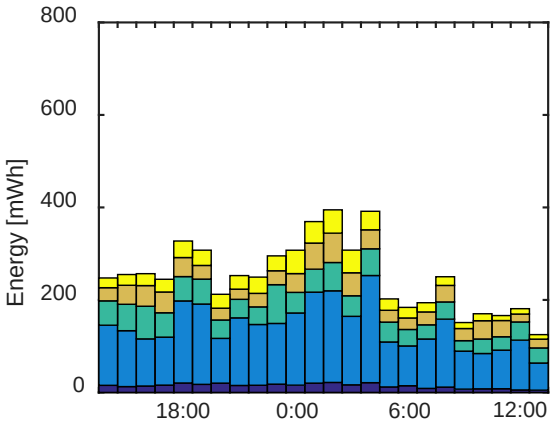

Figure 4.25(b) Hourly distribution of bridge vibration energy between 8th and 9th November 2014

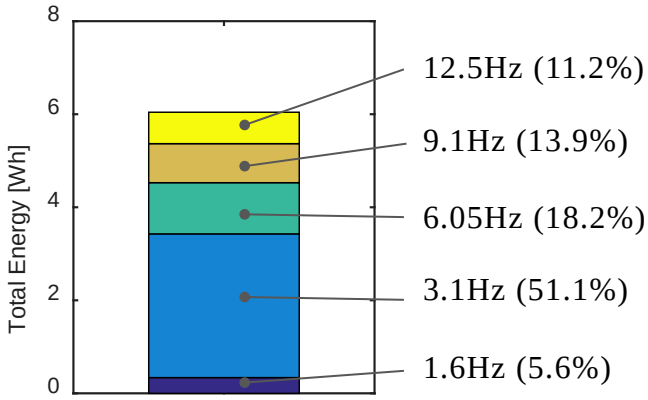

Figure 4.25(c) Distribution of total bridge vibration energy between 8th and 9th November 2014

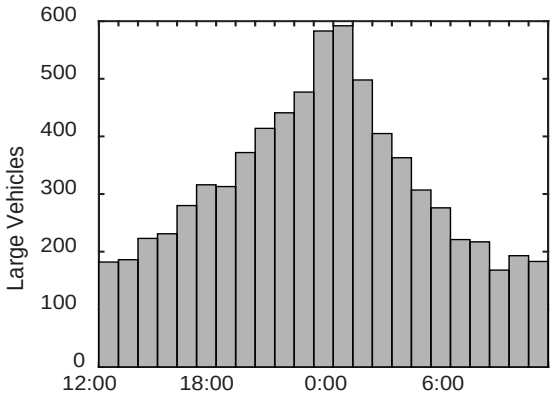

Figure 4.26(a) Hourly traffic of large vehicles between 25th to 26th November 2014

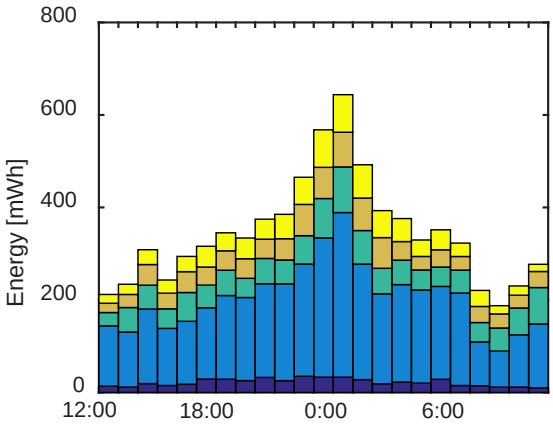

Figure 4.26(b) Hourly distribution of bridge vibration energy between 25th to 26th November 2014

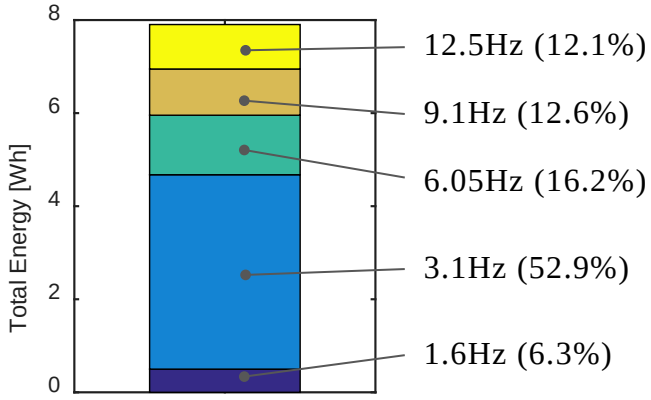

Figure 4.26(c) Distribution of total bridge vibration energy between 25th to 26th November 2014

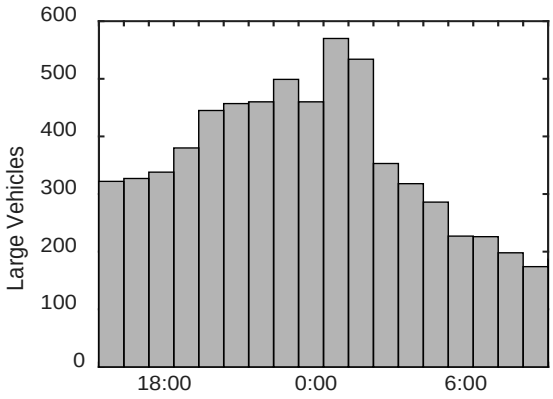

Figure 4.27(a) Hourly traffic of large vehicle between 17th to 18th November 2015

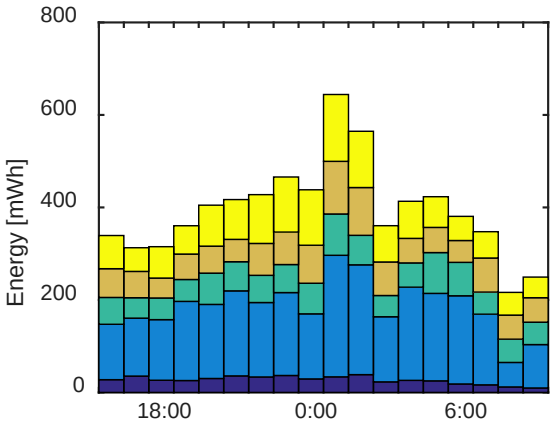

Figure 4.27(b) Hourly distribution of bridge vibration energy between 17th to 18th November 2015

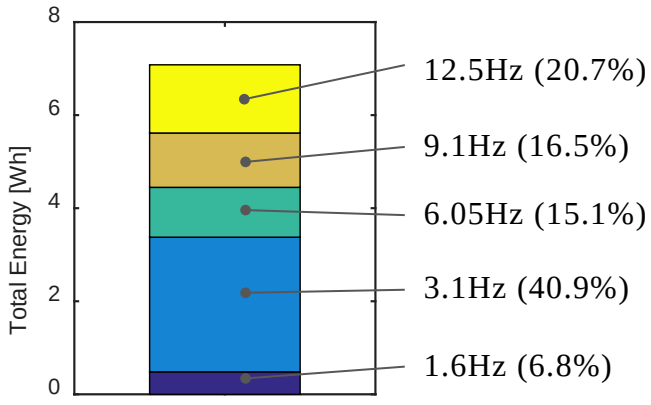

Figure 4.27(c) Distribution of total bridge vibration energy between 17th to 18th November 2015

Chapter 5

Efficiency Enhancement of Power Generators for Energy Harvesting

Abstract

Based on the findings in the field experiments, a potential of the efficiency enhancement of power generators was revealed. In this chapter, a structural design of power generators has been considered for the purpose of applying TMG to constructively use vibrations of bridge structures. Yoke shapes and permanent magnet shapes were considered as design parameters. Based on the findings in parametric studies, the nonlinearity of the damping force of power generation can be controlled and the magnetic spring force can also be considered. Finally, a power generator for the TMG system has been designed and developed, and its performance has been experimentally demonstrated.

5.1. Overview

In the previous chapters, TMG was applied to an actual expressway bridge and watt order power was generated from vibrations of the bridge structure. In addition, to make use of the energy harvested from bridge vibrations, batteries were successfully charged. There is potential for these charged batteries to be used for monitoring systems of bridge structures. However, the structural design of power generators for effective power generation from vibrations of bridge structures has not yet been established. A high performance power generator was used in **Chapter 4** to achieve high electric damping forces under low vibration frequencies of bridges. Although watt order power was obtained from actual vibrations of the bridge structure, the fabrication cost of the power generator was the greatest in the TMG system. Hence for practical use of TMG, the specifications of power generators should be controlled for improving its use.

To investigate the structural design of power generators, Zhu et al. **[83]** proposed a power generator with vertical magnetic flux. The characteristics of electric power generation and damping force of the power generator were analytically and experimentally demonstrated. A power generator with radial magnetic flux has also been proposed and it has been found to generate higher voltage with a smaller magnet volume than the power generator with vertical magnetic flux **[41,43]**. However, it should be noted that the structural design for a radial magnetic flux is generally more complicated than power generators with vertical magnetic flux.

In this study, for the harvesting of energy generated from vibrations of bridge structures, power generators have been enhanced considering their structural design. In addition, the nonlinear characteristics of power generation and magnetic springs were investigated. If the characteristics of power generators can be controlled and designed, factors such as the cost effectiveness of TMG can be further improved.

5.2. Design Concept

Figure 5.1 shows a model electromagnetic power generator. The electromagnetic power generator consists of a moving part and fixed part. The moving part consists of external magnets and a magnet yoke, while the fixed part consists of an electric coil and a coil yoke. By inducing velocity to the magnetic field generated by the permanent magnet, an induced electromotive force is generated at the coil. To simplify the analysis, the power generator has been expressed by an axis-symmetric model (**Figure 5.2**).

5.2.1. Analysis Model

The structural design of a power generator has been conducted using Finite Element Analysis (FEA). In this study, COMSOL® ver.5.2 has been used as the FEA software for electromagnetic analysis. The material properties and conditions of FEA are shown in **Table 5.1** and **Figure 5.3**. As shown in **Figure 5.3**, the nonlinear characteristic of the yoke material (steel: SS400) has been considered in this analysis model. **Figure 5.4(a)** shows an entire view of the analysis model, and **Figure 5.4(b)** shows one part of the model in closer detail. As shown in **Figure 5.4(c)**, the moving part of the analysis model slides up and down within a range of ±20 mm. BDF (Backward Differentiation Formula) method is applied as a time stepping method. To enhance electromagnetic power generators, not only should the accuracy of analysis be considered, but also the analysis time, since iterative FEA is carried out to design dimensional parameters of electromagnetic power generators.

5.2.1.1. Analysis Accuracy and Analysis Time

In order to obtain high computational accuracy of FEA results, it is important to consider the following factors

(a) The aspect ratio of elements

(b) Mesh size

(c) Absolute and relative tolerance

Since the aspect ratio of elements can be considered when creating a mesh, the influence of (b) mesh size and (c) absolute and relative tolerances, on analysis accuracy and analysis time was investigated. The most accurate FE model is shown in **Figure 5.5**, which is a closer view of **Figure 5.4(b)**. A triangular second-order Lagrangian element is applied. The number of degrees of freedom are 569.6 k, the absolute tolerance is 10^{-5} and the relative tolerance is 10^{-6}. Although this is a highly accurate result, it is not practical as the mesh size and tolerances were greatly reduced in the model, which greatly increases the computational time accordingly.

As shown in **Figure 5.6(a)** to **Figure 5.6(d)**, four finite element models with different mesh sizes (number of degrees of freedom = 113.7×10^3, 73.8×10^3, 32.4×10^3, 16.7×10^3) were considered. First, the influence of the various relative tolerances on the analysis error and the analysis time were investigated as shown in **Figure 5.7** and **Figure 5.8** (the absolute tolerance is fixed at 0.001). The analysis error is evaluated by the electromotive force value that is expressed by the following equation.

$$\text{analysis error} = \sqrt{\frac{\sum_x \left(V(x) - V_0(x)\right)^2}{\sum_x V_0{}^2(x)}} \tag{5.1}$$

Where, $V(x)$ is the induced electromotive force [V] of the analysis model, $V_0(x)$ is the induced electromotive force [V] of the model shown in **Figure 5.5** (degrees of freedom: 569.6 k, absolute tolerance: 10^{-5}, relative tolerance: 10^{-6}). As **Figure 5.7** indicates, when the relative tolerance decreases, the analysis error decreases also, hence the analysis accuracy increases. However, a decrease in analysis error, namely the improvement of the analysis accuracy, does not occur when the relative tolerance is 0.001 or less. As shown in **Figure 5.8**, the smaller the relative tolerance, the longer the analysis time, which is unfavorable. However, the analysis time does not increase when the relative tolerance is 0.001 or less. Moreover, the larger the number of elements, the longer the analysis time, which again is unfavorable, and there is also no considerable difference in the analysis accuracy.

Next, the influence of the various relative tolerances on the analysis accuracy and the analysis time are indicated in **Figure 5.9** and **Figure 5.10** (the absolute tolerance is fixed at 0.00001). As shown in **Figure 5.9**, if the absolute tolerance reduces from 0.001 to 0.00001, the analysis accuracy increases, namely the analysis error decreases

by approximately 50% or more. However, the analysis accuracy does not increase when the accuracy of the relative tolerance is around 0.001 or less. As **Figure 5.10** indicates, the smaller the relative tolerance, the longer the analysis time. In particular, the analysis time increases sharply, as the analysis time increases if the relative tolerance is less than 0.001.

Based on these findings, the balance between analysis accuracy and analysis time has been considered, and it has been concluded that the appropriate analysis tolerance of about 1% will be used in this study. The analysis degree of freedom will be between 30000 to 40000 (30 to 40 k, similar to model C shown in **Figure 5.6(c)**), with an absolute tolerance of 0.001, and relative tolerance of 0.001.

5.2.2. Target Design Parameters

5.2.2.1. Electromotive Force Coefficient

Based on Faraday's law of electromagnetic induction, when the moving part is shifted, the non-load induced voltage $E(t)$ is applied to both ends of the coil in proportion to the amount of change in the magnetic flux $\varphi(t)$ in the coil, as shown in the following formula.

$$E(t) = \frac{\delta\phi(t)}{\delta t} \tag{5.2}$$

In **Chapter 2**, the magnetic flux was treated as a constant, irrespective of the position of the moving part $x(t)$ [mm]. The electromotive force coefficient was expressed as a constant by using the relationship where the change in the magnetic flux was proportional to the velocity of the moving part as shown in the formula.

$$\frac{\delta\phi(t)}{\delta t} \propto \frac{\delta x(t)}{\delta t} \tag{5.3}$$

However, it is expected that this linear relationship is not applicable when the position of the moving part moves greatly. Therefore, the electromotive force E has been considered as a function of not only time t, but also of the position of the moving part x.

$$k_{emf}(x) = \frac{E(x,t)}{v(x,t)} \tag{5.4}$$

in which k_{emf} is the electromotive force coefficient [Vs/m], and $v(x,t)$ is the velocity of the moving part of the electromagnetic power generator. As shown in **equation (5.4)** the electromotive force coefficient $k_{emf}(x)$ [V.s/m] is considered as a function of the position of the moving part.

5.2.2.2. Maximum Electric Damping Coefficient

Electric power is generated when the moving part is forced to move by external loads. The relationship between the electric power and the power of the external forces is expressed as follows.

$$F(x,t)v(x,t) = E^2(x,t)\left[\frac{R}{(R+r)^2} + \frac{r}{(R+r)^2}\right] \tag{5.5}$$

Where, the first right term of the equation expresses the induced electric power to the electric resistance R, and the second right term of the equation expresses the induced electric power in the internal coil of the power generator. $F(x,t)$ [N] is proportional to the velocity of the moving part. Therefore, $F(x,t)$ can be expressed with the electric damping coefficient $c(x)$ [N.s/m] as follows.

$$F(x,t) = c(x)\cdot v(x,t) \tag{5.6}$$

$$c(x) = \frac{k_{emf}^2(x)}{r}\frac{1}{R_r+1} \tag{5.7}$$

Where, $R_r = R/r$ is the resistance ratio. The resistance ratio is a dimensionless parameter, therefore, it is clear that $k_{emf}^2(x)/r$ has the same dimension with the damping coefficient [N.s/m]. **Equation (5.7)** demonstrates that the equivalent electrical damping coefficient increases when the resistance ratio R_r decreases.

The total electric power generation [VA or N.m/s] by combining the above equations, and considering the electromagnetic power generator to include equivalent damping becomes

$$W_{total}(t) = (c_{eh}(x) + c_{el}(x))\dot{x}^2(t) \tag{5.8}$$

Where $\dot{x}(t)$ is the velocity, and $c_{eh}(x)$ and $c_{el}(x)$ are damping coefficients due to harvested electric power and electrical loss respectively. These equivalent electrical damping coefficients can be defined as

$$c_{eh}(x) = \frac{k_{emf}^2(x)}{r}\frac{R_r}{(1+R_r)^2}, \qquad c_{el}(x) = \frac{k_{emf}^2(x)}{r}\frac{1}{(1+R_r)^2} \tag{5.9}$$

5.2.2.3. Magnetic Spring Force Effect

The moving part is influenced by the magnetic force which occurs between the permanent magnet and the coil yoke. This force is generally called cogging force. In general, the higher the cogging force, the higher the moving resistance. This causes a decrease in power generation efficiency. However, in this study, the cogging force has been treated as the restoring and repelling forces towards the neutral position of the moving part (x = 0mm), similar to the spring force of a tuned mass system. This effect, namely the magnetic spring effect, is considered in the use of the power generator.

5.3. Design of Power Generator

The ability of power generation is highly influenced by the yoke shapes of power generators, since the magnetic path through the coil, from the north-pole to the south-pole, is controlled by the yoke shapes. The magnetic path is generally called magnetic circuit. The magnet shape of power generators is also important, since the magnetomotive force in the magnetic circuit is induced by the magnet shape. Therefore, the yoke and magnet shapes should be designed to increase the magnetic flux passing through the coil.

In this study, the yoke and magnet shapes were designed to control the characteristics of power generators. Design parameters with seven dimensions, namely magnet yoke tooth height, My_th, magnet yoke width, My_w, coil yoke tooth height, Cy_th, coil yoke tooth width, Cy_tw, magnet height, M_h, magnet yoke height, My_h, and coil yoke height, Cy_h, were introduced as shown in **Figure 5.2**. The corresponding dimensional values are indicated in **Table 5.2**. In addition, the air gap between the moving part and the fixed part should be as small as possible, since the magnetic resistance in the magnetic circuit is higher in the air than in the steel yoke. An air gap of 0.5mm has been selected for this study and this value is realistic, considering the balance between the accuracy of assembly and fabrication cost.

Based on the findings obtained from the experiments of harvesting energy on the trial bridge in **Chapter 4**, two important requirements for power generators were discovered;

(a) high efficiency for small vibrations

(b) wide stroke range for large vibrations

In addition, a reduction of the friction force and a reduction of the fabrication cost are also important. To reduce the friction force, the shaft part was made non-magnetic to eliminate the horizontal absorption force with the bearing part, and to reduce the frictional resistance. The air gap between the moving part and the fixed part was designed as 0.5mm, and this design can be achieved with basic fabrication accuracy. For this reason, fabrication costs can be reduced by one order from the conventional power generator used in **Chapter 4**.

5.3.1. Parameter Design Method of Power Generator

In this study, dimensional parameters of power generators have been considered to obtain the required power generation and the required damping effect of power generators. **Table 5.2** shows the design parameters of the power generator, the initial power generator values, and parameter value limitations. The objective function F_{opt} is shown in **Table 5.3**. To take into consideration the two aforementioned important requirements for power generators, (a) high efficiency for small vibration and (b) wide stroke range for large vibration, were separately studied. As indicated by the blue rectangle in the left hand figure or the red rectangle in the right hand figure of **Table 5.3**, the objective function F_{opt} is the minimum of the electromotive force coefficient k_{emf} [V.s/m] in the stroke range $X_{min} \leq X \leq X_{max}$ [mm]. Combinations of design parameters that maximize the objective function F_{opt} were identified by iterative calculations of the FEA analysis for (a) and (b), respectively. The parameters identified are shown in **Table 5.3**.

As indicated in **Table 5.3**, the electromotive force coefficient k_{emf} [V.s/m] and the stroke range (X_{max} - X_{min}) [mm] are in a trade-off relationship. Therefore, multi-objective functions (a) high efficiency for small vibration, and (b) wide stroke range

for large vibration were introduced to the power generator for harvesting energy from vibrations of bridge structures. By controlling the balance between the electromotive force coefficient and stroke range, appropriate dimensional parameters for power generators has been proposed. Designed power generators satisfy the required power generation performance by using multi-objective functions.

5.3.2. Iteration Procedure

Since the computational complexity increases in iterative computations of FE models, efficient FEA with an appropriate balance between analysis accuracy and analysis time has been acquired by using the analysis conditions discussed in **Section 5.2.1.1**. The dimensional parameters were designed to maximize the multi-objective functions by using a dynamic search method. The dynamic search method can be considered as a generalized version of Newton's method. Through a trial and error procedure, it was concluded that this method is effective to obtain an enhanced power generator.

5.3.3. Design of Power Generator

To attain the best performance of TMG, multi-objective functions were decided based on the two requirements of the power generator as follows.

(a) High efficiency for small vibrations

To maximize the minimum electromotive force coefficient k_{emf} within a ±2 mm stroke range.

(b) Wide stroke range for large vibrations

To satisfy the minimum required electromotive force coefficient of k_{emf} = 100 [V.s/m] within a ±10 mm stroke range.

These objective functions are indicated in **Figure 5.11**. The red area shows the objective function for high efficiency for small vibrations, the blue area shows the objective function for wide stroke range for large vibrations. **Figure 5.11** shows also the examples of characteristics of the electromotive force coefficient versus displacement of the moving part by gray dotted lines. The target parameters are

indicated in **Figure 5.2**. First, FEA results are checked if the electromotive force coefficient satisfies the objective function for wide stroke range (blue area in **Figure 5.11**), and next, parameters are changed to maximize the objective function for high efficiency (red area in **Figure 5.11**) which satisfy the two objective functions simultaneously. Finally, the design parameters were determined through iterative FEA using the direct search method as shown in **Table 5.4**. Determined characteristics of the electromotive force coefficient versus displacement of the moving part is shown in **Figure 5.11** by a red line.

5.4. Experimental Evaluation

Based on the designed dimensional parameters, an electromagnetic power generator has been developed (**Figure 5.12**). The three key characteristics of the electromagnetic power generator, namely the electromotive force coefficient k_{emf}, the dynamic friction force and the magnetic spring force, were experimentally evaluated.

5.4.1. Electromotive Force Coefficient k_{emf}

The newly developed electromagnetic power generator was set on an excitation machine as shown in **Figure 5.12**. The moving part of the power generator was forced to slide up and down by the actuator. The electromotive force coefficient k_{emf} was obtained from the experimentally measured induced voltage. The electromotive force coefficient was designed to satisfy the required efficiency within the wide stroke range and obtain high efficiency within the short stroke range. To evaluate the nonlinear characteristics of the voltage induction, the triangular wave excitation was carried out (5 mm/s, ±20 mm). The sampling rate was 1000 Hz.

Figure 5.13 shows the induced voltage and the velocity of the moving part, which was obtained by division of the displacement of the actuator. **Figure 5.14** shows the relationship between the electromotive force coefficient and the position of the moving part. The blue line shows the electromotive force when the moving part slides upwards, while the red line shows the electromotive force when the moving part slides

downwards. As shown in **Figure 5.14**, the electromotive coefficient is a function of the position of the moving part, and this characteristic is the same as the designed values in FEA. The errors in the designed values from FEA were 10 % or less. The cause of the difference between the two lines is considered to be due to the hysteresis effect.

5.4.2. Dynamic Friction Force

Friction force is one of the largest losses when harvesting vibration energy, and it occurs mainly on the shaft holders of the power generator. In addition, the larger the friction force, the shorter the rating life of the shaft holders. Therefore, the friction force should be evaluated clearly. The experiment system is shown in **Figure 5.12**. The induced force to the moving part was measured by the strain load cell (capacity: 5kN, output: 2 mV/V).

Figure 5.15 shows the relationship between the induced force and the position of the moving part. The upper line shows the induced force when the moving part slides upwards. The lower line shows the induced force when the moving part slides downwards. Therefore, the dynamic friction force can be obtained by

$$\text{Dynamic friction force} = (\text{upper line} - \text{lower line}) / 2 \tag{5.10}$$

The relationship between the dynamic friction force and the position of the moving part is shown in **Figure 5.16**. Based on the results, the rating life of the shaft holders of the power generator were evaluated. The rating life of shaft holders is normally expressed as a distance as follows.

$$L = \left(\frac{f_H \cdot f_T \cdot f_C}{f_W} \frac{C}{P} \right)^2 \cdot 50 \ \text{[km]} \tag{5.11}$$

where, L is rating life [km], f_H is hardness factor, f_T is temperature factor, f_C is contact factor, f_W is weighted factor, C is basic load [N] and P is working load [N]. To estimate the rating life time, a converting formula was introduced.

$$L_y = \frac{L}{2 \cdot l_s \cdot n_1 \cdot 526} \ \text{[year]} \tag{5.12}$$

Where, L_y is rating life [year], l_s is stroke [m] and n_1 is number of cycles per minute [cpm]. Based on the specification of the applied shaft holders, the basic load and

factors are shown C = 412 N, f_H = 0.8, f_T = 1.0, f_C = 0.81 and f_W = 2.0. From the experimental results, the working load to the shaft holders was selected as P = 100 N, since the variation below the working load is advantageous for the rating life and is not a problem. From the experimental result on the bridge, the average stroke and number of cycles per minute were selected as l_s = ±5 mm, n_1 = 100 cpm. According to these formula, the rating life of the two linear bushes used in the power generator are 120 km or 13.5 years or more.

5.4.3. Magnetic Spring

The magnetic spring force is obtained as the average of the upper and lower lines of the force-displacement graph (**Figure 5.15**) namely

Magnetic spring force = (upper line + lower line) / 2 (5.13)

Figure 5.17 shows the relationship between the magnetic spring force and the position of the moving part. The aforementioned characteristics can be used for designing TMG.

5.4.4. Design of TMG

To enable the best performance of TMG, a nonlinear characteristic of the electromagnetic power generator, namely the electromagnetic damping force $F_e(x,\dot{x})$ that is induced by an electromotive force and a magnetic spring force $F_m(x)$, was considered. The analysis model is indicated in **Figure 5.18**. In this analysis model, nonlinear characteristics of the developed power generator and friction forces σ_1 and σ_2 are considered. The electromagnetic damping force is expressed as follows.

$$F_e(x,\dot{x}) = \frac{\{k_{emf}(x)\}^2}{R+r}\cdot\dot{x}^2 \tag{5.14}$$

Where, $k_{emf}(x)$ is the electromotive force coefficient [V.s/m], R is external electric load [Ω], r is DC resistance of the coil [Ω], x is the position of the moving part of the power generator from its neutral position. The nonlinear characteristics of electromotive force coefficient $k_{emf}(x)$ and magnetic spring force $F_m(x)$ were experimentally evaluated

(**Figure 5.14** and **Figure 5.17**). By using this analysis model, TMG can be tuned to bring out the best performance of the efficiency enhanced power generator.

5.5. Summary

In this chapter, an effective structural design of a power generator has been proposed to control the specifications of power generators to adapt with TMG for effective energy harvesting from vibrations of bridge structures. In addition, the nonlinear characteristics of power generation and magnetic springs were investigated with FEA to obtain the best performance of TMG. The following results were obtained.

A) The yoke and magnet shapes in the power generator have been designed to control the characteristics of power generators. Considering the magnetic circuit, seven dimensional parameters of power generators have been selected as design parameters.

B) A design method has been proposed using multi-objective functions to satisfy the two important requirements for the power generator, namely high efficiency for small vibrations, and a wide stroke range for large vibrations.

C) With the proposed design method, the power generator has been designed and developed. The characteristics of the power generator have been verified through experiment.

In addition, if the dynamic friction loss can be reduced to 1 N or less, TMG systems could harvest energy even from vibrations induced by small vehicles. Efficiency of power generation could be further improved if the air gap between the moving part and fixed part could be reduced, or if the volume of neodymium magnet and/or the coil could be increased.

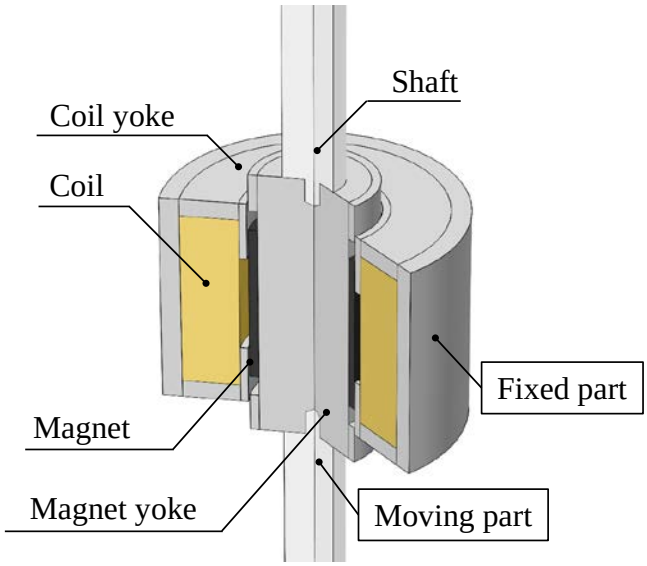

Figure 5.1 A model of electromagnetic power generators

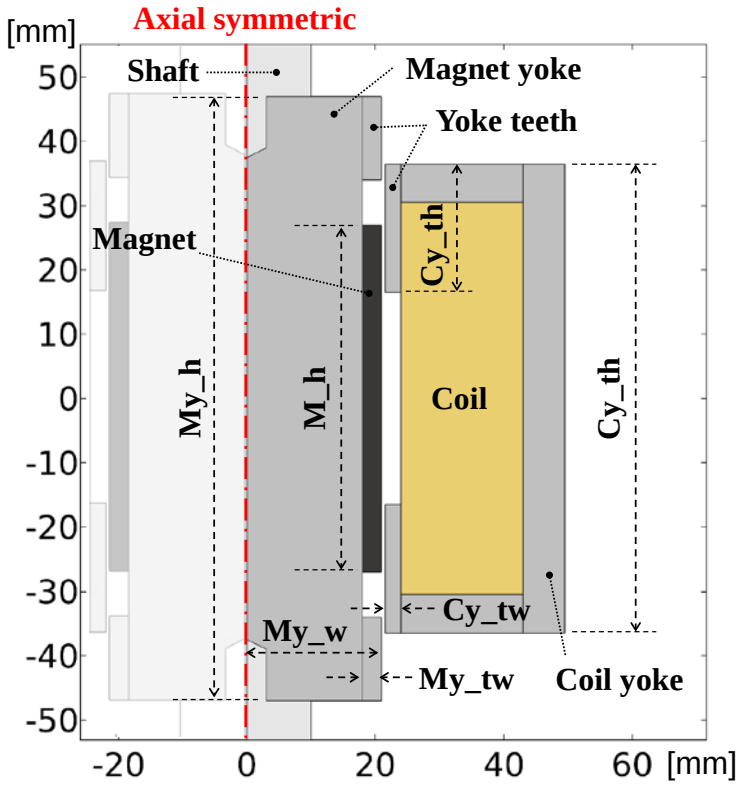

Figure 5.2 Analysis model of electromagnetic power generators by 2D axial symmetric model

Table 5.1 Relative permeability of each material of the power generator, magnetic flux density of the neodymium magnet, and coil turns for Finite Element Analysis

Yoke (steel: SS400)	$\boldsymbol{\mu_{yoke}}$	-
Air	μ_{air}	1.00
Coil (cooper)	μ_{coil}	1.00
Neodymium magnet	μ_{mag}	1.05
	B_r	1.2 [T]
Coil turns	N	1300

Note: Nonlinear relative permeability of the yoke material μ_{yoke} is shown in **Figure 5.3.**

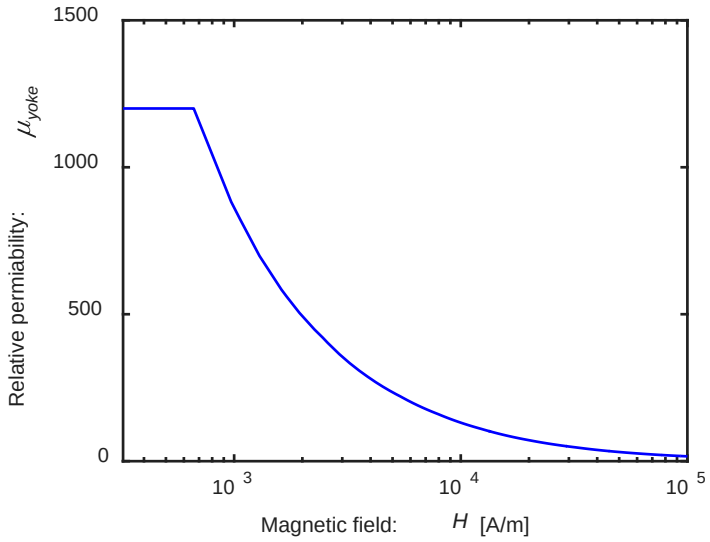

Figure 5.3 Nonlinear characteristic of relative permeability of yokes (steel: SS400)

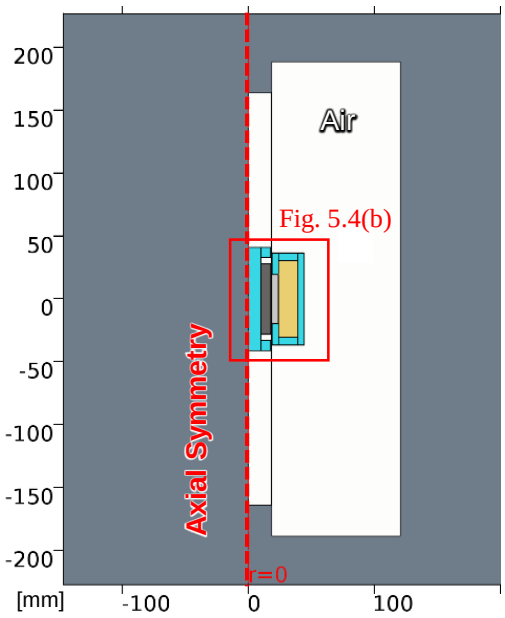

Figure 5.4(a) Entire view of the analysis model

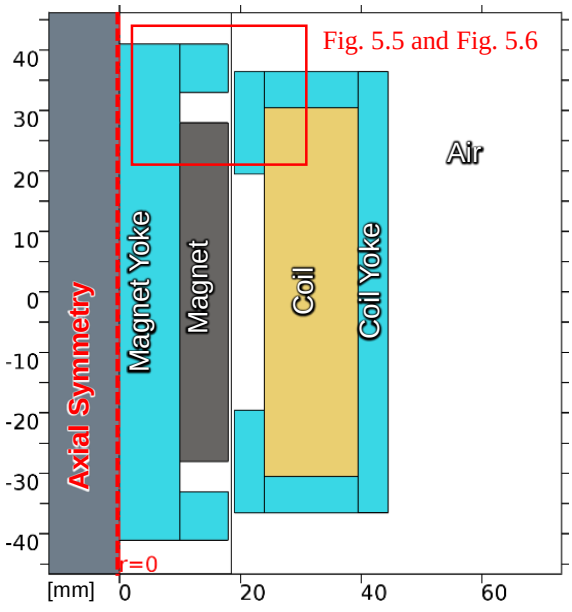

Figure 5.4(b) A closer view of the analysis model

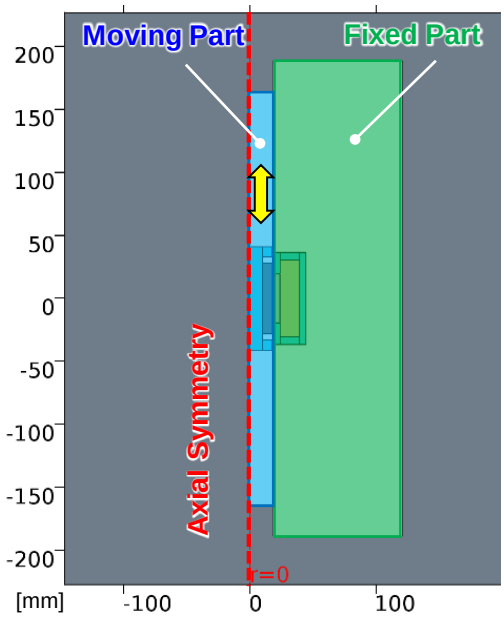

Figure 5.4(c) Entire view of the moving part and the fixed part of the analysis model

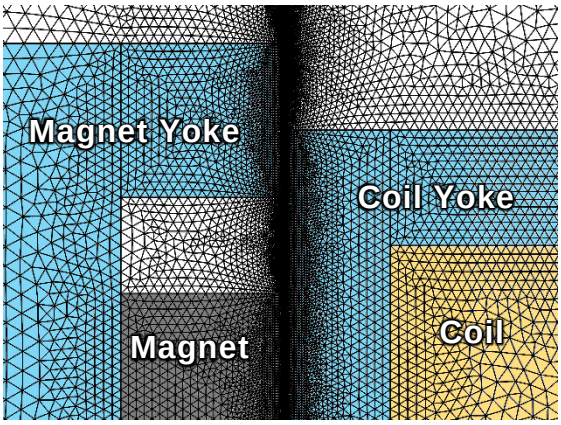

Number of degrees of freedom = 569.6k

Figure 5.5 Element division of the most accurate Finite Element model

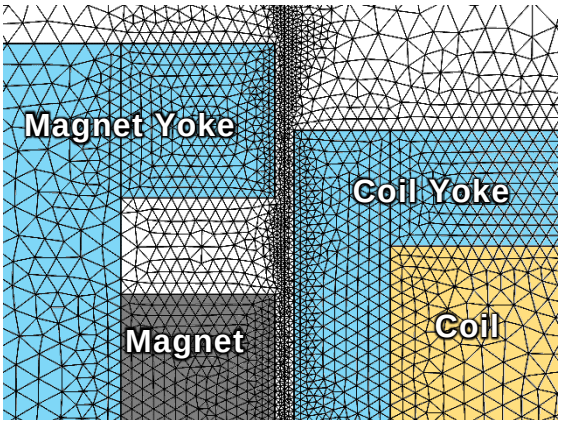

Number of degrees of freedom = 113.7k

Figure 5.6(a) FE model A

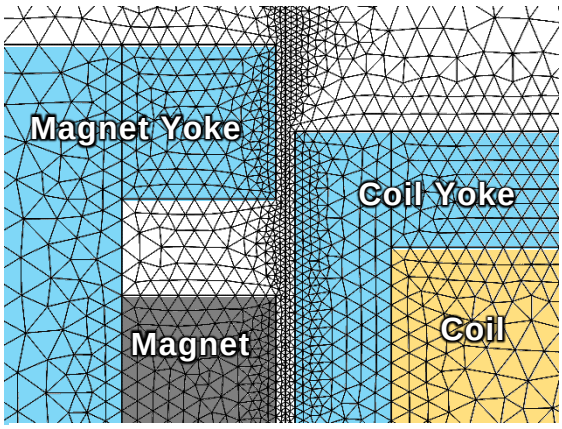

Number of degrees of freedom = 73.8k

Figure 5.6(b) FE model B

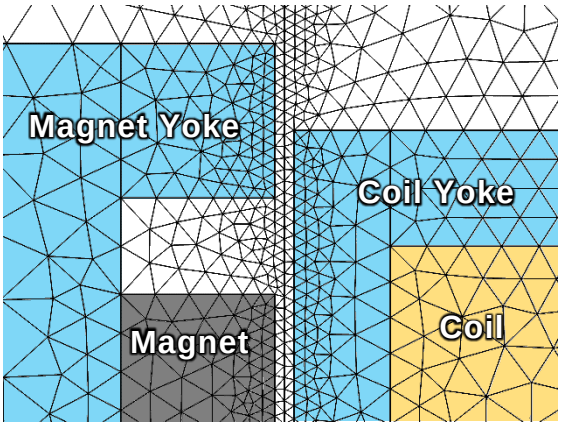

Number of degrees of freedom = 32.4k

Figure 5.6(c) FE model C

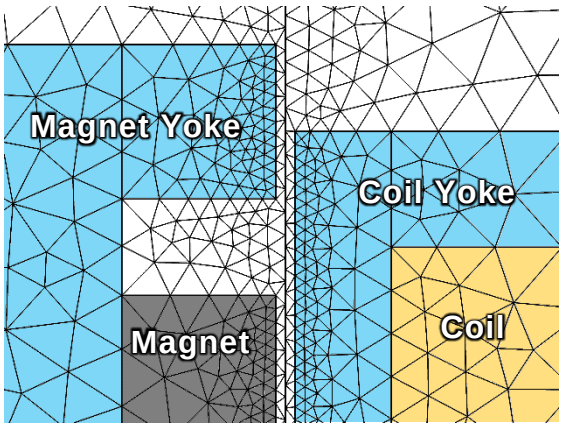

Number of degrees of freedom = 16.7k

Figure 5.6(d) FE model D

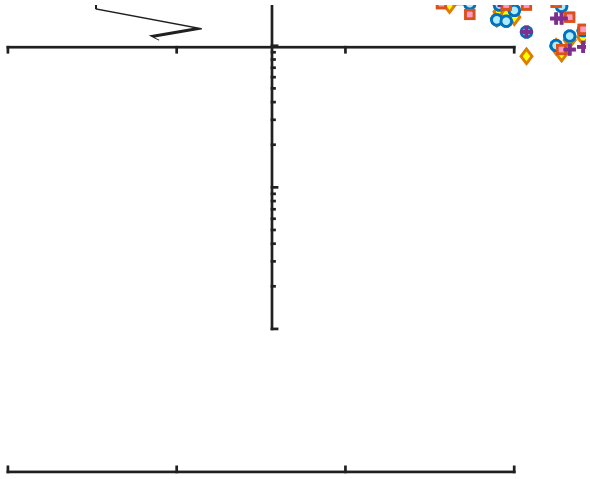

Figure 5.7 Relationship between analysis accuracy for voltage generation and relative tolerance of various FE models

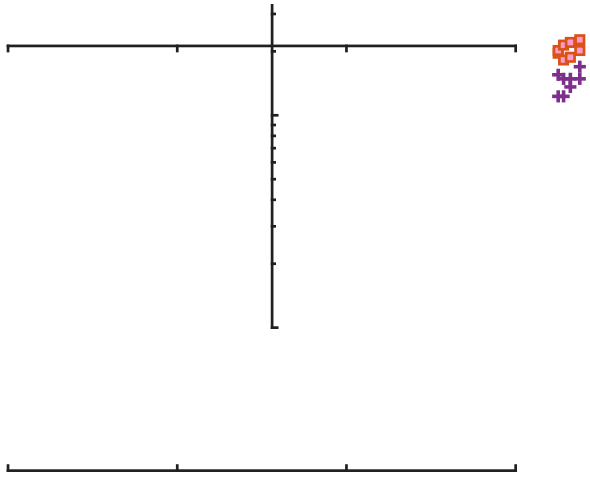

Figure 5.8 Relationship between analysis time and relative tolerance of various FE models

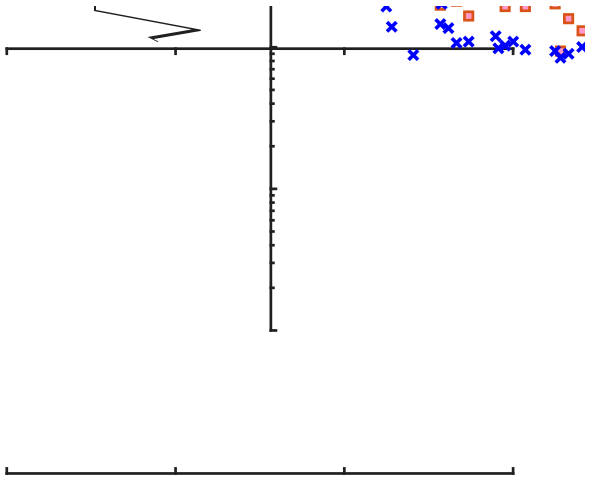

Figure 5.9 Relationship between analysis accuracy and relative tolerance in the case of two different absolute tolerances

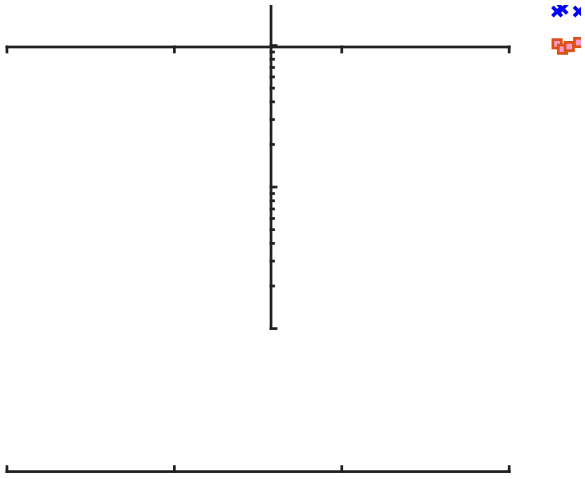

Figure 5.10 Relationship between analysis time and relative tolerance in the case of two different absolute tolerances

Table 5.2 Initial value of dimensional parameters of the power generator and limitations

	Parameters	Initial Value	Lower Bound	Upper Bound
My_h	Magnet yoke height	82[mm]	70[mm]	110[mm]
Cy_h	Coil yoke height	73[mm]	65[mm]	95[mm]
Cy_th	Coil yoke tooth height	17[mm]	3[mm]	Cy_h/2
My_th	Magnet yoke tooth height	8[mm]	3[mm]	(My_h-56[mm])/2
My_w	Magnet yoke width	10[mm]	5[mm]	17[mm]

Table 5.3 Two different design objective functions F_{opt} and the identified dimensional parameters of the power generator

(a)	**(b)**
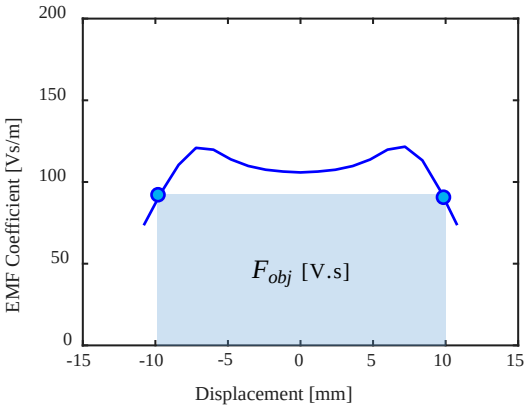	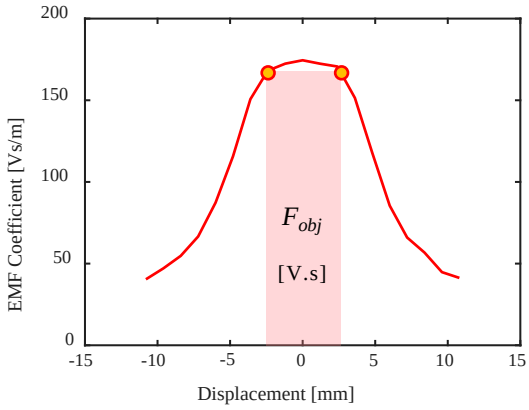
Electromotive force coefficient and displacement	Electromotive force coefficient and displacement
-10 mm ≤ X ≤ 10 mm	-2.5 mm ≤ X ≤ 2.5 mm
Objective of design parameters: maximizing F_{obj} $F_{obj} = \min\left[k_{emf}(X)\right] \cdot (X_{\max} - X_{\min})$	
$\max\left[F_{obj}\right] = 1.796$ V.s	$\max\left[F_{obj}\right] = 0.807$ V.s
My_h = 105.1 mm Cy_h = 76.3 mm Cy_th = 21.1 mm My_th = 7.1 mm My_w = 14.9 mm	My_h = 94.5 mm Cy_h = 82.1 mm Cy_th = 17.8 mm My_th = 10.0 mm My_w = 14.9 mm

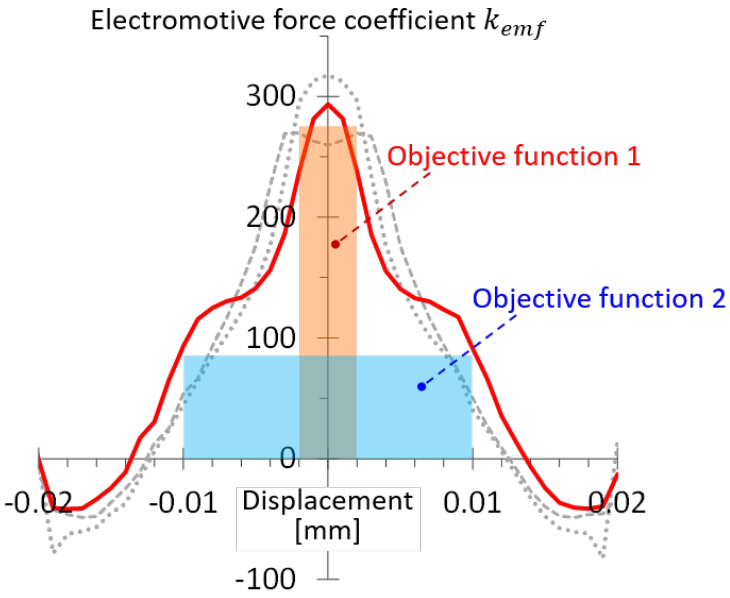

Figure 5.11 Electromotive force coefficients verses displacement for various combination of parameters for multi-objective functions

Table 5.4 Designed dimensional parameters of the power generator

Magnet yoke tooth height	My_th	13.0 mm
Magnet yoke width	My_w	18.0 mm
Coil yoke tooth height	Cy_th	20.0 mm
Coil yoke tooth width	Cy_tw	2.5 mm
Magnet height	M_h	54.0 mm
Magnet yoke height	My_h	95.0 mm
Coil yoke height	Cy_h	74.0 mm

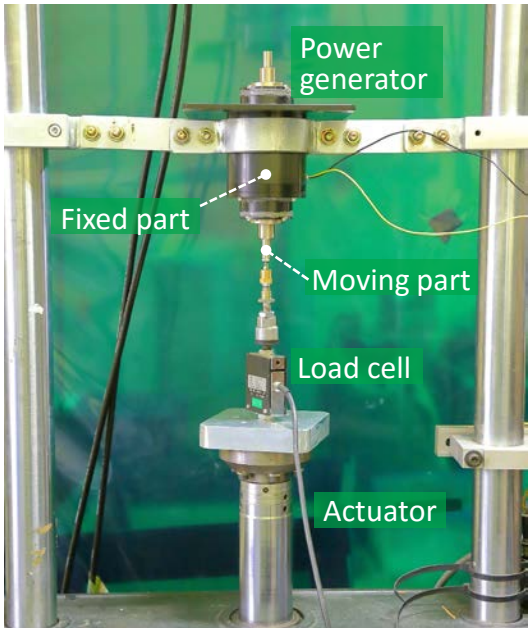

Figure 5.12 Power generator and equipment of experimental evaluation test using an excitation machine

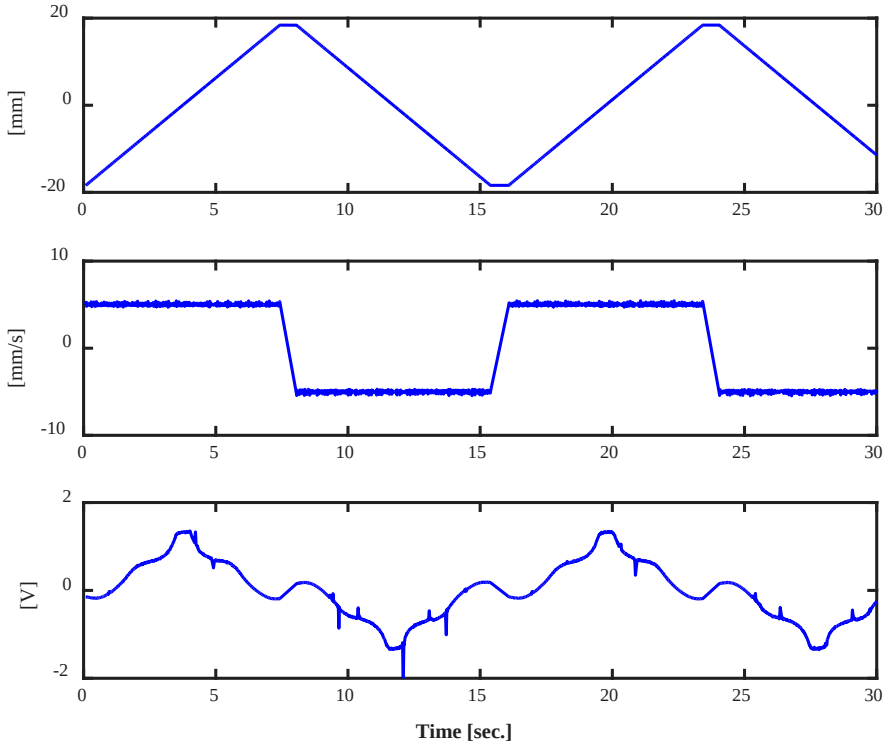

Figure 5.13 Displacement applied to the moving part, velocity of the moving part, and induced voltage signal of the power generator in the experimental evaluation test

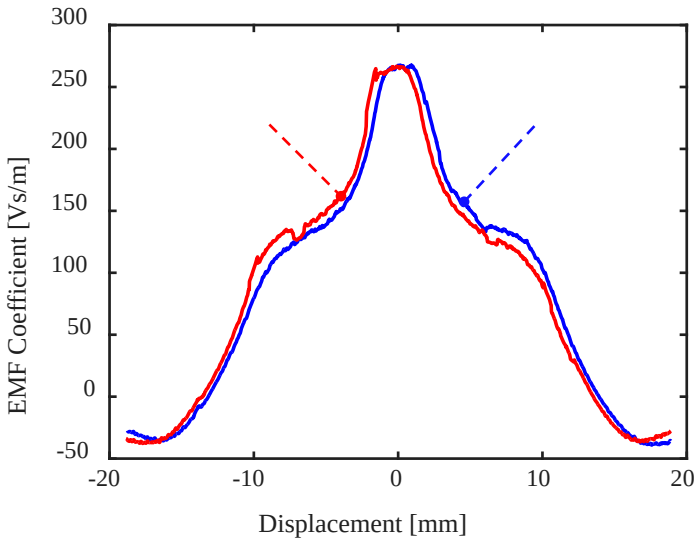

Figure 5.14 Electromotive force coefficients of displacement in the experimental evaluation test

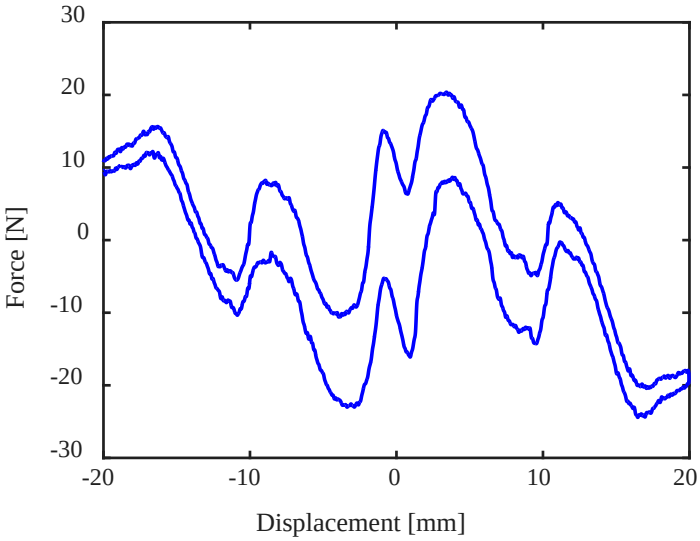

Figure 5.15 Relationship between force and position of the moving part of the power generator

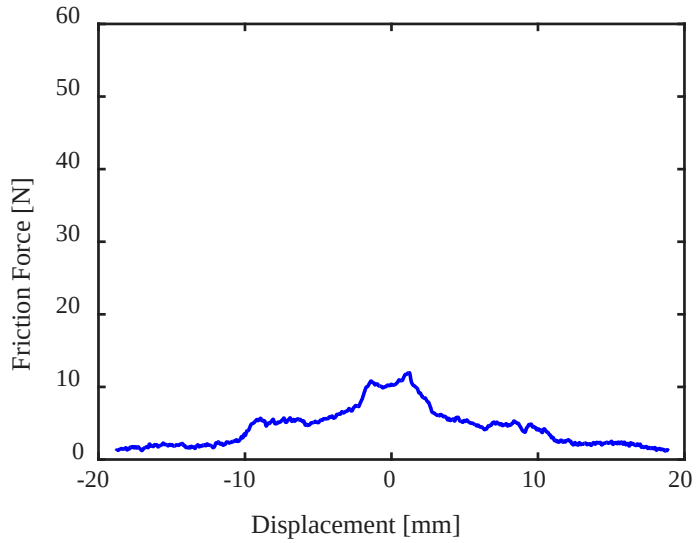

Figure 5.16 Relationship between friction force and position of the moving part of the power generator in the experimental evaluation test

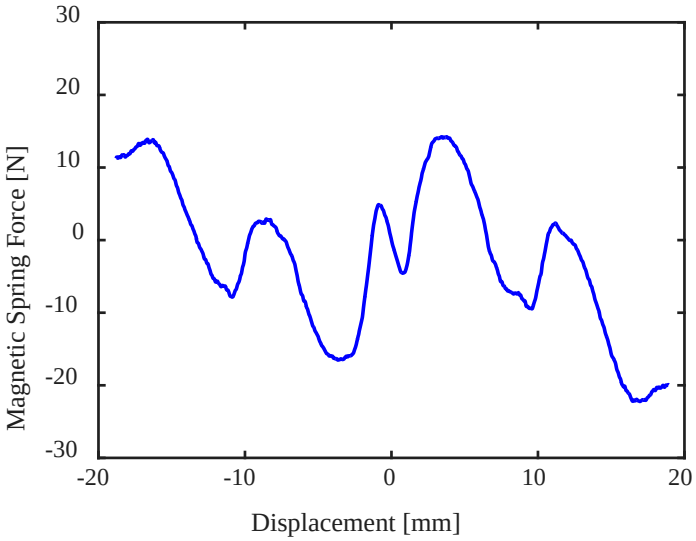

Figure 5.17 Relationship between magnetic spring force and position of the moving part of the power generator in the experimental evaluation test

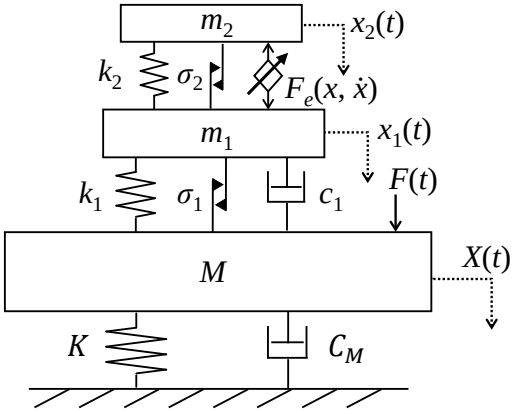

Figure 5.18 Analysis model of bridge-TMG system using nonlinear characteristics of the developed power generator and friction forces

Chapter 6

Proposal of Uses of the Developed Energy Harvesting System

Abstract

In this chapter, an application and operation method of a prototype TMG for vibrations of bridge structures has been investigated. From experiments using the developed device on the existing bridge, the performance of harvesting energy was demonstrated. In addition, it was attempted to supply the harvested electric energy to a monitoring system of a bridge structure.

6.1. Overview

To apply TMG for health monitoring of bridge structures, reliability and efficiency should be considered, and it is also necessary to establish an application procedure to harvest energy. In **Chapter 4**, an application procedure of TMG was proposed. In **Chapter 5**, for effective energy harvesting from vibrations of bridge structures, the efficiency enhanced power generator was then actually developed.

In this chapter, to consider the reliability of TMG systems, attempts were made to store the harvested energy in batteries and use them in a health monitoring system of bridge structures. In addition, long-term harvesting energy was evaluated based on the numerical analysis result. The nonlinear characteristics of power generation and magnetic springs were considered, and so these characteristics were actively incorporated into the TMG design. It is considered that these characteristics improve the ability of power generation of entire TMG systems.

6.2. Application of TMG Systems

According to the application procedure defined in **Chapter 4**, it has been attempted to charge lithium ion secondary batteries using the harvested energy and moreover, the harvested energy has been used to operate a monitoring system.

6.2.1. Target Power for Monitoring Systems of Bridge Structures

To consider supplying electricity to health monitoring systems of bridge structures, the target harvesting energy must be determined. However, monitoring plans depend on each bridge structure and target to be monitored, and the required power varies depending on sensing devices used for monitoring. To detect the bridge structural conditions, bridge structural vibrations are generally used in many researches. For example, bridge structural vibrations are measured by accelerometers for five minutes every four hours, during two to four weeks for each season in reference **[50]**. In other researches, the bridge vibration acceleration data for several minutes are acquired per

day, or bridge vibration acceleration during disasters, such as earthquakes or typhoons, are measured using trigger functions. Considering these existing health monitoring using accelerometers of bridge structures, the required harvesting energy for each monitoring plan was calculated. As examples, four monitoring plans were proposed in this study to evaluate the required harvesting energy for health monitoring systems of bridge structures.

- Plan A: 5 minutes measurement per day is carried out everyday
- Plan B: 5 minutes measurement per hour is carried out two days per month
- Plan C: 5 minutes measurement per hour is carried out one week per quarter
- Plan D: 24 hours continuous measurement per quarter

In these health monitoring plans, bridge structural accelerations were continuously measured during the measuring periods. In plan A and plan B, the bridge vibration modal analysis is mainly focused. In plan C, the bridge vibration modal analysis under traffic induced vibration is focused. To measure the bridge vibration mode, a plural number of sensing devices is generally used. In plan A to plan C, five sensing devices are considered to be supplied electricity from one TMG as an example. On the other hand, in plan D, continuous traffic induced vibrations is focused for the purpose of such as weigh-in-motion. Since MEMS sensors and wireless data transfer systems have rapidly been developed in recent years, a monitoring device using a wireless communication system equipped with a MEMS accelerometer was selected (**Figure 6.1**). The specifications of the monitoring device used in this study are shown in **Table 6.1**. The sampling rate of the acceleration measurement of bridge structural vibration is generally within the range between 100 Hz and 500 Hz. Each monitoring plan and its power consumption was then evaluated in **Table 6.1**.

6.3. Experimental Application of TMG Systems for Health monitoring systems of Bridge Structures

6.3.1. Experiment for Power Generation

The designed TMG for the third vertical vibration mode (6.1 Hz) was installed onto the decided location, namely 18 m from the start of the bridge. To evaluate characteristics of power generation on the existing bridge, a one-day experimental measurement was carried out. To consider the long-term usage of TMG, TMG was covered with an aluminum case to protect it from weather influences. The designed external electric load for the power generation was 40 Ω. Tuning frequencies of the main mass f_1 and second mass f_2 were 6.73 Hz and 10.2 Hz, respectively. These parameters were designed using the proposed analysis iteration flow shown in **Figure 3.7** in **Chapter 3**. As indicated in **Figure 6.2**, the hourly harvested energy was obtained. As shown in **Figure 6.2**, the average hourly harvested energy in the one-day measuring period was 2.3 mWh. Hence, the average harvested power generation was 2.3 mW in one day. This power is of the same level as the experiment in **Chapter 4**, yet the fabrication cost of the power generator is one order smaller. The instantaneous maximum power generation was around 1 to 3 W. This power is also of the same level as the experiment in **Chapter 4**.

Based on the findings obtained in the experiments, first, the average harvested energy and instantaneous maximum power generation were of the same level as the experiment in **Chapter 4**. Second, TMG was adapted not only for smaller bridge vibrations, but also for dominant excitation by traffic loads.

6.3.2. Application TMG to A Monitoring System of Bridge Structure

In the experimental application of TMG to the trial bridge in **Chapter 4**, the charging circuit, which consists of the super capacitor array and the rectifier circuit with shottky barrier diodes, was developed so that harvested energy can charge batteries (**Figure 6.3**). The super capacitor array had low internal resistance and high electricity storage efficiency. However, a large spontaneous discharge occurred at 3 V or more in the experiment. Another problem was that the cost per energy density was

higher than that of a common used secondary battery, such as a lithium ion battery, by an order of one or more. To solve these problems, lithium ion secondary batteries were used. Although the internal resistance of the lithium-ion secondary battery is double or more than that of the super capacitor (**Figure 6.4**), the spontaneous discharge amount is smaller by one order or less. In addition, the charged energy in the lithium ion secondary battery can be easily used for the monitoring device since only a small change in voltage occurs. The battery device consists of two AA-size lithium ion batteries connected in series.

The charged electric energy in the battery was supplied to the monitoring device and it was attempted to continuously operate the monitoring system of the bridge structure (**Figure 6.5**). The monitoring plan was that five minutes of acceleration was measured, and next, wireless data was transmitted to the base station once an hour. This plan simulates the proposed monitoring plan A, B and C (**Table 6.1**).

The time series measured charged electric energy in the lithium ion batteries is shown by a red line in **Figure 6.6**. The battery device consists of two AA-size lithium ion batteries connected in series, and the combined battery voltage is between 2.2 and 2.7 V. As shown in **Figure6.6**, the charging and consuming of batteries were repeated in one-hour cycles. The battery energy was mainly consumed when the monitoring device was communicating with the base station and transferring the sensing data once an hour. At first, the voltage gradually decreased with repeating charging and consuming energy. However, the battery voltage started to increase during a period of daytime. The smaller the battery voltage, the smaller the rate at which the battery voltage decreases. Therefore, it is possible that the energy supply and consumption can be balanced when battery voltage is low.

To consider the effect of the energy harvested, the energy consumed by the monitoring device was estimated and is indicated with the black line in **Figure 6.6**. The lower limitation of the operating voltage of the monitoring device is around 2.3 V. As shown in **Figure 6.6**, the operating life-time of the monitoring device was extended by suppling the electric energy from bridge vibration. In this experiment, the monitoring plan with high frequency measurements of five minutes monitoring period once an hour was selected, namely simulating the proposed monitoring plan A, B and C (**Table 6.1**). Based on the results, it is estimated that the consumed energy by the

monitoring device during the three days measuring period can be compensated with around three days of charging batteries by TMG.

There are three solutions to improve the charging efficiency.

(i) increasing the induced voltage

(ii) reducing the necessary voltage of the monitoring device

To increase the induced voltage, the number of turns of the coil should be increased. This change is not difficult and can be attained with slight change in fabrication cost. It is also considered to reduce the necessary voltage of monitoring devices. TMG can be further developed if these problems are solved.

6.3.3. Evaluation of Energy Harvesting in Long-Term Uses

For practical application of TMG systems, it is important to comprehend how much power generation can be expected in long-term use. In addition, it is also important to verify if the designed TMG can satisfy the required power generation and if the stroke of the power generator is not over the limit. The numerical simulation of energy harvesting in a bridge-TMG system was therefore carried out. The analysis model was shown in **Chapter 5** (**Figure 5.18**), and **Table 6.2** shows parameters used in the numerical simulation. In this research, in order to comprehend the power generation characteristics of TMG in detail, bridge acceleration data from one-day (between 25th to 26th November 2014) was used. The acceleration data length can be further reduced to simplify this verification procedure. The analysis results are shown in **Figure 6.7**. The average harvested energy was 3.86 mWh/h in one day.

A method to estimate the amount of long-term energy harvested is proposed by using the relationship between short-term energy harvested and traffic of large vehicles, as demonstrated in the application experiment on the bridge in **Chapter 4**. The proposed procedure for evaluating long-term energy harvested is indicated in **Figure 6.8**. First, the average energy harvested per large vehicle, named hereafter unit

harvesting energy, is obtained by dividing the energy harvested by the traffic of large vehicles. Next, the long-term harvested energy is estimated by multiplying the long-term traffic of large vehicles by the unit harvesting energy.

The phenomena of harvesting energy from vibrations of bridge structures can be considered as scattered induced random vibration due to traffic loads that reach the TMG through multiple paths. Rayleigh distribution is used to evaluate the expected value of unit harvesting energy **[91-93]**. Rayleigh distribution is as follows.

$$P(x) = \frac{x}{b^2} \exp\left[-\frac{x^2}{2b^2} \right] \tag{6.2}$$

$$\hat{b} = \sqrt{\frac{1}{2n} \sum_{i=1}^{n} X_i^2} \tag{6.3}$$

$$\hat{X} = \hat{b} \sqrt{\frac{\pi}{2}} \tag{6.4}$$

Where, $\hat{b}$ is the Rayleigh parameter and $\hat{X}$ is the expected value. By using the results obtained in **Figure 6.7**, the expected value of unit harvesting energy $\hat{X}$ and 95 % confidence level $\hat{X}_{95}$ have been evaluated as indicated in **Table 6.3**. Next, based on the long-term traffic data (in this study, data from 7th November 2014 to 12th December 2014 were used), the long-term harvesting energy was evaluated (**Figure 6.9** and **Table 6.3**). The expected value of harvesting energy per a day $\hat{E}$ is 68.6 mWh/day, which is the average calculated from five weeks' worth of data. **Table 6.9** indicates the balance between the energy supply from TMG and energy consumption by monitoring systems in each monitoring plan (shown in **Table 6.1**). The expected value of harvesting energy $\hat{E}$ can sufficiently supply required energy for the monitoring plans A, B and C. In case of plan D, the expected value of harvesting energy $\hat{E}$ can enable long battery life. As results, long-term applicability of the TMG system was evaluated based on the numerical analysis.

6.4. Summary

For the practical use of TMG, a TMG system design procedure has been proposed considering the demand electric power, the cost effectiveness and the long-term applicability. In addition, it has been attempted to charge batteries using the harvested energy. The key factors of this chapter are summarized below.

A) In the experiments, energy harvested by TMG from vibrations of bridge structures were found to satisfy the general use of monitoring systems, which was the aim of the tuning design.

B) The harvested energy could be stored in secondary lithium-ion battery devices and used for health monitoring systems of bridges. TMG can therefore improve the service life of monitoring systems.

C) Moreover, long-term applicability of the TMG system was evaluated based on the numerical analysis. The nonlinear characteristics of power generation and magnetic springs were considered into the evaluation procedure.

In addition, the applicability of TMG could be further improved if the energy loss during battery charging is decreased by increasing the voltage induced by power generators, by reducing the necessary voltage of monitoring devices.

Figure 6.1 Example of health monitoring device (wireless data transmission, 3-axis MEMS accelerometers, voltage sensor, temperature and humidity sensors)

Table 6.1 Configuration of a monitoring system and required energy for monitoring plans

Wireless Structural Sensing & Logging Device for Bridges (3-Axis MEMS Accelerometers, Voltage sensor, Temperature & Humidity Sensors) 6mA (Sensing), 33mA (Communication) @ 2.5V Sampling rate: 128 Hz (Accelerometers)				
	Measurement	Period of Time	Number	Required Energy
Plan A	5 mins / day	everyday	5	23mWh/day
Plan B	5 mins / hour	2 days / month	5	36mWh/day
Plan C	5 mins /hour	1 week /quarter	5	42mWh/day
Plan D	24 hours	1 day / quarter	1	101mWh/day

Table 6.2 Parameters of the analysis model of Bridge-TMG system

m_2	Second mass	32 kg
k_2	Coil spring of second mass	131.4 kN/m (10.2 Hz)
σ_2	Friction force (second mass & power generator)	6.0 N
$F_e(x,\dot{x})$	Electromagnetic damping force Magnetic spring force	$F_e(x,\dot{x})$ $F_m(x)$
R	External electric load	40 Ω
r	DC resistance	10 Ω
m_1	Main mass	104 kg
k_1	Coil spring of main mass	186.0 kN/m (6.73 Hz)
c_1	Viscous damping	44.0 N.s/m (0.5 %)
σ_1	Friction force of the first mass	1.0 N
M	Bridge modal mass	320000 kg
K	Bridge modal stiffness	470.1 MN/m (6.1 Hz)
C_M	Bridge modal viscous damping	417.0 kN.s/m (1.7 %)

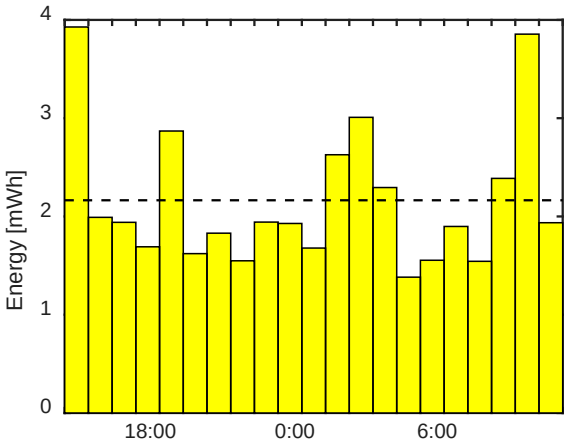

Figure 6.2 Experimental result of the hourly harvested energy from bridge vibrations of the trial bridge

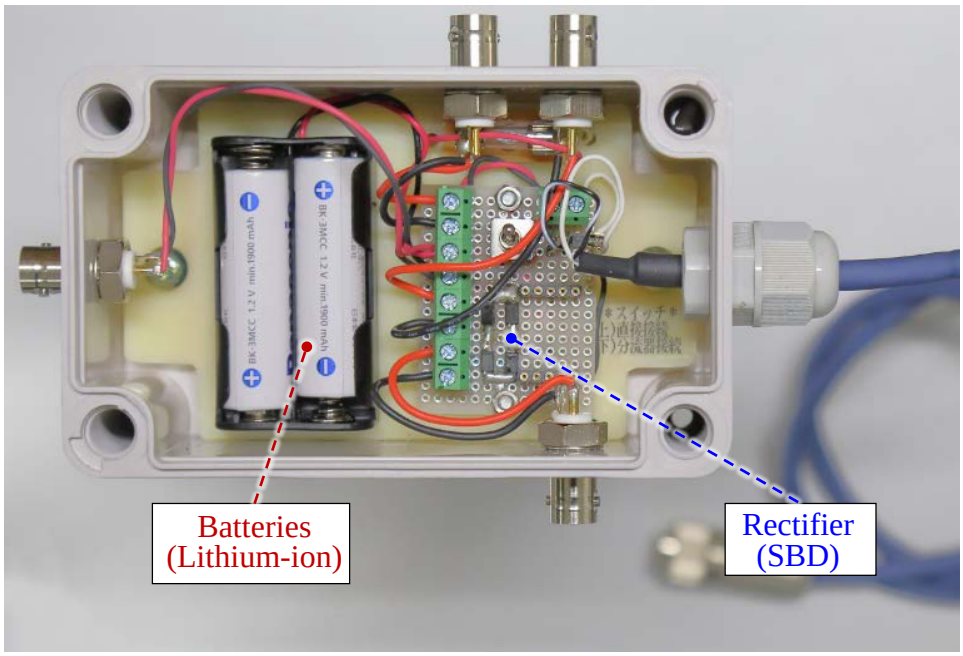

Figure 6.3 Charging circuit using lithium-ion batteries and schottky barrier diodes (SBD)

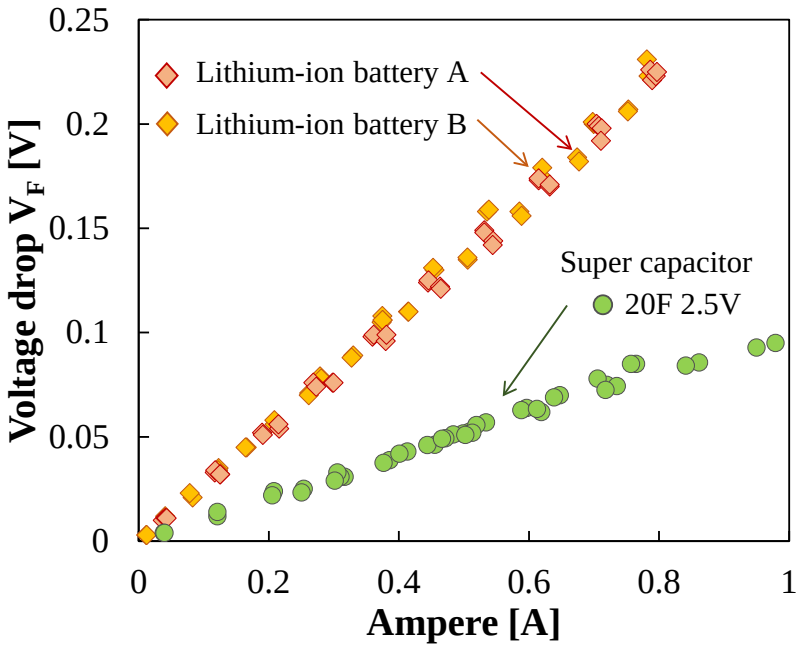

Figure 6.4 Comparison of voltage drop of lithium-ion batteries and a super capacitor (Experiment)

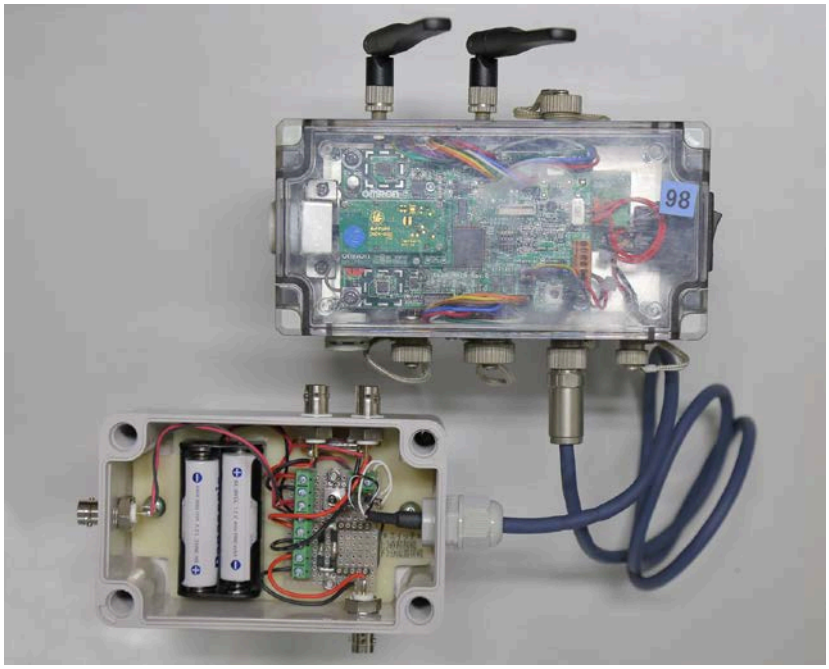

Figure 6.5 Proposed continuous health monitoring system suppling harvested energy

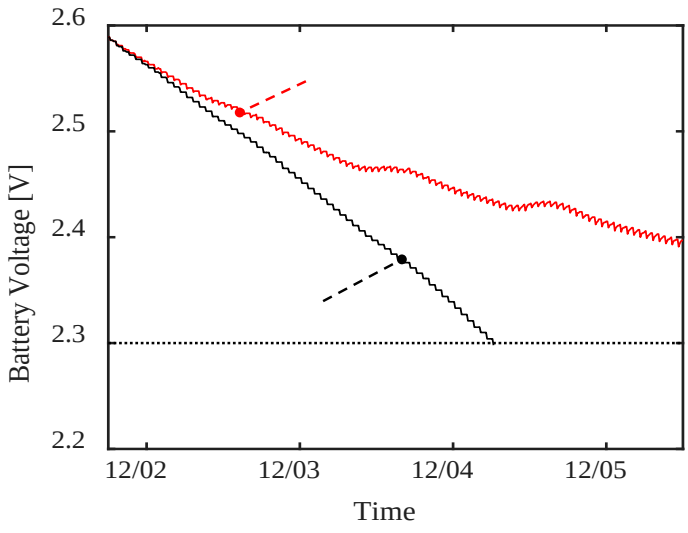

Figure 6.6 Battery voltage – time with supplying electricity to the monitoring system

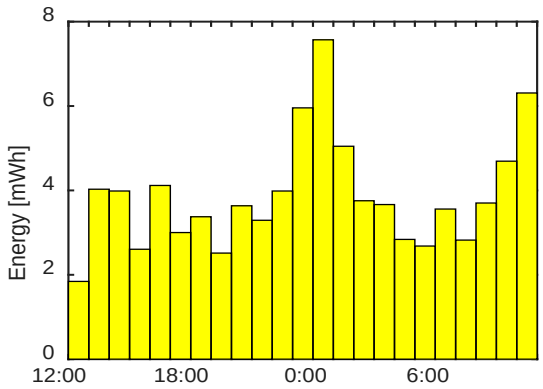

Figure 6.7 Evaluation of harvested energy (numerical analysis)

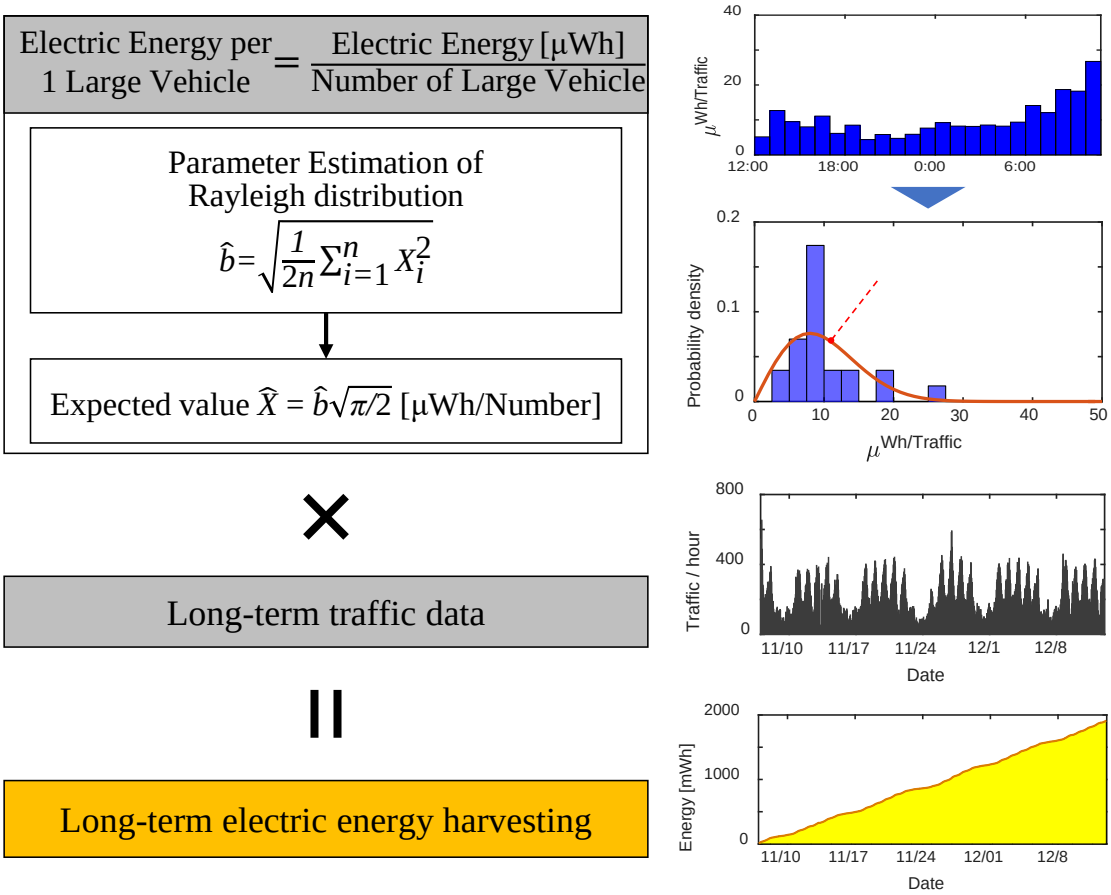

Figure 6.8 Evaluation procedure of long-term electric energy harvesting

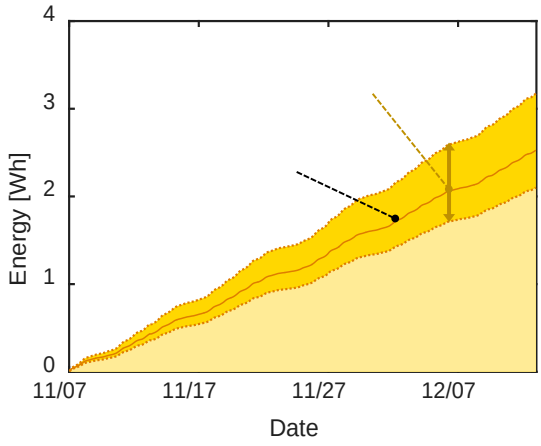

Figure 6.9 Evaluation of long-term electric energy harvesting based on the numerical analysis

Table 6.3 Unit energy harvesting per large vehicle and evaluated long-term harvested energy (average in 5 weeks)

Unit energy harvesting per large vehicle (Used traffic data: 2014/11/25 12:00 ~ 2014/11/26 11:00)		
Expected value	$\widehat{X}$	13.2 μWh/Truck
95% confidence level	$\widehat{X}_{95}$	11.0~16.6 μWh/Truck

Evaluated long-term harvested energy (average in 5 weeks) (Used traffic data: 2014/11/07 0:00 ~ 2014/12/12 24:00)		
Expected value	$\widehat{E}$	68.6 mWh/day
95% confidence level	$\widehat{E}_{95}$	60.0~91.4 mWh/day

Table 6.4 Evaluation of power supply in each monitoring plan

Plan A	Sufficiently supply: 261%~397%
Plan B	Sufficiently supply: 167%~254%
Plan C	Sufficiently supply: 143%~218%
Plan D	Long-life battery: 2.5~10.5 times

Chapter 7

Conclusions

The results of these investigations support the following conclusions related to the objectives of this study.

I. Investigation of the structural characteristics of an energy harvester

Characteristics of an energy harvester, named Tuned Mass Generator (TMG), have been theoretically explained for harvesting energy to achieve greater power generation from bridge vibrations using an equivalent electric circuit of a power generator. It was also found that dual-mass systems have several advantages over single-mass systems for robustness and efficiency of power generation. Based on these findings, TMG using a tuned dual-mass system and electromagnetic power generator has been proposed.

II. Proposal of a parameter design method for effective energy harvesting

A multi-physics parameter design method has been proposed to tune TMG. Results from the parametric studies shown that for effective energy harvesting, first, it is essential to determine the relationship between the required characteristics for electromagnetic power generators, and second, TMG requires a robust parameter design for uncertain bridge vibration, accuracy of assembling TMG and tuning errors.

III. Evaluation of the applicability of TMG to an existing bridge

To investigate the configuration of TMG considering the performance of energy harvesting, a prototype TMG has been applied to an existing expressway bridge. Subsequently, performances of the tuning design of TMG were demonstrated through an experiment on the trial bridge. In addition, the energy harvested from vibrations of bridge structures was found to satisfy the energy required for the general use of monitoring systems.

IV. Enhancement of a power generators efficiency

An effective structural design of a power generator has been proposed to control the specifications of power generators to adapt with TMG systems for effective energy harvesting from vibrations of bridge structures. In addition, the nonlinear characteristics of power generation and magnetic springs were investigated with FE analysis to obtain the most effective performance of TMG. A design method was

proposed using multi-objective functions to satisfy the two important requirements for power generator, namely high efficiency for small vibrations and wide stroke range for large vibrations. Enhanced performances of the power generator were verified through experiment.

V. Development of a TMG system that includes a health monitoring system of bridge structures

To achieve practical use of TMG and to consider the reliability and long-term applicability of the TMG system, attempts were made to store the harvested energy in batteries and use them in a health monitoring system of bridge structures. Nonlinear characteristics of power generation and magnetic spring effect, and other characteristics were actively incorporated into the design procedure to improve the ability of power generation of the entire TMG system. In addition, it was demonstrated that the energy harvested could be stored in the secondary lithium-ion batteries and consequently used for a health monitoring system of bridges.

Finally, a method to harvest bridge vibration energy has been successfully achieved using a developed TMG system. A health monitoring of bridge structures using a TMG system has been proposed and the ability for continuous health monitoring has been demonstrated.

Vibration-based energy harvesting using TMG has several advantages over other power sources, such as solar power generation. First, a stable electric energy can be generated from bridge structures where a common traffic volume of large vehicles is expected, such as expressway. Second, energy harvesting using TMG does not affected by weather conditions and even a power failure, due to such as lightning and strong wind. Third, TMG system can reduce a long-term maintenance cost and an environmental load since the TMG system can reduce power line installation work, and the electricity rate is not required. In addition, TMG has a potential to monitor the structural behavior using generated voltage signals, since TMG generate electricity according to vibrations of bridge structures.

The proposed method in this research can be applied to various bridges, of which the dominant natural frequency is higher than 5 Hz such as middle span bridges. To obtain greater energy, it is essential to correspond to a lower natural frequency of bridges. However, at present, it is difficult to achieve the greater harvesting energy from bridge vibrations, because of the mechanical systems such as the stroke of coil springs and the friction loss. The efficiency and applicability of TMG could be further improved if TMG could be applied to lower bridge vibration modes.

Recommendations

The practical power generation according to the required energy level for monitoring systems is demanded. Since monitoring plans for bridge structures have been discussed in various studies, several required energy levels were examined by considering monitoring plans (plan A to D) in this study. It is possible to harvest energy from bridge vibrations for regular monitoring, which obtains dynamic behaviors of bridge structures using accelerometers. However, in order to measure dynamic behavior continuously, a larger generated electric power is required. By improving the efficiency and enabling power generation at lower frequencies, TMG can achieve the required energy level for such as continuous dynamic monitoring of bridge structures. From the conclusions of this study, the following are proposed as further potential enhancements of harvesting energy from vibrations of bridge structures.

(a) If the dynamic friction force can be reduced to the 1N or less, TMG could harvest energy even from vibrations induced by small vehicles or from wind induced vibrations. The friction force could also be improved considering the mechanical devices used in the power generator.

(b) TMG applicability could be further improved if the charging energy loss was decreased by improving the induced voltage of the power generator, by reducing the necessary voltage of the monitoring device, or by boosting the battery voltage to the required voltage of the health monitoring device.

References

[1] LEE J.W., KIM J.D., YUN C.B., YI J.H., and SHIM J.M., “Health-monitoring method for bridges under ordinary traffic loadings”, *Journal of Sound and Vibration*, Vol. 257(2), pp. 247-264, 2002.

[2] ZHANG Q. W., “Statistical damage identification for bridges using ambient vibration data”, *Journal of Computers and Structures*, Vol. 85(7–8), pp. 476–485, 2007.

[3] ALI M. R., OKUMATSU T., OKABAYASHI T., and JAWAID B. A., “Dynamic characteristics estimation from the ambient vibration of existing bridge by realization theories”, *Journal of Structural Engineering*, Vol. 55A, pp. 284-294, 2009.

[4] MIKI C., KOTO Y., SASAKI E., SAITO K., and ISHIKAWA Y., “Long-Term Monitoring of AN Urban Expressway Bridge Using Optical Fiber Sensor System”, *Journal of Japan Society of Civil Engineers*, Vol. 71A, No. 3, pp. 416-428, 2015.

[5] FUKADA S., MUROI T., MOMIYAMA Y., and KAJIKAWA Y., “Dynamic response of bridge affected by road roughness with a long spatial wavelength in monitoring before and after repair”, *Journal of Japan Society of Civil Engineers*, Vol. 67A, No. 1, pp. 121-136, 2011.

[6] MIAO S., VEERMAN R., KOENDERS E., and KNOBBE A., “Modal Analysis of a concrete highway bridge-structure calculations and vibration-based results”, *The 6th international conference on structural health monitoring of intelligent infrastructure*, pp. 9-11, Hong Kong, Dec. 2013.

[7] ZUO L., SCULLY B., SHESTANI J., and ZHOU Y, “Design and characterization of an electromagnetic energy harvester for vehicle suspensions”, *Journal of Smart Materials and Structures*, Vol. 19, No. 4, pp. 1-5, 2010.

[8] YOSHIDA Y., KOBAYASHI Y., and UCHIMURA T., “Development of the monitoring system that operates with the power generated from the bridge vibration”, *Journal of Japan Society of Civil Engineering*, Vol. 70/A1, No. 2, 2014, pp. 282-294.

[9] YOSHIDA Y., KOBAYASHI Y., and WADA K., “Application of the power storage device by energy harvesting from the bridge vibration for the structure monitoring”, *Journal of Structural Engineering*, Vol. 61A, pp. 532-543, 2015.

[10] INOUE R., “Eco-conscious construction vibration reduction method using vibration energy harvester”, Takenaka technical research report, No. 68, pp. 1-8, 2012.

[11] INOUE R., ABE T., and HIRABAYASHI S., “Vibration energy harvesting using air-conditioning ducts: part 2: Verification experiment using vibration energy harvester and sensor module”, *Summaries of technical papers of annual meeting Architectural Institute of Japan*, pp. 1351-1352, 2013.

[12] TANAKA M., and SUZUKI M., “Development of Power Supply Unit for Anomaly

Defection Sensors in Ground Coils of Superconducting Maglev", *Railway Technical Research Institute Report*, Vol. 27, No. 7, pp. 17-22, 2013.

[13] CASSIDY I.L., SCRUGGS J.T., BEHRENS S., and GAVIN H.P., "Design and experimental characterization of an electromechanical transducer for large-scale vibratory energy harvesting applications", *Journal of Intelligent Material Systems and Structures*, Vol. 22, pp. 2009-2024, 2011.

[14] SHEN W., ZHU S., and XU Y., "An experimental study on self-powered vibration control and monitoring system using electromagnetic TMD and wireless sensors", *Sensors and Actuators* A: Physical, Vol. 180, pp. 166-176, 2012.

[15] CHOI Y. T., and WERELEY N. M., "Self-powered magnetorheological dampers", *Journal of Vibration and Acoustics*, Vol. 131(4), pp. 1-5, 2009.

[16] MAŚLANKA M., "Free vibrations of a cable with an attached MR damper-experimental analysis of amplitude dependent damping", *Proceedings of the 7th International Symposium on Cable Dynamics*, pp. 415-422, Austria, 2007.

[17] PRAKASH P., and PANDEY A. K., "Performance of MR damper based on experimental and analytical modeling", *Proceedings of the 22nd International Congress of Sound and Vibration*, pp.1-5, Italy, 2015.

[18] OSAFUNE T., NAKAMURA S., MIZUNO K, KATO H., and UETA T., "Study on impact absorbing momentum exchanging damper for suppression of road bridge vibration", *Journal of Structural Engineering*, Vol. 56A, pp. 237-250, 2010.

[19] MOHAMED G., MANSOUR K., MUHAMMAD T. B. Y., and MOHAMMAD A., "Shock vibration control using a novel impact damper", *Proceedings of the 22nd International Congress of Sound and Vibration*, Italy, 2015.

[20] SEMERCIGIL S. E., COLLETTE F., and HUYNH D., "Experiments with tuned absorber—Impact damper combination", *Journal of Sound and Vibration*, Vol. 256(1), pp. 179-188, 2002.

[21] FUJINO Y., "同調質量ダンパー（TMD に関して）－最近の成果をまじえてー", 片山技法, No. 13, pp. 2-10, 1993.

[22] SET

[23] O K., "Trends in Vibration Controlling Equipments", *Journal of Japan Society of Mechanical Engineers*, Vol. 51C, No. 472, pp. 3165-3171, 1983.

[24] SEMERCIGIL S. E., LAMMERS D., and YING Z., "A new tuned vibration absorber for wide-band excitations", *Journal of Sound and Vibration*, Vol. 156(3), pp. 445-459, 1992.

[25] LANG Z. Q., JING X. J., BILLINGS S. A., TOMLINSON G. R., and PENG Z. K., "Theoretical study of the effects of nonlinear viscous damping on vibration isolation of sdof systems", *Journal of Sound and Vibration*, Vol. 323(1–2), pp. 352-365, 2009.

[26] KANEKO I., and KATSUKAWA T., "Powerful TMD for bridges strongly shaken by a reaction force from an abutment", Kumagai technical research report, pp.12-20, 1996.

[27] IGARASHI A., and HASEGAWA N., "Evaluation of response displacement reduction effect by TMD application to a bridge girder supported by elastomeric isolation bearings", *Journal of Japan Society of Civil Engineers*, Vol. 66A, No.1, pp. 196-200, 2010.

[28] MA S., and SEMERCIGIL S. E., "A modified passive tuned absorber for secondary systems under random excitation", *Journal of Sound and Vibration*, Vol. 208(3), pp. 349-366, 1997.

[29] FOISAL A. R. M., HONG C., and CHUNG G. S., "Multi-frequency electromagnetic

energy harvester using a magnetic spring cantilever", *Journal of Sensors and Actuators*, Vol. 182A, pp. 106-113, 2012.

[30] NERVES A. C., and KRISHNAN R., "A strategy for active control of tall civil structures using regenerative electric actuators", *Proceedings of the 11th American Society of Civil Engineers Mechanics Conference*, pp. 503-506, Florida, 1996.

[31] PALOMERA A. R., CONNOR J. J., and OSCHENEDORF J. A., "Feasibility study of passive electromagnetic damping systems", *Journal of Structural Engineering*, Vol. 134(1), pp. 164–170, 2008.

[32] ZHU S., SHEN W., and XU Y., "Linear electromagnetic devices for vibration damping and energy harvesting: Modeling and testing", *Journal of Engineering Structures*, Vol. 34, pp. 198-212, 2012.

[33] LIU J. Q., FANG H. B., ZHENG Y. X., MAOB X. H., SHENA X. C., CHENA D., LIAOB H., and CAIA B. C., "A MEMS-based piezoelectric power generator array for vibration energy harvesting", *Microelectronics Journal*, Vol. 39(5), pp. 802-806, 2008.

[34] ROUNDY S., WRIGHT P. K., and RABAEY J., "A study of low level vibrations as a power source for wireless sensor nodes", *Journal of Computer Communications*, Vol. 26(11), pp. 1131-1144, 2003.

[35] UMEDA M., SAKAI Y., and NAKAMURA K., "Self-generation door alarm system using impact induced piezoelectric vibration", *IEEJ Transactions on Sensors and Micromachines*, Vol. 123E, No. 12, pp. 534-540, 2003.

[36] SUZUKI Y., EDAMOTO M., KASAGI N., KASHIWAGI K., MORIZAWA Y., YOKOYAMA T., SEKI T., and Oba M., "Micro electret energy harvesting device with analogue impedance conversion circuit", *Proceedings of Power MEMS 2008 + micro EMS 2008*, pp. 7-10, Japan, 2008.

[37] MARBOUTIN C., SUZUKI Y., and KASAGI N., "Optimal design of micro electret generator for energy harvesting", *7th Int. Workshop Micro and Nanotechnology for Power Generation and Energy Conversion Applications (Power MEMS 2007)*, pp. 141-144, Freiburg, 2007.

[38] YAMAGUCHI H., SASAKI E., and MINESAWA G.V., "Development of passive velocity sensors using power generation with vibrated electret", *Journal of Japan Society of Civil Engineering*, Vol. 70A1, No. 2, pp. 150-160, 2014.

[39] SUZUKI Y., MIKI D., EDAMOTO M., and HONZUMI M., "A MEMS electret generator with electrostatic levitation for vibration-driven energy-harvesting applications", *Journal of Micromechanics and Microengineering*, Vol. 20, No. 10, 2010.

[40] MATSUMOTO K., SARUWATARI K., and SUZUKI Y., "Prototyping of battery-less wireless sensor node using electret-based kinetic energy harvesting", *IEEJ Transactions on Sensors and Micromachines*, Vol. 132C, No. 3, pp. 344-349, 2011.

[41] AKAZAWA T., MURAO K., and OKADA Y., "Study of Linear Alternator for Free Piston Stirling Engine", *The Symposium on Stirling Cycle*, Vol. 9, pp. 33-34, 2005.

[42] AKAZAWA T, MURAO K., HIRATA K., and HOSHINO T, "Development of high efficiency stirling engine", *The Symposium on Stirling Cycle*, Vol. 9, pp.105-106, 2005.

[43] HOSHINO T., YOSHIHARA S., AKAZAWA T., and MURAO K., "Performance testing of new type linear alternator", *The Symposium on Stirling Cycle*, Vol. 10, pp. 109-110, 2006.

[44] HOSHINO T., "Design and fabrication of opposed-piston linear alternator for Stirling engine", *The Symposium on Stirling Cycle*, Vol. 5, pp. 5-8, 2001.

[45] TAKESHIMA R., SEHNAWI R. A., NAKAJIMA A., NAKAMURA S., and YOKOKAWA H., “A study on change of vibration property of bridge structure with RC pier in different vibration level”, *Journal of Japan Society of Civil Engineers*, Vol. 70A1, No. 4, pp. 130-139, 2014.

[46] SAITO T., NAKAJIMA A., TAKESHIMA R., and SEHNAWI R. A., “Experimental investigation on vibrational property change of bridge model under various input level”, *Journal of Structural Engineering*, Vol. 59A, pp. 261-271, 2013.

[47] YOSHIOKA T., HARADA M., YAMAGUCHI H., and ITOU S., “A study on the vibration characteristics change of the steel truss bridge by the real damage of diagonal member”, *Journal of Structural Engineering*, Vol. 54A, pp. 199-208, 2008.

[48] OKUMATSU T., YAMAZAKI A., NAKAMURA S., KOMATSU M., and NISHIKAWA T., “Investigation on variation of natural frequency of a steel langer bridge accompanied by temperature change”, *Proceedings of constructional steel*, Vol. 21, pp. 484-491, 2013.

[49] YAMAGUCHI H., TAKANO H., OGASAWARA M., SHIMOSATO T., KATO M., and OKADA J., “Identification of dynamic characteristics by field vibration test in Tsurumi Tsubasa bridge”, *Journal of Japan Society of Civil Engineers*, No .543/I-36, pp. 247-258, 1996.

[50] KAWASHIMA K., OGIMOTO H., WATANABE G., and NISHI H., “Damping characteristics of a PC cable-stayed bridge based on measured strong motion records”, *Journal of Japan Society of Civil Engineers*, Vol. 65A, No .2, pp. 426-439, 2009.

[51] OKUMATSU T., OKABAYASHI T., TASHIRO D., KANAMEYA T., AHMAD J. B., “Observation of natural frequency of a steel langer truss bridge by the remote monitoring system”, *Journal of Structural Engineering*, Vol. 53A, pp.844-852, 2007.

[52] OKUMURA T., OKABAYASHI T. MOTOYAMA M., MOMIYAMA Y., and MUROI T., “振動遠隔モニタリングによる PC 主桁橋梁の固有振動数の長期的変動について”, *土木学会西部支部研究発表会*, pp. 83-84, 2009.

[53] IGUSA T., and XU K., “Vibration control using multiple tuned mass dampers”, *Journal of Sound and Vibration*, Vol. 175(4), pp. 491-503, 1994.

[54] YAMAGUCHI H., KABELOVA Q., and KIKUCHI J., “Vibration control of structures with multiple tuned mass dampers”, *Journal of Structural Engineering*, Vol. 40A, pp. 897-903, 1994.

[55] SGOBBA S., and MARANO G.C., “Optimum design of linear tuned mass dampers for structures with nonlinear behavior”, *Journal of Mechanical Systems and Signal Processing*, Vol. 24(6), pp. 1739-1755, 2010.

[56] LEE C.L., CHEN Y.T., CHUNG L.L., and WANG Y., “Optimal design theories and applications of tuned mass dampers”, *Journal of Engineering Structures*, Vol. 28(1), pp. 43-53, 2006.

[57] HORIUCHI H., FUJISAWA N., and TSUMURA N., “Practical formulas for estimating design parameters of TMD”, *Journal of Structural Engineering*, Vol. 37A, No. 2, pp. 781-788, 1991.

[58] KAMIYA K., KAMAGATA K., MATSUMOTO S., and SETO K., “Optimal design method for multi dynamic absorber”, *Journal of Japan Society of Mechanical Engineers*, Vol. 62C, No. 602, pp. 22-27, 1996.

[59] PAN G., and YASUDA M., “Robust Design Method of Multi Dynamic Vibration Absorber”, *The Japan Society of Mechanical Engineering*, Vol. 71C, No. 712, pp. 3430-3436, 2005.

[60] YAMASHITA S., OOKUMA M., SETO K., and NAGAMATSU A., “Simultaneous

optimum design method of dynamic absorbers for controlling multimode", *The Japan Society of Mechanical Engineering*, Vol. 57C, No. 534, pp. 399-406, 1991.

[61] IWANAMI K., and SETO K., "The optimum design method for dual dynamic dampers and its effectiveness", *The Japan Society of Mechanical Engineering*, Vol. 50C, No. 449, pp. 44-52, 1984.

[62] FUJINO Y., SUN L., and YAMAGUCHI H., "A simulation study on effectiveness of multiple TMD and multiple TLD.", *Journal of Structural Engineering*, Vol. 38, No. 2, pp. 825-836, 1992.

[63] SUMIYOSHI B., and INOUE H., "Numerical study on robustness for frequency response of plural TMD system", *Journal of Structural Engineering*, Vol. 46A, No. 2, pp. 565-574, 2000.

[64] ABE M., and FUJINO Y., "Dynamic characterization of multiple tuned mass damper (MTMD) and its frequency band width", *Journal of Japan Society of Civil Engineering*, No. 465/ I-23, pp. 87-96, 1993.

[65] YOSHIZUMI F., SANO K., and INOUE H., "Optimum robust design for a-few-TMD systems", *Journal of Structural Engineering*, Vol. 48A, pp. 329-338, 2002.

[66] ABE M., and FUJINO Y., "Efficiency and design formulas of multiple tuned mass dampers (MTMD)", *Journal of Japan Society of Civil Engineering*, Vol. 465/I-23, pp. 97-106, 1993.

[67] TAMAKOSHI T., and YOKOI Y., "Annual Report of Basic Data on Road Structures", *Technical Note of National Institute for Land and Infrastructure Management*, No.822, 2015.

[68] ARROYO E., BADEL A., FORMOSA F., WU Y., and QIU J., "Comparison of electromagnetic and piezoelectric vibration energy harvesters: Model and experiments", *Journal of Sensors and Actuators*, Vol. 183A, pp. 148-156, 2012.

[69] SCRUGGS J. T., and IWAN W. D., "Control of a civil structure using an electric machine with semiactive capability (ASCE)", *Journal of Structural Engineering*, Vol. 129(7), pp. 951–959, 2003.

[70] SCRUGGS J. T., and IWAN W. D., "Structural control with regenerative force actuation networks", *Journal of Structural Control and Health Monitoring*, Vol. 12(1), pp. 25-45, 2005.

[71] CASSIDY I. L., SCRUGGS J. T., BEHRENS S., and GAVIN H. P., "Design and experimental characterization of an electromechanical transducer for large-scale vibratory energy harvesting applications", *Journal of Intelligent Material Systems and Structures*, Vol. 22(17), pp. 2009–2024, 2011.

[72] STEPHEN N., On the maximum power transfer theorem within electromechanical systems, Journal of Mechanical Engineering Science, Vol. 220(8), pp. 1261-1267, 2006.

[73] KONG N., HA D. S., ERTURK A., and INMAN D. J., "Resistive impedance matching circuit for piezoelectric energy harvesting", *Journal of Intelligent Material Systems and Structures*, Vol. 21(13), pp. 1293-1302, 2010.

[74] LEFEUVRE E., AUDIGIER D., RICHARD C., and GUYOMAR D., "Buck-boost converter for sensorless power optimization of piezoelectric energy harvester", *IEEE Transactions on Power Electronics*, Vol.22(5), pp. 2018-2025, 2007.

[75] HOANG T., KANG D., and LEE J., "Comparisons between various designs of transverse flux linear motor in terms of thrust force and normal force", *IEEE Transactions on Magnetics*, Vol. 46(10), pp. 3795-3801, 2010.

[76] TANG X., LIN T., and ZUO L., “Electromagnetic vibration energy harvesting with high power density using a magnet array”, *Proceedings of Active and Passive Smart Structures and Integrated Systems*, Vol. 8341, California, 2012.

[77] CHANG J., KANG D., LEE J., and HONG J., “Development of Transverse Flux Linear Motor with Permanent-Magnet Excitation for Direct Drive Applications”, *IEEE Transactions on Magnetics*, Vol. 41, No. 5, 2005.

[78] POLINDER H., MECROW B.C., JACK A.G., DICKNISON P.G., MUELLER M.A., “Conventional and TFPM Linear Generators for Direct-Drive Wave Energy Conversion”, *IEEE Transactions on Energy Conversion*, Vol. 20(2), 2005.

[79] BAOMING G., ALMEIDA A. T., and FERREIRA F. J. T. E., “Design of transverse flux linear switched reluctance motor”, *IEEE Transactions on Magnetics*, vol. 45, no. 1, pp. 113–119, 2009.

[80] LIU C. T., and KUO J. L., “Experimental investigation and 3-D modeling of linear variable-reluctance machine with magnetic-flux decoupled windings”, *IEEE Transactions on Magnetics*, Vol. 30, No. 6, pp. 4737–4739, 1994.

[81] KANG D. H., “Increasing of thrust force in transverse flux machine by permanent-magnet screen”, *IEEE Transactions on Magnetics*, Vol. 41, No. 5, pp.1952–1955, 2005.

[82] WENLONG L., CHAU K. T., and CHING T. W., “A Six-Phase Transverse-Flux-Reversal Linear Machine for Low-Speed Reciprocating Power Generation”, *The 2015 IEEE International Electric Machines and Drives Conference (IEMDC)*, pp. 618-623, 2015.

[83] FRANZITTA V., VIOLA A., and TRAPANESE M., “Design of a transverse flux machine for power generation from seawaves”, *Journal of Applied Physics*, Vol. 115(17), 2014.

[84] ZHU S., SHEN W., and XU Y., “Linear electromagnetic devices for vibration damping and energy harvesting: Modeling and testing”, *Journal of Engineering Structures*, Vol. 34, pp. 198-212, 2012.

[85] TANG X., and ZUO L., “Enhanced vibration energy harvesting using dual-mass systems”, *Journal of Sound and Vibration*, Vol. 330, pp. 5199-5209, 2011.

[86] ZUO L., and CUI W., “Dual-functional energy-harvesting and vibration control: Electromagnetic resonant shunt series tuned mass dampers”, *Journal of Vibration and Acoustics*, Vol. 135(5), 2013.

[87] KAITO K., MATSUOKA K., WATANABE T., SOGABE M., and FUJINO Y., “Vibration monitoring for railway bridges using passing train load”, *Journal of Japan Society of Civil Engineers*, Vol. 66F, No .3, pp. 382-401, 2010.

[88] SETO K., OOKUMA M., YAMASHITA S., and NAGAMATSU A., “An Estimation Method of Equivalent Masses for a Multi-Degree of Freedom System”, *Journal of Japan Society of Mechanical Engineers*, Vol. 53C, No .485, pp. 52-58, 1987.

[89] OKAZAKI N., NARABAYASHI T., and ICHIZAKA A., “Damping Ratio Evaluation of the Conventional-model Estimated Formulas by the Half Power Method and Proposal of the Practical Exact Formulas”, *Journal of Micromechatronics*, Vol. 48, No. 2, pp. 20-31, 2004.

[90] Research Committee on Fatigue Diagrams of Helical Compression Springs, “Study on fatigue diagrams of helical compression springs”, *Journal of Transactions of Japan Society of Spring Engineers*, Vol. 2015, No. 60, pp. 51-105, 2015.

[91] TAGUCHI N., HANAZATO T., IKEDA Y., and ISHIDA R., “Dynamic loads of traffic-induced ground vibrations on road: Predictional method of environmental ground vibrations Part 2”, *Journal of Environmental Engineering*, Vol. 73, No. 633, pp. 1241-1247, 2008.

[92] SIDDIQUI M. M., “Some Problems Connected with Rayleigh Distributions”, *Journal of Research of the National Bureau of Standards-D. Radio Propagation*, Vol. 66D, No. 2, pp.167-174, 1962.

[93] KUNDU D., and RAQAB M.Z., “Generalized rayleigh distribution: different methods of estimation”, *Computational Statistics and Data Analysis*, Vol. 49, pp. 187-200, 2005.

[94] AHMED A., AHMAD S. P., and RESHI J. A., “Bayesian analysis of rayleigh distribution”, *International Journal of Scientific and Research Publications*, Vol. 3(10), 2013.